ABSTRACT

WILLOUGHBY, JULIE ANN-CROWE. Design & Synthesis of Silicone Elastomer Networks with Tunable Physico-Chemical Characteristics. (Under the direction of Jan Genzer.)

We have engineered functional surfaces via the manipulation of silicone elastomers (SEs). The most common silicone, poly(dimethylsiloxane) PDMS, can be both challenging and advantageous in the design of surfaces due to its inherent inertness and flexibility of the siloxane backbone. This unique polymer is approaching a $10 billion dollar market attributed to its formulation in a wide array of applications; from the personal care industry to the electronics industry. While it can be used for many applications, surface design with PDMS usually requires a chemical or physical modification of the polymeric network. In addition, surface characteristics are tailored for specific functions since there is not one surface that fits all end-uses. In studying the intrinsic behavior of engineered SEs, we asked questions regarding surface stability, environmental conformation and adaptability, and tuning physical features.

We report on the formation of responsive surfaces with tailorable surface-reconstruction kinetics and switching hysteresis by thiol-ene radical addition of mercaptoalkanols with variable lengths to poly(vinylmethylsiloxane) networks. Exposing the modified surfaces to water led to a rearrangement of the hydrophilic alkanes at the surface. The rearrangement kinetics decreases with increasing number of the methylene spacers (n) in the mercaptoalkanol. The response kinetics is found to be very fast for n = 2 and 6. For instance, upon exposing to water, the water contact angle on 3-mercaptopropanol-based surfaces decreases by $\approx 35^{o}$ at the rate of 2^{o}/second. The high flexibility of the siloxane

backbone endows these materials with switching longevity; the materials were able to switch their wettability over 10 cycles with minimum hysteresis. Increasing the number of methylene spacers to n = 11 decreases the surface reorganization dramatically. Formation of semi-crystalline regions in such materials (detected via IR) is responsible for initial "sluggish" kinetics and eventual surface "freezing".

The effects of surface chemistry and topology on cellular adhesion and proliferation have been studied extensively in the past. However, little work exists that aims at probing the effects of surface morphology and elastic modulus on cell behavior. To achieve timely and comprehensive experimental design, there is need for the availability of novel substrata with tunable mechanical properties (or compliance) at the micro and meso-scale level ranging from individual cells to whole tissues. Despite expansive research that has targeted the understanding of cellular response to its host scaffold, the choice of material and extrapolation of findings from one cell/material system to another has proven difficult. Thus establishing general relationships between substrate compliance and cell behavior cannot be considered independent of the material and cell type.

In our work, we have explored creating surfaces from SEs comprising gradients in stiffness (or elastic modulus), by controlling the degree of cross-linking. Network regions consisting of higher cross-linking demonstrate a greater elastic modulus. We present two methods to control the mechanical properties of silicone elastomers. The first technique utilizes interdiffusion of multiple SEs with varied molecular weights that are subsequently cross-linked into a network. The second method involves synthesizing a UV-curable SE. This method controls the degree of cross-linking by regulating the intensity of the UV light via a transparency with tunable transmittance placed on top of the SE film. Our results show

that it is possible to generate compliance gradients through either route, enabling a large range of both gradient patterns and stiffness.

Design & Synthesis of Silicone Elastomer Networks with Tunable Physico-Chemical Characteristics

by

Julie Ann-Crowe Willoughby

A dissertation submitted to the Graduate Faculty of
North Carolina State University
in partial fulfillment of the requirements for the Degree of
Doctor of Philosophy

Chemical and Biomolecular Engineering
Raleigh, North Carolina, USA
2007

Approved by

Jan Genzer Chair of Advisory Committee	Saad Khan
Joseph DeSimone	Orlando Rojas

DEDICATION

Many times, it is tempting to wait to dedicate a work until it is complete. Throughout my tenure at North Carolina State University, where the defense of my thesis work seemed far removed, I sometimes thought about to whom I would dedicate my work. The doctoral pursuit is not easy and it is your loved ones that keep you going. Above all, this work would not have been possible without my faith in God and the strength given to me to believe in myself. Beyond this it is easy to say that the companionship of my young son, Quentin, throughout this journey has made light of failed experiments, tough exams and tiring nights. When I look back over the last five years, I am not the proudest of my doctorate work but of the fine son I am raising in the process. His attendance of thermodynamics, kinetics and polymer classes when he was only five seems likely it will have some positive impact on him—hopefully the gift of loving to learn, that hard work does persevere and that with faith in all that is good, nothing is impossible.

I dedicate this work to all those who believed in me when I didn't—my parents, my brothers and sisters, my sons Luke, Quentin, and Chandler, and most of all my husband, George, who's gift of a positive outlook on life has encouraged me when I needed it most!

BIOGRAPHY

Julie Ann-Crowe Willoughby was born in 1969 in Cincinnati, Ohio. Her parents, Dave and Marion Crowe raised her and her six siblings in Northern Kentucky. They presented her with the gift of learning that was embraced by the faculty of Notre Dame Academy where Sister Mary Ethel, SND encouraged her to pursue whatever science she deemed interesting. It was Sister Ethel's enthusiasm for learning, insistence that chemistry was easy and eternal patience with her young students that inspired Julie to study chemical engineering at the University of Kentucky. The fact that her brother, Dan, also assured her there would be plenty of male counterparts in her engineering versus nursing classes was especially appealing after attending the all-girls high school and made the initial decision easy. By good fortune, Julie landed a student co-operative position with the Dow Corning Corporation her first year in college that enabled her to pay her way through college and gain an appreciation for what it meant to be an engineer. The position that started in 1988 exposed her to the basic silane-manufacturing site in Carrollton, Kentucky and later in research & development at the corporate headquarters in Midland, Michigan. She became a full-time employee with the company in 1992 upon receiving her Bachelor of Science in Chemical Engineering degree and left her Kentucky home for Michigan.

In 1997, she was blessed with her son Keith Quentin Hayes, III. After juggling motherhood and a full-time career, she decided that a stint in academia would give her the flexibility to achieve whatever she desired with her profession. So ten years after graduating from undergrad, she and Quentin moved to warmer weather in 2002 to start fall classes in the

chemical engineering doctorate program at North Carolina State University under the excellent guidance of her advisor, Professor Jan Genzer.

New Year's Day 2007, she was married to George Spicer Willoughby, III. They live in Cary, North Carolina and are blessed with three sons, Luke, Quentin, and Chandler. Upon completing her Doctorate requirements, Julie plans to work for MeadWestvaco in Raleigh, North Carolina.

ACKNOWLEDGMENTS

It is with sincere gratitude that I thank my research advisor, Professor Jan Genzer, for all that he has afforded me over the last five years. His encouragement, high standards for research, constructive feedback on everything from experimental design, presentation skills, to scientific writing have been invaluable to my experience in graduate school. His caring attitude about all his lab members is quite evident as well as his desire to have a good time while at work, making the journey through grad school more enjoyable. He gave me the freedom to pursue my research ideas and the flexibility to get it done in the manner that made a life-work balance possible. I've thought many times how it was my good fortune to land in his group.

I would be remiss in not thanking some other people in the department that made it possible for me to find the strength to continue that first semester in the program. Returning to a rigorous academic course load after ten years was more challenging than I anticipated, combined with the new reality of single motherhood almost made the task impossible. Carol Hall gave me the encouragement and support needed to rearrange my course load in a more manageable fashion, Saad Khan refused to give up on me even after I told him I was through, and Jan Genzer arranged for me to get in the laboratory those first few months where the smell of silanes made me feel oddly at home. George Roberts, as was his nature, provided support and guidance for maneuvering one's way through graduate school. I was also fortunate to get to work with Professor Peter Fedkiw as a teaching assistant in Transport

Phenomena where he gave me ample opportunity to teach and work with the undergraduates. This in addition to General Electric's Faculty for the Future fellowship, under the mentorship of Professor Saad Khan, gave me invaluable experience in teaching and additional financial support for my son and me. I would also like to thank Dr. Khan for serving on my dissertation committee, unlimited use of his laboratory and for all the enjoyable conversation regarding grad school, classes, and life! Josh Manasco, one of Dr. Khan's graduate students, ran DSC samples for me while I was writing my thesis. Josh, your help was invaluable and I'll run GPC samples for you whenever I can!

I want to thank Professor Joe DeSimone for delivering the most enjoyable class I've had while in school. I was always eager to attend his polymers class even though it pointed out everything I didn't know and thought I did while working in industry! His enthusiasm for the subject and concern for his students' understanding of the material makes me very thankful I signed up for this elective. I also would like to thank him for his willingness to discuss research whenever I wanted and for serving on my dissertation committee.

I would like to thank Professor Orlando Rojas for being my non-departmental member of my dissertation committee. His obvious enthusiasm for academic research and collaboration is inspiring. I have several people who helped me with techniques that made part of my research possible. Dr. Simon Lappi has been extremely instrumental in my understanding of FTIR and was always open to me running experiments in his lab offering whatever assistance he could. I thank Dr. Hanna Gracz for her assistance with NMR and last minute help on peak

assignments. I thank Dr. Orlin Velev for the use of his microscope, Dr. Russ Gorga for discussions on dynamic mechanical analysis and unlimited use of his laboratory, and Dr. Laura Clarke for intriguing discussions on dielectric spectroscopy. I appreciate all the help and opinions that our research associate, Dr. Kirill Efimenko, has given to me throughout my years in the department. His research provided the foundation for my dissertation work.

I thank all the support personnel who made graduate school flow much more seamlessly—Saundra Doby, Diane Harper, Sandra Bailey, and Sheila Hayes. Your work keeps this department running and I haven't forgotten the coffee I owe you Diane for your last minute help for my Schoenborn presentation. I promise to get it before I leave.

I am very fortunate for my classmates (a/k/a "babes") my first two years—April, Amy, Dana, and Alison made tough work fun. Our coffee trips and support of each other's work was a true network of friendship! All the discussions regarding research and life with April, Alison, Angelica and Chris usually accompanied by wine made the graduate endeavor one of true higher learning! Angelica and Chris, you were the best roommates—Quentin and I were very lucky to have you with us for two years. Angelica, your knowledge of rheology astounds me and the willingness you have to help us all is truly admirable.

I value and appreciate the work that Kathy Fraley did on our cell proliferation project. Your efficiency and quick grasp of the research is impressive; you'll do great wherever you go. I also thank Michael Weiger for working with us, patiently explaining the functions of cells

and for being the great friend you are over the last five years. I am very grateful we started this journey together and you'll be done before you know it!

I had the good fortune of joining the Genzer research group at the tail-end of his "first" set of students, doctors Tao Wu, Jim Semler, Rajendra Bhatt, Mike Tomlinson, Bin Wei, and Randy Petrie were great fun to work with, provided their expertise whenever asked, and have all moved on as successful scientists! My completion of my dissertation work, introduces the second wave of Genzer students—Dr. Tiffany Bailey, Dr. Insun Park, Jason Stone, Young Jhon, Erich Bain, Evern Ozcam, Omer Gozen, Shafi Arifuzzaman, and SaloTurgman. I think our group dynamics has made the research journey all that much better for the fun and fellowship we share. I wish you all the best in your continued endeavors! Evern, I can't thank you enough for all your enthusiasm and hard work on my project!

In addition to all the great people I met through the department, I have also had several people support me as a parent throughout the years, especially the Berkowitz family. Patricia your willingness to take Quentin whenever I needed those first few years made all the difference. I am thankful for the support network Quentin and I received while he was at Cathedral School. Having him in such a wonderful environment so close to NC State was very reassuring and made my job as a parent and graduate student much easier!

I am sure I forgetting others and if I have, please know that I am truly grateful for whatever support you gave me. Although this acknowledgement is threatening to be longer than my

dissertation, I have to recognize some very special people. To my parents for believing in me, and the encouragement you have given me throughout my life. Even when you weren't sure of what I was doing, you have always been there. Although distance separates us physically, you are always close to my heart! My dear sister Karen, for being there this past year, I am so thankful you moved to Raleigh and part of our everyday life. Donna, Dan, Martin, Christine and Meghan, you've always been there with your encouragement and help as well. I don't know how I got so lucky to have such a wonderful family.

I can't express in words the love and support I have received from my husband George, who has watched and supported my frantic last days in graduate school. To Papa, you are the roots of our family. To Quentin, Luke and Chandler, you have shown me the beauty of life, the inquisitiveness to learn, and to just have a good time. Now that my "thing" is done, the computer can be yours again and I promise not to have the zombie look in my eyes that you said was "thesis, thesis, and thesis". Here's to more fun and us!

Finally, I would like to acknowledge the funding agencies for financially supporting the research presented in this dissertation and to Dow Corning Corporation for introducing me to the wonderful world of silicones.

TABLE OF CONTENTS

PAGE

LIST OF FIGURES ..... **xiv**

LIST OF SCHEMATICS ..... **xxi**

LIST OF TABLES ..... **xxii**

CHAPTER 1: WHY STUDY SILICONE ELASTOMERS? **1**

1.1 Motivation 1

1.2 References 8

CHAPTER 2: MANIPULATING SILOXANE SURFACES **10**

2.1 Introduction 10

2.2 Surface Modification of PDMS 11

2.2.1 Obtaining Hydrophilicity 11

2.2.1 Surface Stability 16

2.3 Conclusion 24

2.4 References 26

CHAPTER 3: RESPONSIVE SILOXANE-BASED POLYMERIC SURFACES **30**

3.1 Introduction 30

3.2 Modes of Polymeric Surface Dynamics 31

3.2.1 Wettability Studies 32

3.2.2 Surface Segregation 33

3.2.3 Surface Reorientation....35
3.2.4 Dynamic Interplay Between Segregation and Reorientation....37
3.3 Switchable Surfaces....39
3.3.1 Polymers on ”Hard“ Surfaces....39
3.3.2 Polymers on “Soft” Surfaces....41
3.4 Rubber Elasticity and the Siloxane Bond....42
3.5 Surface Reconstruction and Reversibility....43
3.6 Rapid Formation of Hydrophilic Surfaces....47
3.7 Conclusion....49
3.8 References....50
Appendix 3.1 Generating PVMS networks—Materials and Methods....53
A3.1 PVMS Synthesis....53
A3.2 PVMS Network Formation....58
A3.3 Surface Reorientation....58
A3.4 References....60
CHAPTER 4: MODIFIED PVMS SURFACES....61
4.1 Introduction....61
4.2 Thiol-ene Addition Reaction on PVMS networks....62
4.3 Tailored Wettability Switching Kinetics and Reconstruction Reversibility....67
4.3.1 Modification of PVMS with Mercaptoalkanols....68
4.4 Determination of Semi-crystallinity....75
4.5 Confirmation of Temperature Transitions....81

4.6 Conclusion 86
4.7 References 88
Appendix 4.1 Materials and Methods 92
A4.1 Modification of PVMS Networks 92
A4.2 Infrared Spectroscopy 93
A4.3 Differential Scanning Calorimetry 94
A4.4 Dynamic Rheology 94
A4.5 Dynamic Mechanical Analysis 94
A4.6 References 95
CHAPTER 5: PDMS-PVMS NETWORKS 96
5.1 Introduction 96
5.2 Making siloxane substrates with modulus gradients via interdiffusion 100
5.3 Wettability of PDMS-PVMS DPX-Y Substrates 107
5.4 Designing substrates for cell migration/proliferation studies 110
5.5 Morphology studies 116
5.6 Conclusion 120
5.7 References 123
Appendix 5.1 Materials and Methods 125
A5.1 Preparation of DPX-Y PDMS-PVMS networks 125
A5.2 Preparation of diffusion gradients 125
A5.3 Wettability measurements 125
A5.4 Dynamic Rheology and Dynamic Mechanical Analysis 126

A5.5 Dynamic Cell proliferation protocol 126

A5.6 Cell suspension and counting 126

CHAPTER 6: UV-CURABLE NETWORKS 128

6.1 Introduction 128

6.2 UV-Curable Siloxanes 131

6.3 Synthesis of 3-mercaptopropylmethyl-terminated PVMS 132

6.4 Formation of UV-curable PVMS networks 139

6.5 Conclusion 148

6.6 References 149

Appendix 6.1 Materials and Methods 151

A6.1 Synthesis of PVMS-SH 151

A6.2 Network Formation 151

A6.3 Nanoindentation 151

A6.4 NMR Spectroscopy 153

A6.5 References 156

CHAPTER 7: SUMMARY AND OUTLOOK 157

7.1 Summary 157

7.2 Recommendations for Future Work 160

7.2.1 Surface modification of PVMS via UV-activation 164

7.2.3 Additional mechanical analysis 166

7.2.3 Surface Segregation of PDMS-PVMS 166

7.3 References 168

LIST OF FIGURES

PAGE

Figure 1.1: Annual and projected growth of the United States silicone demand.....3

Figure 1.2: Supply and demand for silicones by category (top) and application (bottom).....5

Figure 2.1: The siloxane backbone has a high degree of flexibility unparallel in organic polymers due to its large Si-O-Si bond angle and length 10

Figure 2.2: Dependence of a) the advancing contact angles of deionized water ($\theta_{adv,DIW}$), b) the contact angle hysteresis of deionized water ($\theta_{adv,DIW}$- $\theta_{rec,DIW}$), and c) the surface energy on the UVO treatment time for Sylgard-184 exposed to UVO60 (squares), UVO90 (circles), and UV90 (up-triangles). In part a) each point represents an average over 5 measurements on various areas of the same sample (the error associated with these measurements is smaller than r1.5 °). The lines are guides to the eye.....15

Figure 2.3: Etched PDMS surface containing micro-, submicro-, and nano-composite structures shows a self-cleaning effect with water CA as high as 162° and SA lower than 5°. 17

Figure 2.4: A) Schematic illustrating the mechanism of increased packing density of a self- assembled monolayer after mechanically stretching the substrate. B) Representation showing the higher water contact angle for MAMs on PDMS versus SAMs on PDMS. 20

Figure 2.5: Water contact angles for mechanically-assembled monolayers made of semifluorinated alkanes on siloxane elastomers. 21

Figure 2.6: Advancing (z) and receding ({) contact angles of DI water, θ_{DIW}, on H8-MAMs prepared by vapor deposition of OTS as a function of the stretching of the PDMS substrate, Δx. The dashed line denotes the value of θ_{DIW} for a crystalline array of $-CH_3$ groups.....22

Figure 2.7: Water stability data for H8-MAM, H16-MAM, F8H2-MAM, structures, all stretched to ε_x=70 %. Also included are data for F8H2-SAM.....24

Figure 3.1: Comparison of (v, ", x , z) experimental and (‘, |, ¨, ’, •) calculated surface tensions for D, Z-terminated PDMS: (v, ‘) carboxypropyl-terminated, (", |) aminopropyl-terminated, (x , ¨) hydroxypropyl-terminated, and (z , ’) methyl-terminated. 32

Figure 3.2: (Left) Dependence of advancing contact angle of water on heating time against vacuum at 100°C for low energy (top left) and high-energy (bottom left) groups. (Right) Dependence on contacting media for various reconstructive behaviors. 36

Figure 3.3: Contact angle of water (pH 1) on samples of PE-COOH after treatment in hot distilled water (pH 6-7, 100°C, 30 s) as a function of the contact angle prior to heating in water. Prior to the treatment in water, samples were partially reconstructed by heating under vacuum at 78 or 100°C or by heating in perfluorodecalin (100°C), to attain the various values of T. 38

Figure 3.4: (a) Chemical oxidation of poly(4-methyl styrene) with cobalt (II) acetate. (b) Schematic representation of the surface reconstruction of a chemically modified glassy polymer below and above its bulk glass-transition temperature. 40

Figure 3.5: Contact angles of water (pH=1) for two separate samples of PBD-ox cycled repeatedly against deionized water at 80 and at 43 °C. The error bars one standard deviation above and below the mean of the contact angle measurements. 42

Figure 3.6: Illustration of the differences in surface rearrangement between PDMS and PVMS elastomers. The vinyl moiety has a higher affinity for water relative to the methyl group. 44

Figure 3.7: Time dependence of water contact angle measured on model PDMS networks („), Sylgard-184 networks (..), and bare PVMS networks (z). The error bars represent an average over 3 measurements performed on three different areas of the same sample.....45

Figure 3.8: Change of the contact angle with increasing time for model PDMS networks (a, „), Sylgard-184 networks (b, ..), and bare PVMS networks (c, z). 46

Figure 3.9: Images of water droplet spreading on PVMS-UVO surfaces treated for various UVO times (ordinate) collected at various time intervals after depositing the droplet (abscissa). The numbers indicate the water contact angle that was evaluated from the images of the water droplets.....48

Figure A3.1: Differential refractive index (dn/dc) values for PVMS in to HPLC-grade toluene. 55

Figure A3.2: GPC traces for the 90° light scattering detector for a typical run of PVMS during the step-condensation process of vinyl methyl silanols. Molecular weight for each trace is listed in Table 3.1. Average polydispersity index is 3.0.....57

Figure 4.1: ATR-FTIR spectra of bare PVMS (solid line) and PVMS after thiol-ene addition of 1-dodecanethiol, PVMS-S-$(CH_2)_{11}CH_3$ (dashed line). The PVMS network was prepared by cross-linking PVMS chains (MW = 39 kDa) with a 70% excess of TEOS cross-linker. Vinyl peaks at 960, 1407, and 1587 cm^{-1} in the thiol-ene modified sample are not present. The inset shows photographs of water droplets on PVMS and PVMS-S-$(CH_2)_{11}CH_3$ samples. 63

Figure 4.2: Illustration of the reversible nature of a dual-energy siloxane substrate. When the –COOH functionalized surface is exposed to water, the –COOH reorient to the surface to maximize their contact with water. Removal from the aqueous environment returns the substrate to the original state.. 64

Figure 4.3: Time-dependent water contact data for PVMS substrates (Molecular weight is 39 kDa, *R*=1.7 moles of cross-linker/moles of polymer): bare PVMS („), 1-dodecanethiol-modified PVMS (PVMS-S-$(CH_2)_{11}CH_3$, S), and 3-mercaptopropionic acid modified PVMS (PVMS-S-$(CH_2)_2$COOH, ¡). Average error in contact angle measurement is ±1.5 degrees.. 65

Figure 4.4: Ability of PVMS-S-$(CH_2)_2$COOH to reverse its wettability behavior.....67

Figure 4.5: Time dependence of the deionized water wettabilities for PVMS-C_n-OH surfaces. The error for $_{DIW}$ is r1.5û.....69

Figure 4.6: Illustration of dynamic contact angle method. The surface reconstruction occurs during stage 3 where the wetting force can be isolated due to negligible volume changes and zeroing the balance to eliminate the gravitational force from the measurement. 71

Figure 4.7: Time dependence of the deionized water wettabilities for PVMS-C_n-OH surfaces. The error for $_{DIW}$ is r1.5û.....73

Figure 4.8: Contact angle hysteresis (' T= $T_{advancing}$- $T_{receding}$) for each DCA cycle of the following substrates: PVMS (J), PVMS-S-$(CH_2)_2$OH (F), PVMS-S-$(CH_2)_6$OH({), and PVMS-S-$(CH_2)_{11}$OH (S). 74

Figure 4.9: Photographs of mercaptoalkanol-modified PVMS substrates in front of an opaque background; MPVMS NPVMS-S-C_6OH and OPVMS-S-C11OH. The opaqueness of Ois indicative of crystallites. 76

Figure 4.10: A sample of PVMS-S-$(CH2)_{10}$OH observed with optical microscopy (at 5X and in reflectance mode).....77

Figure 4.11: Dynamic rheology on PVMS and mercaptoalkanol-modified PVMS substrates. Runs performed at sequential operational temperatures (T): a) T = 23ûC, b) T = 50ûC, and c) T=23ûC. Average standard deviation is ± 33 kPa. 78

Figure 4.12: ATR-FTIR data within the methylene stretching region for PVMS and the mercaptoalkanol-modified samples. The resultant chromatogram for each specimen was deconvoluted with multi-peak Guassian fits using OriginLab. The higher wavenumber peak is the characteristic asymmetric methylene stretching vibrations and the lower wavenumber is the characteristic symmetric methylene stretching vibrations. As crystallinity increases, the frequency vibrations shift to lower wavenumbers. 79

Figure 4.13: ATR-FTIR data recorded between 23-55^{o}C for PVMS-S-$(CH2)_{11}$OH. As the temperature increases the material transitions through a melting region and loses some crystallinity. This is reflected in an upward frequency shift for the characteristic asymmetric and symmetric methylene stretching vibrations with increasing temperature (see inset).....81

Figure 4.14: Differential scanning calorimetry for PDMS, PVMS and PVMS modified substrates. Heating rate was 3^{o}C/minute, see text for details. 83

Figure 4.15: Dynamic mechanical analysis for PVMS and PVMS-mercaptanol modified substrates. Temperature ramps were performed at a heating rate of 3^{o}/minute and at 1 Hz. Amplitude was set within the linear viscoelastic regime. Main graph is the measured storage modulus (E'-closed symbols) and loss modulus (E"-open symbols). Inset graph is tan delta (E'/E"). 85

Figure 5.1:VSMC spreading increases and F-actin becomes well defined with increasing PAAM stiffness. The arrow shows the direction of increasing elastic modulus. A) Phase contrast image of VSMCs on the gradient gel modified with type 1 collagen; the scale bar is 500 microns. Individual panels (B-E) show representative fluorescent images of F-actin stained with rhodamine-phalloidin. B is from the softer region of the gel (i.e., the leftmost 0.7 mm portion of the gel). (C,D) are from the intermediate regions (i.e. the middle 1.4 mm portion of the gel), and (E) is from the stiffer region of the gel). The scale bar is 50 micron. 97

Figure 5.2: Interdiffusion formulations for the PDMS-PVMS blend. Degree of polymerization for PDMS was 11, 15, or 78. The nomenclature for formulations is DPX-Y where X represents the degree of polymerization for the PDMS-hydride terminated fluid and Y is the number of vinyls targeted for cross-linking.. 102

Figure 5.3: Interdiffusion of three formulations of PVMS_PDMS networks. Storage modulus was measured on an ARES 2000 rheometer at 1 radians/second within the linear viscoelastic regime. The first set of data (∨) was collected after a 3-day cure time in a 70°C oven and the second set was collected after an additional 5-day room temperature cure time ('). The samples were taken from the same cured substrate. 103

Figure 5.4: Dynamic mechanical analysis data for DP 11-250 (A) and DP11-75 (B) performed at 1 Hz. Storage modulus („) and loss modulus (†) plotted as a function of temperature. 106

Figure 5.5: Static contact angle (A) and wettability rate changes (B) for PVMS_PDMS DPX-Y networks DP11-250 („), DP11-75 (x), PVMS ('), and Sylgard 184 ( ). 108

Figure 5.6: The contact angle hysteresis (' T= $T_{advancing}$ - $T_{receding}$) via DCA as a function of cycle number for PVMS (') and DP11-250 („). Each cycle consisted of immersing the substrate, holding at constant volume for 8.5 minutes and withdrawing the substrate. Substrates were quickly blow-dried with nitrogen between cycles. 109

Figure 5.7: NIH 3T3 fibroblast cell counts cultured in DMEM media with 0.1% FBS and 1% PS/G at 37°C. Cells were suspended with trypsin, diluted in PBS, and injected into a hemocytometer for manual counting. 112

Figure 5.8: NIH3T3 mouse fibroblast growth on A) DP11-75, B) DP11-250 and C) polystyrene substrates. Magnification is at 20X (bar = 5 microns). Photos taken 48 hours after initial seeding. 114

Figure 5.9: Images of substrates A) DP11-75 and B) DP11-250 after exposure to a 20 Pg/ml FITC-labeled fibronectin solution. After the substrates were rinsed several times with PBS, the samples were imaged with a 20X (bar = 5 microns) lens transmittance mode optical microscope. 115

Figure 5.10: DP11-75 (A) and DP11-250 (B) phase separation images from phase contrast optical microscopy using a 10X lens in reflectance mode (bar = 200 Pm). 116

Figure 5.11: Phase separation images from phase contrast optical microscopy using a 10X lens in reflectance mode. Images for DP11-45 (A-C) and DP11-160 (D-F) were taken after A,C) initial cure (t = 0), B,D) after 4 weeks, and C,F) then after exposure to water. 118

Figure 5.12: Elastic modulus as a function of frequency for Sylgard 184 (') and the high and low modulus (DP11-250 („) and DP11-75("), respectively) substrates used in the 2nd cell proliferation study. 119

Figure 5.13 A) Cell proliferation results for the 2nd round of substrates evaluated with NIH 3T3 fibroblast cell cutured in DMEM media with 0.1% FBS and 1% PS/G at 37°C. Cells were suspended with trypsin, diluted in PBS, and counter via a BD coulter counter. B) Same samples and cell counting procedure as in (A) except the substrates were pretreated with deionized water to force the phase separation to equilibrium in an aqueous environment. 122

Figure 6.1: "Methods for generating elastic substrata with gradients in mechanical properties. (A) Acrylamide is photopolymerized under transparency masks with varying degrees of opacity. The radial gradient pattern boxed on the left can be used to create a substrate shown on the right with the 'map' of its mechanical properties (Young's modulus). (B) Acrylamide is photopolymerized using a combination of microfluidics and photopolymerization. The gradient generator is used to create a gradient in the crosslinker (bis-acrylamide). The width of the gel is 3 mm, and the gradient in the Young's modulus (as determined from atomic force microscopy) is approximately 12 Pa/μm. In (A), the lighter the shading, the higher the compliance. In (B), the lighter the shading, the lower the compliance." 129

Figure 6.2: FTIR spectra for PVMS (Dow Corning PJ Fluid®) (A) and after the end-capping reaction with mercaptopropylmethyldiethoxy silane (B). Peak (1) is the –OH stretching and peak (2) is the Si-O stretching from the terminus groups of PVMS (Si-OH). Note that these peaks are absent in the lower spectrum. 134

Figure 6.3: ^{1}H NMR for PVMS (A) and PVMS-SH (B). ^{13}C NMR for PVMS (C) and PVMS-SH (D). See text for explanation of chemical shifts. 136

Figure 6.4: GPC traces for PVMS (A) precursor (n=300) and the resultant PVMS-SH terminated fluid (B). Peak 1 is the liner siloxane fluid, Peak 2 is likely low molecular weight.....137

Figure 6.5: Molecular weight distribution for mercapto-endcapped PVMS with the starting PVMS fluid possessing a Mw of 28 kDa (A) versus 1.5 kDa (B). 138

Figure 6.6: Dynamic rheology frequency sweep data for a network of 65/35 PVMS-SH/PVMS. UV cured at 365 nm for 7 (..), 17 ( ), and 27(c) minutes. Scan performed at 30°C and at low strain (0.1%) determined to be within the LVE region. The inset shows the range of G' versus cure time. 142

Figure 6.6: Dynamic Mechanical Analysis for PVMS cured via an alkoxy mechanism (A) and 100% PVMS-SH UV-crosslinked material (B). UV cure performed at 365 nm for 7 minutes. Storage modulus E'(closed symbols J , S), loss modulus E" (open symbols F , U) and tan delta (z, {) as a function of temperature (Frequency = 1 Hz and set amplitude of 30 micron for LVE region).. 144

Figure 6.8: Illustration of gradient/pattern formation of UV-curable PVMS-SH fluid.. 146

Figure 6.9: Nanoindentation of PVMS-SH cured networks. Material was cured beneath a patterned mask for a specified amount of time. The boxed region in the lower mask is the area tested with nanoindentation. Gradients in modulus were successfully produced with this technique.....147

Figure 7.1: ATR-FTIR spectra for A) untreated side of PVMS and B) treated with Z-mercaptohexanyl bromoisobutryrate. 161

Figure 7.2: A) ATR-FTIR spectra of a PVMS surface modified with L-cysteine. The presence of a broad carbonyl peak –COOH is indicative of the cysteine molecule and B) optical microscopy illustrates a dramatically different surface morphology than standard.....163

LIST OF SCHEMATICS

PAGE

Scheme A3.1: Synthesis routes for poly(vinylmethylsiloxane). Method (A) is step-condensation polymerization and Method (B) is kinetically controlled anionic ring opening polymerization. 54

Scheme 5.1: Schematic of PVMS_PDMS crosslinking mechanism. The amount of hydride-terminated PDMS determines the degree of crosslinking 100

Scheme 6.1: Schematic for making mercapto-terminated poly(vinylmethylsiloxane). Reaction is done in reflux mode at 60°C for 5 hours. 132

Scheme 6.2: Steps to making a UV-cured PVMS network. The UV exposure duration dictates the degree of crosslinking.....139

Scheme 6.3: General thiol-ene photopolymerization process.. 140

Scheme 6.4: Rearrangement to -Si-S- due to thermal instability of the Si-C-C-S bond. Scheme redrawn from reference 6.13. 141

LIST OF TABLES

PAGE

Table A3.1 Properties of PVMS polymers whose trace scans are show in Figure A3.2.....56

Table 4.1: Summary of temperature transitions for PDMS, PVMS and PVMS-modified substrates via DSC and DMA measurements. T_D is assumed to be the glass transition temperature. T_D is assumed to be a melting transition. See text for the description of T_E.....86

Table 5.1 : Elastic moduli of various soft human tissues.....98

Table A6.1: NMR instrument parameters for 1H, 13C, and 29Si.. 154

CHAPTER 1: Why study silicone elastomers?

1.1 Motivation

Engineering functional surfaces is necessary to produce efficacious characteristics that positively influence its performance in specific applications. Surfaces are tailored for specific function such as biocompatibility; biocompatible devices are implanted and interact with cellular components in a manner dependent on the surface chemistry, topology, and morphology of the implant. Studying the intrinsic behavior of engineered surfaces typically involves understanding surface stability and surface dynamics. The scope of this Ph.D. thesis entails controlling the surface behavior of silicone elastomers. Silicones are both advantageous and challenging to use in surface design. These traits evolve from silicones' uniqueness of its fundamental polymer characteristics.

Silicones, the generic terminology for siloxanes, are hybrid materials comprising an inorganic Si-O backbone with pendant organic groups. The most widely-used silicone is poly(dimethylsiloxane) (PDMS), which has two pendant groups made of methyl. PDMS is employed in numerous applications that often have contrasting end-use such as anti-foaming applications or, on the opposite spectrum, foam-stabilizing additives. The ability to perform well in these opposing applications makes it easy to understand why PDMS has remained a material of choice in studying surface activity driving forces[1,2]. The physical polymeric behavior is dictated by the fundamental properties of intermolecular forces between pendant groups, the size of pendant groups, and chain flexibility. Chemical consequences are derived from a polymer's bond energy and polarity attributes. For example, PDMS can be used in high temperature applications due to the higher Si-O bond energy of about 100 kJ/mole more

than the C-C or C-O bond energy[1]. In contrast, fluorocarbons would be preferred over silicones in highly alkaline conditions. This is due to the polarity of the Si-O bond, which makes it susceptible to hydrolysis by water due to electrophilic or nucleophilic attack at the extremes of pH.

The unique surface properties of PDMS arise from the material's deviation in surface energy behavior. The simple pattern of a reduction in surface energy equating to an increase in hydrophobicity and a reduction in interfacial energy against water is not the rule for PDMS[3]. Instead, the high backbone flexibility, imparted from the asymmetric bond angles of Si-O-Si and O-Si-O and the longer bond lengths for Si-O compared to C-C, allows for various chain orientations depending on the type of the interface. For instance, due to attractive/repulsive interactions, the methyl substituents along the Si-O-Si backbone will orient to the surface at an air-interface yet bury themselves beneath the polymer surface at a water-interface to adopt their lowest surface energy configuration. This is not the case in a hydrocarbon system, where the methyl groups are present at fixed bond angles with steric restrictions[1-3]. The backbone flexibility is also reflected in the difference of rotational potential energy in the siloxane bond (3 kJ/mol) versus a hydrocarbon bond, such as polyethylene (14 kJ/mol) [4]. This imparts almost zero restriction to the barriers of rotations for PDMS and affords its stature as the polymer with one of the lowest known glass transition temperatures.

These unique material properties have afforded the silicone industry an economic advantage in that it is a material, which finds it way into applications ranging from lipstick to electrical device encapsulants. Today, the silicone/siloxane market is valued at $9.3 billion dollars [5-7]. Figure 1.1 shows the growth of the silicone industry since 1998 and its projected

annual growth of 5% per year through 2012. This overall dollar amount equates to about 1.1 million metric tons for 2005. Figure 1.2 depicts the breakdown of the silicone finished goods categories - elastomers, fluids and resins. These finished goods account for about 80% of the total silicone demand. Although comparing with its hydrocarbon counterparts can be difficult due to different applications and markets, one category, the total synthetic and natural rubber elastomer market, is about 15 million metric tons per year[8,9]. While the silicone elastomers constitutes just a fraction of this market, their growth in the high-value electronics and medical fields promises high growth for the next 5 years[5,10,11].

From Figure 1.2 it is apparent that both silicone fluids and silicone elastomers enjoy

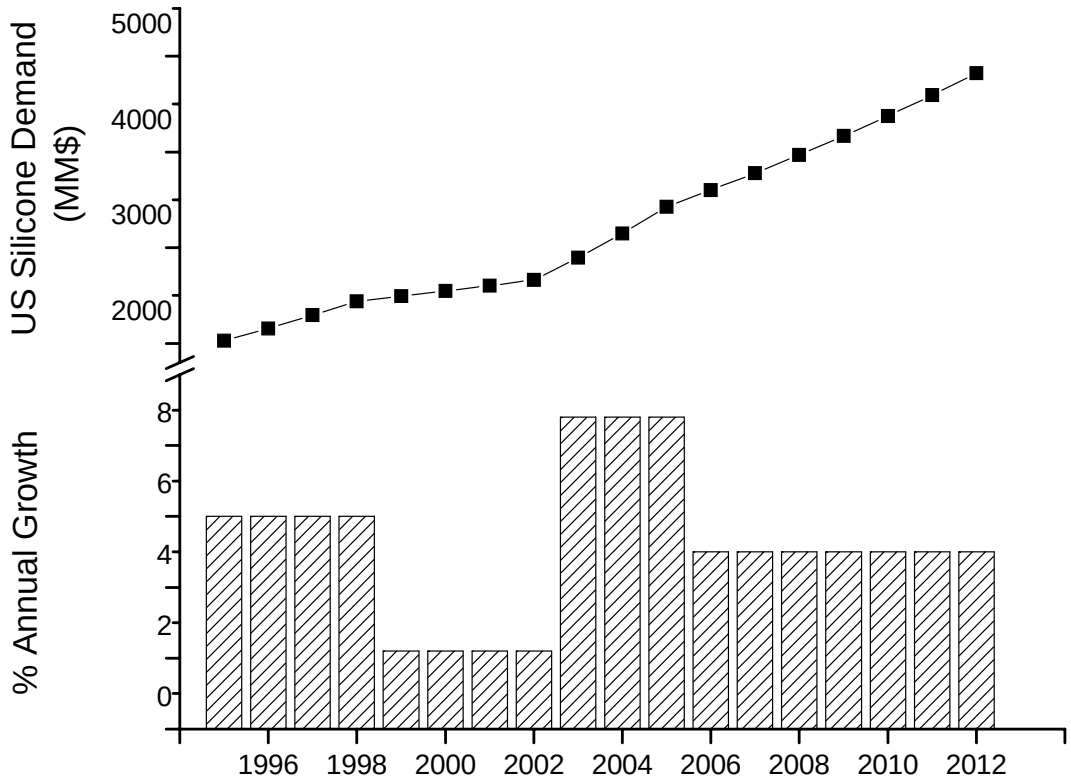

Figure 1.1: Annual and projected growth of the United States silicone demand. Plotted from values found in references 5.7-9.

almost equal consumption by industry and consumers. While elastomers may be as common as the $3 tube of bathroom caulk, we were intrigued by the possibilities of modifying and studying their surface properties. Our interest in silicone elastomers stems from their uniqueness as dual solid/liquid materials. Once PDMS is cross-linked, it is a solid at room temperature, yet its liquid-like nature between cross-link junctions would remain intact. Upon further surface modification, we postulated that we would be able to design surfaces with a particular function and probe their response in various environments. This brings us back to understanding the fundamental surface properties of PDMS elastomers.

Previous work on PDMS elastomers from our group is described in Chapter 2 of this Ph.D. Thesis. The flexibility of the siloxane backbone makes surface reorientation inevitable with a surface modification of differing surface energy than the Si-O backbone. Genzer and Efimenko circumvented this trait by imparting a stable low-energy surface by limiting the surface mobility of PDMS through a clever mechanical design[12]. This work was the basis for transitioning from stable surfaces to responsive surfaces. Generating a material platform that could be tuned to either resisting reconstruction or rapidly responding to the environment seems challenging with a molecule that is intrinsically flexible and free to reorient to its preferred configuration. It was first necessary to understand the kinetic of the restructuring of the backbone and pendant groups in relation to the environment. In order to accomplish this, we needed a substrate and a method that could clearly delineate between configuration states.

Chapter 3 of this Ph.D. Thesis addresses the responsive nature of the silicone backbone with the introduction of a new substituent for the silicon atom. Dual-energy substituents allow for probing wettability differences with simple contact angle measurements. This

necessitated the synthesis of siloxane homopolymer with these attributes that could also be cross-linked into a solid network. Hydroxy-terminated poly(vinylmethylsiloxane) (PVMS) afforded this capability and the restructuring kinetics between differing surface-energy states was characterized with changes in the water contact angle over time. This paved the way to the generation of responsive silicone surfaces and we defined a goal of insuring a rapidly reconstructive surface with a measurable surface energy state that was both large in magnitude and capable of continued oscillation.

We determined that we could design responsive materials by functionalizing the PVMS

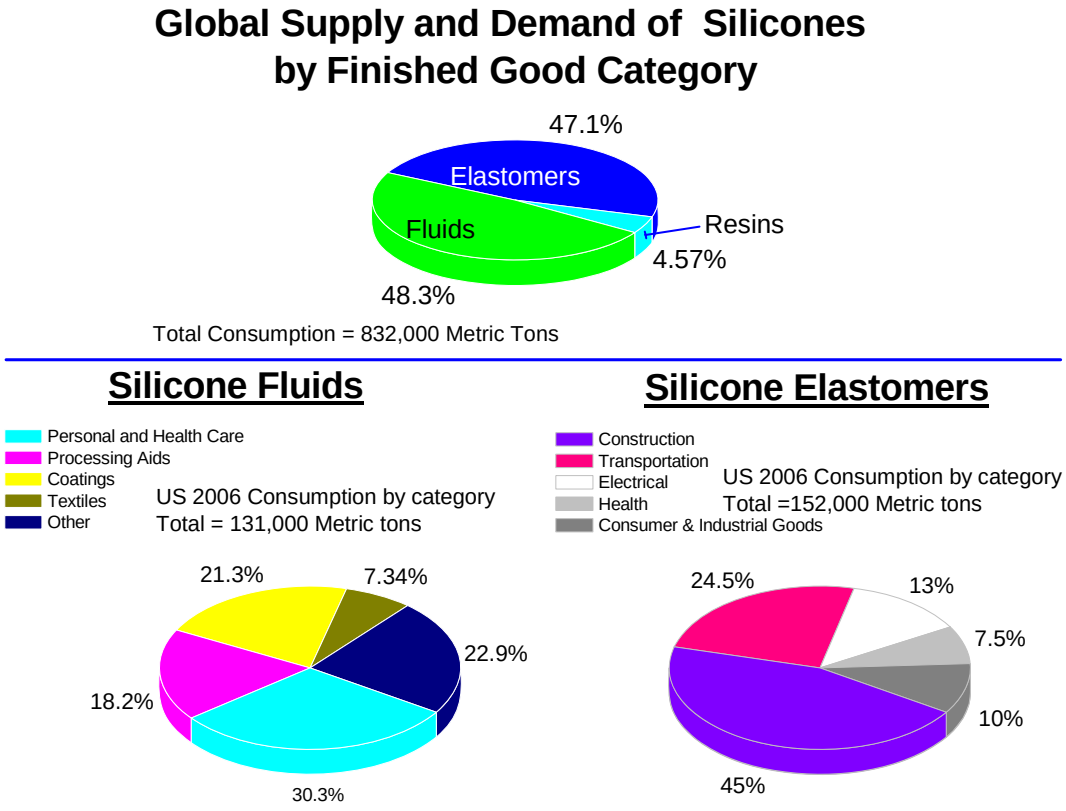

Figure 1.2: Supply and demand for silicones by category (top) and application (bottom). Plotted from values found in references 5,7-9.

surface enabled by the reactivity of the vinyl bond. Tuning the wettability, surface reconstruction, and minimizing the hysteresis between states, was enabled by imparting the surface with either liquid-like or solid-like characteristics. Chapter 4 discusses the thiol-ene modifications to PVMS networks and the investigation of induced crystallinity as a function of the methylene spacer group on the contrasting substituent from the methyl group.

Aside from the intriguing surface behavior of siloxane networks, we anticipate a continued surge in technological advances for the application of silicones in such fields as tissue engineering. The 15-year ban on silicone breast implants imposed by the FDA in 1992 has been reversed as science prevailed with the most comprehensive biocompatible studies of their continued safety and efficacy after human implantation[13,14]. This creates a constructive platform for scientists who continue to study silicones use for biological advances in aid of improving quality of life. Due to silicone's excellent material properties imparting chemical and thermal stability, low surface tension, hydrophobicity, and gas permeability in medical application requiring such characteristics, they can enjoy, without media skeptics, their status as one of the most thoroughly tested and important biomaterial[15]. The advances in tissue engineering continue to challenge and probe our understanding of material properties at the cellular level. Our role as material scientists is to design materials that can probe cell-surface interactions due to such changes as surface chemistry, topology, and morphology. We conclude this thesis work by providing materials with cross-linking mechanisms that are capable of generating silicone substrates with gradients in modulus on the micro-scale as described in Chapters 5 and 6. As PDMS imparts the intrinsic inertness that is desired and fine-tuned in a plethora of applications, our continued use of PVMS provides a material platform capable of subsequent modification as outlined in our work on responsive surfaces.

Our work on manipulating and designing siloxane surfaces is by no means comprehensive; there is always room for continued understanding, validation, and application. The fact that we have successfully demonstrated the potential for siloxane elastomers to be applied in continued scientific advances opens the door for continued research and collaboration across disciplines with a material that continues to prove its benefits with its "peculiar" behavior[16].

1.2 References

1. Owen, M. J. in *Siloxane Polymers* (ed. Clarson, S.) (PTR Prentice Hall, Englewood Cliffs, New Jersey, 1993).

2. Owen, M. J. in *Silicon-Containing Polymers* (ed. Chojnowski, J.) (Kluwer Academic Publishers, Dordrecht, 2000).

3. Owen, M. J. The Surface Activity of Silicones: A Short Review. *Ind. Eng. Chem. Prod. Res. Dev.* **19**, 97-103 (1980).

4. Colas, A. & Cutis, J. in *Biomaterials Science: An introduction to Materials in Medicine* (ed. Buddy Ratner, A. H., Fredrick Schoen, and Jack Lemons) (Elsevier, Inc., 1996).

5. Chang, J. Silicones poised for rapid growth. *Chemical Market Reporter* **269**, 25 (2006).

6. SILICONES. *Adhesives & Sealants Industry* **12**, 15 (2005).

7. Will, R., Lochner, U. & Yoneyama, M. in *Chemical Economics Handbook* (SRI Consulting, 2007).

8. Chang, R. J. & Yoneyama, M. in *Chemical Economics Handbook* (SRI Consulting, 2007).

9. Chang, R. J. in *Chemical Economics Handbook* (SRI Consulting, 2005).

10. Lerner, I. Silicone spans the globe. (Cover story). *Chemical Market Reporter* **269**, 22-23 (2006).

11. Kanar, N. M. Silicone PSAs. *Adhesives & Sealants Industry* **13**, 48-54 (2006).

12. Genzer, J. & Efimenko, K. Creating long-lived superhydrophobic polymer surfaces through mechanically assembled monolayers. *Science* **290**, 2130-2133 (2000).

13. Brandon, H. J., Jerina, K. L., Wolf, C. J. & Young, V. L. Biodurability of retreived silicone gel breast implants. *Plast. Reconstr. Surg.* **111**, 2295 (2003).

14. Brandon, H. J., Jerina, K. L., Wolf, C. J. & Young, V. L. In vivo aging characteristics of silicone gel breast implants compared to lot-matched controls. *Plast. Reconstr. Surg.* **109**, 1927 (2002).

15. Colas, A. & Cutis, J. in *Biomaterials Science: An introduction to Materials in Medicine* (ed. Buddy Ratner, A. H., Fredrick Schoen, and Jack Lemons) (Elsevier, Inc., 1996).

16. Owen, M. J. Why silicones behave funny. *Chemtech* **11**, 288-292 (1981).

CHAPTER 2: Manipulating Siloxane Surfaces

2.1 Introduction

Commercial interest in siloxane elastomers has lasted for over 50 years. The most-widely-used material in this category involves poly(dimethylsiloxane) (PDMS) (R = -CH_3 in Figure 2.1). The high flexibility of the Si-O bond, the greater Si-O-Si bond angle and length relative to the C-C-C bond, and low energy barriers to rotation, contribute to a very low glass transition temperature (T_g) for PDMS (≈150 K)[1]. As a consequence, this low T_g value gives rise to high chain flexibility even at room temperature. In addition, the presence of two stable methyl groups on the silicon atom endows PDMS with chemical and physical resistance. These two characteristics make siloxanes a popular choice for thermal and/or electrical insulators and as barrier sealants or coatings.

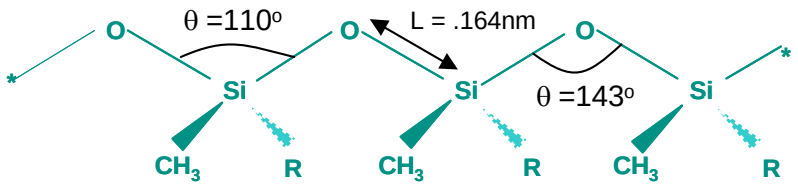

Figure 2.1: The siloxane backbone has a high degree of flexibility unparallel in organic polymers due to its large Si-O-Si bond angle and length.

We have been able to harvest the underlying properties of the extreme flexibility of siloxane elastomers for growth in understanding and manipulating surface design. In order to command a desired response from a surface, altering its chemical make-up is necessary. The inherent inertness of PDMS, however, makes this task challenging. Surface modifications

involving: 1) physical treatments, such as plasma/corona irradiation and ultraviolet (UV) and UV/ozone exposure, 2) chemical oxidation, or 3) a combination of both physical and chemical treatments have been utilized in the past to render the original PDMS either more hydrophobic or hydrophilic[2-7]. One challenge associated with chemical oxidation of siloxane polymers is that the required high basic or acidic conditions promote backbone chain scission and/or degradation. Yet another challenge is the surface stability of a converted hydrophilic PDMS substrate due to the so-called "hydrophobic-recovery". This Chapter discusses the methods of conversion for both hydrophilic and hydrophobic silicone elastomers and our subsequent routes for modifying their surfaces.

2.2 Surface Modification of PDMS

2.2.1 Obtaining Hydrophilicity

There are many instances, where the low surface energy PDMS surface is not always desired. For instance, in blood-contacting devices and adhesive coatings it is paramount to alter the PDMS surface properties as its hydrophobicity results in non-specific protein adsorption[8-10]. Non-specific protein adsorption in biomaterials results in numerous adverse reactions, including coagulation, complement activation, platelet adhesion and activation, and immunological reactions[11,12]. Modification of surfaces has become prevalent for such applications where transformation from hydrophobic (*e.g.*, methyl) to hydrophilic (*e.g.*, hydroxyl-, carboxy- or other hydrophilic group) enables the use of coupling techniques with organic modifiers of varying functionality. In applications where minimal surface reconstruction is required, decreasing polymer bulk and surface mobility is also necessary. One way to achieve this goal is to use a polymer with a glass transition temperature much

higher than its application temperature. This was elegantly demonstrated by Rouse et al.'s work on "frustrated" glassy surfaces, where they manipulated the polymer interface composition by controlling the system temperature[13]. After oxidizing the surface of a model glassy polymer, poly(4-methylstyrene), to obtain hydroxy- and carboxy- surface groups, Rouse and coworkers observed that this surface was "locked" and remained hydrophilic when exposed to air below its bulk T_g. However, for temperatures above T_g, the surface was no longer "frozen" as the chains were allowed to resume their preferred random state. For polymers such as PDMS, where the T_g is much lower than most (if not all) of its applications, hydrophilic stability is difficult to achieve without some change in crystallinity or surface orientation order.

Traditional transformation of the hydrophobic PDMS to a stable hydrophilic state has been achieved via techniques involving physical treatment, such as corona and plasma modification[14,15]. Conventional plasma treatments involve exposing the substrate to a glow discharge between two electrodes or from a radio or microwave frequency generator at low pressures in various gases[14]. X-ray photoelectron spectroscopy (XPS) analysis on oxygen plasma-treated samples confirmed a rapid substitution of carbon atoms by oxygen atoms, which led to the formation of hydrophilic surfaces[16]. This treatment will propagate several hundred nanometers below the surface with irreversible chemical changes at the near-surface region [16-19]. Concurrently, a PDMS surface "skin" is transformed into a thin and brittle silica-like layer. The creation of a silica-like layer leads to crack formation (typically immediately after removing the sample from the plasma treatment apparatus and cooling them down to ambient temperature), causing changes in the PDMS mechanical properties.

The cracks also facilitate the diffusion of uncross-linked PDMS species, typically low molecular weight, to migrate to the surface thereby altering the initial hydrophilic state. While not thoroughly discussed in this chapter, it is recognized that the outcome of corona treatments are very similar to plasma-treated surfaces.

A detailed stability study on plasma-treated silicon rubber was performed by Williams and co-workers[20]. The low-powered plasma treatment occurred in the presence of argon, oxygen, nitrogen, or ammonia gases. A battery of analytical techniques confirmed that the modified surfaces were hydrophilic. For O_2- and Ar-treated samples, there was an increase in wettability, as determined by contact angle, formation of a brittle silica-like layer, and a recovery to a hydrophobic state ("hydrophobic recovery") after aging for 1 month in air. When aged in phosphate-buffered saline (PBS) the hydrophobic recovery of O_2- and Ar-treated samples was reduced. Compared to their O_2- and Ar-modified counterparts, the N_2- and NH_3-treated samples exhibited minimal roughness, as elucidated from atomic force microscopy (AFM), an increase in hydrophilic properties (increase in nitrogen species content), and a similar hydrophobic recovery. Interestingly, there was a difference seen in their biocompatibility despite their hydrophobic recovery patterns. This behavior may be attributed to the degree of roughness and functionality of the samples. Compared to bare PDMS, the O_2- and Ar-treated samples exhibited decreased haemocompatibility (*i.e.*, the time it takes for a foreign blood-contacting device to induce thrombosis)[20]. In contrast, the N_2- and NH_3-modified samples achieved longer blood-contacting times without platelet activation and coagulation than untreated PDMS[20]. This illustrates that surface modification is a multi-faceted design problem involving chemical composition, topography, and

morphology considerations for a given application. Since control of the modification process is difficult with plasma or corona technology, there is a need for other techniques.

In our work, we utilize ultraviolet/ozone treatment (UVO) in order to render PDMS hydrophilic. The UVO method involves a photo-sensitized oxidation process, in which the molecules of the treated material are excited and/or dissociated by the absorption of short-wavelength ultraviolet (UV) radiation (λ_1 = 184.9 nm and λ_2 = 253.7 nm). The organic products of this excitation react with atomic oxygen to form simpler, volatile molecules (typically CO_2), which readily desorb from the surface. Therefore, while ozone is continually formed and consumed by this process, there is a continuous generation of atomic oxygen[21]. Compared to oxygen plasma, UVO treatment is recognized as a milder type of physical modification to polymer surfaces with similar surface changes but with approximately an order of magnitude reduction in processing time[22,23]. This allows for better control of the surface conversion, as different degrees of hydrophilicity will be obtained for different treatment times.

The PDMS elastomer network system that has been widely used in our research involves both model PDMS as well as industrial-grade Sylgard-184 (manufactured by Dow Corning). The latter material comes in a two-part kit that makes Sylgard-184 readily applicable for commercial use. Figure 2.2 depicts the difference in the contact angle of water (a), the contact angle hysteresis (b), and the surface energy (c) for Sylgard-184 surfaces treated with UVO with two different lamps; one that transmits about 65% (UVO60) and the other transmits about 90 % (UVO90) of the shorter wavelength radiation (λ_1 = 184.9 nm)[21].

In addition to contact angle measurements we also used X-ray reflectivity and near-edge x-ray absorption fine structure (NEXAFS) spectroscopy to characterize the formation of the silica-like layer. Our results revealed that when exposed to UV, Sylgard-184 underwent chain scission of both the main backbone and the methyl side-groups. The radicals formed

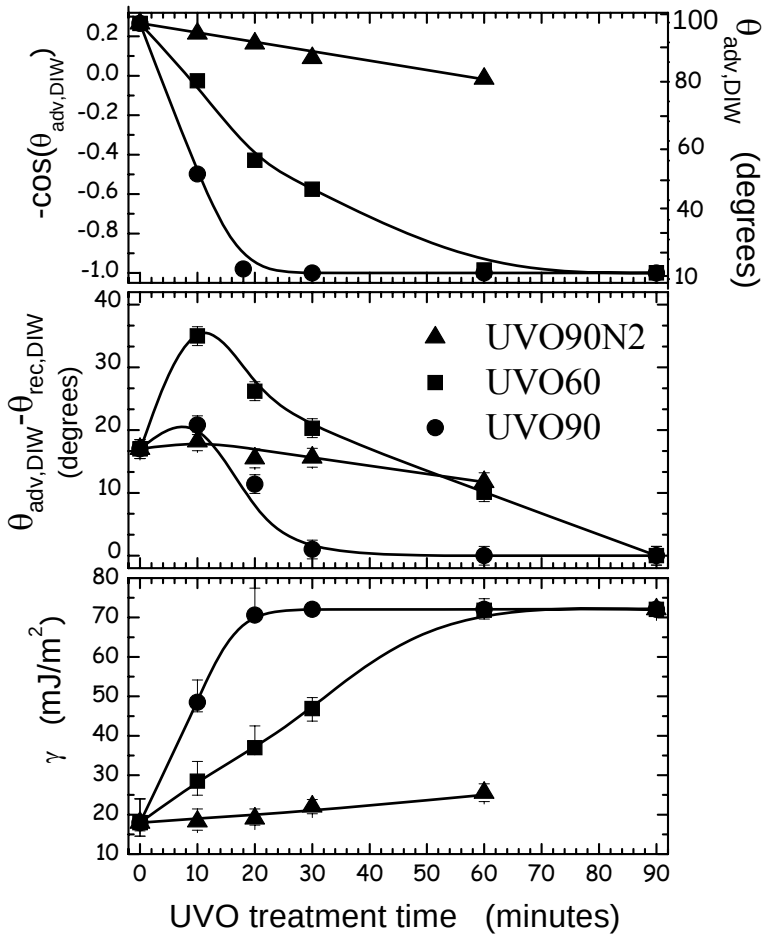

Figure 2.2: Dependence of a) the advancing contact angles of deionized water ($\theta_{adv,DIW}$), b) the contact angle hysteresis of deionized water ($\theta_{adv,DIW}$- $\theta_{rec,DIW}$), and c) the surface energy on the UVO treatment time for Sylgard-184 exposed to UVO60 (squares), UVO90 (circles), and UV90 (up-triangles). In part a) each point represents an average over 5 measurements on various areas of the same sample (the error associated with these measurements is smaller than ±1.5°). The lines are guides to the eye. [21].

during this process recombined forming a network whose wetting properties were close to those of untreated Sylgard-184. In contrast to the UV radiation, the UVO treatment created a large number of hydrophilic groups (*e.g.*, -OH) to the surface and sub-surface structure of Sylgard-184. The material density distribution within the first ≈5 nm of Sylgard-184 was most affected by the UVO treatment. The electron density near-surface region reached about 50 % of that of silica, as measured by the x-ray reflectivity technique[21].

An important observation from our work was that the silica fillers in Sylgard-184 did not alter its surface properties during and after UVO treatment. Comparison of our results with previous studies on silica filler containing PDMS materials concluded that the silica fillers were rarely seen in the sub-surface region of oxygen plasma PDMS films. As Sylgard-184 is a convenient commercial material to use, we combined its fabrication with a mechanical technique to create highly-hydrophobic surfaces that resist reconstruction.

2.2.2 Surface Stability

We mentioned earlier that hydrophobic recovery from the physically-modified surfaces created with UVO or oxygen plasma treatment prevented surface stability as the surfaces lost their original hydrophilic properties. Ironically, this phenomenon is advantageous for outdoor insulator applications. PDMS elastomers used in areas with high air-born pollution are subject to contamination deposits, which cause electrolyte film formation on the insulator resulting in current leakage and dry-band arcing. The corona discharge causes an initial wettability increase but recovers to its original hydrophobic state within 100 minutes, as tracked using AFM[18,24]. In addition, the adhesive force was found to increase immediately

after the electrical exposure but eventually returned to it original value of the unexposed surface[18,24]. While this type of "oscillating behavior" with PDMS elastomers allows the long-term vitality of the application even with the intermittent surface instability, there is still a great need for a surface with intrinsic stability.

The attraction of naturally occurring super hydrophobic surfaces (*e.g.*, lotus leaf effect) has inspired researchers to develop clever surface designs[25]. For example, thermoresponsive polymers and manipulation of surface roughness has resulted in surfaces with water contact angles exceeding 140° [6,26]. Recently, Jin and co-workers used a laser-etching method to produce super hydrophobic self-cleaning surfaces with PDMS[26]. They created PDMS with micro-, submicro-, and nano-composite surface structures by etching micropillars into PDMS and also spin-coating PDMS on polycarbonate nanopillar surfaces. These etched surfaces showed extremely high water contact angles of 160˚C and minimal wettability hysteresis (*cf.* Figure 2.3).

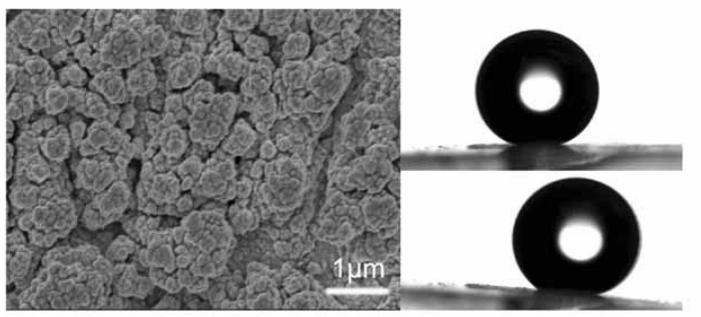

Figure 2.3 : Etched PDMS surface containing micro-, submicro-, and nano-composite structures shows a self-cleaning effect with water CA as high as 162°. Copyright © 2005 WILEY-VCH Verlag GmbH & Co. KGaA, Weinheim[26].

Attaching various organic modifiers to a surface is another way to alter surface properties of materials. One common technique is the deposition of self-assembled monolayers (SAMs) producing high quality and structurally-defined surfaces of specific chemical functionality[27,28]. Traditionally, SAMs have been formed with thiol or disulfide molecules on gold substrates or chlorosilanes molecules on silica substrates (molecules of various ω-terminus functionality). The deposition of SAMs onto polymer surfaces allows for specific tailoring of surface properties, *i.e.*, wetting and lubrication. Recognizing the fact that wetting properties of SAMs and their subsequent stability depend on a delicate interplay between the chemical functionality and the degree of order (including packing) within the SAM, our laboratory capitalized on the inherent siloxane elasticity to manipulate monolayer packing and surface modification of PDMS to control the grafting density of organosilane SAMs[2]. Specifically, we developed a method leading to the formation of mechanically assembled monolayers (MAMs). This technique (*cf.* Figure 2.4) is based on mechanically stretching PDMS sheets, and "activating" the surface via UVO treatment. Surface-bound hydroxyl groups on the UVO-modified PDMS were subsequently used as attachment points for semifluorinated organosilanes (SFO). After releasing the initial strain, the sheets returned to their original size thus "squeezing" the SFOs into densely populated arrays.

In Figure 2.5 we plot the results for the monolayers formed with $F(CF_2)_8(CH_2)_2SiCl_3$ (F_8H_2) on three substrates: PDMS, PDMS with an elongation (Δx) of 70%, and PDMS (Δx=70%) after aging for six months in a humid environment[2]. Not only did the water contact angle increase to values ≈130˚, but it also lost very little hydrophobicity after prolonged water exposure for the MAMs-PDMS fluorinated sample. While some

hydrophobicity is lost for the aged sample, it is minimal and still far more hydrophobic than the "conventional" SAMs-PDMS fluorinated sample (no stretching involved). Experiments using NEXAFS established that the high hydrophobicity and stability of the surfaces resulted from close packing of the semifluorinated groups on the surface that hindered the motion of the surface-grafted molecules.

MAMs of hydrocarbon-based silanes, $H(CH_2)_nSiCl_3$ (Hn-MAM), were also evaluated for hydrophobic performance[29]. It is known that as the length n of the hydrocarbon increases, the structure of a self-assembled monolayer transitions from a liquid-like to a solid-like state[30-32]. An increase in crystallinity should result in reduced mobility of the polymer surface. We evaluated this concept in hydrocarbon MAMs by probing the boundary between the liquid- and solid-like transition with "short" (n=8) and "long" (n=16) alkane molecules grafted onto PDMS surfaces. Grafting densities of the alkane-based silanes were varied by stretching the substrate to different elongations (Δx) prior to the UVO treatment. The packing density of the alkane chain increased with increasing the sample elongation prior to the organosilane deposition. We hypothesized that if the alkane chains were densely packed on the PDMS surface, neighboring chains should restrict their mobility even if the alkane chain lengths were less than the commonly accepted crystalline transition state of n = 12. To test this theory, we studied the behavior of MAMs prepared from n-octyltrichlorosilane (H8-MAM).

(A)

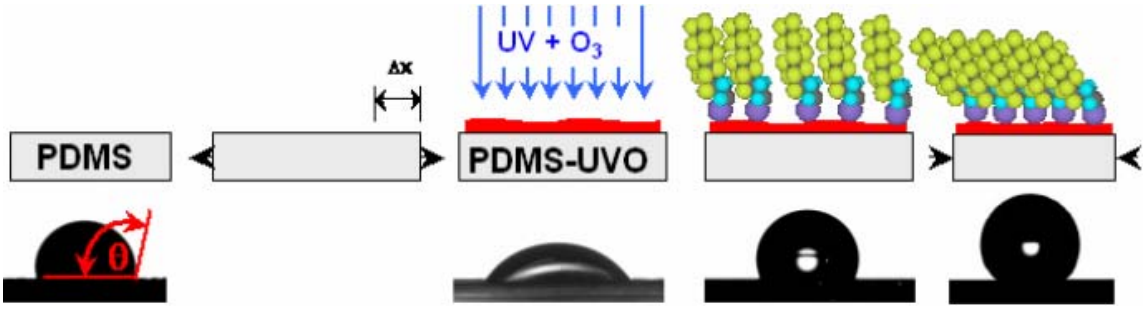

(B)

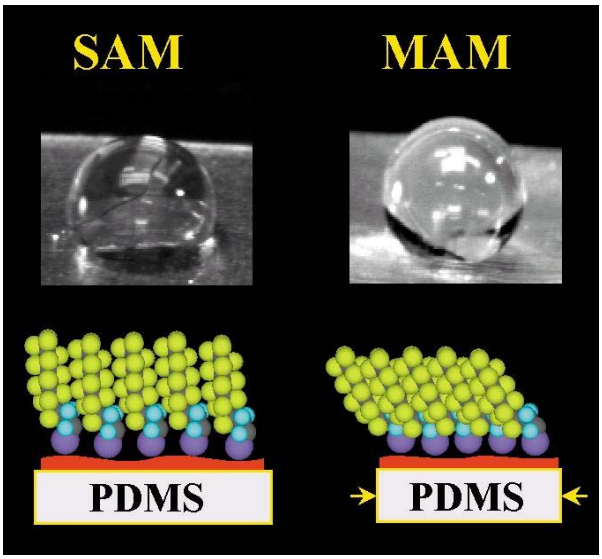

Figure 2.4: A) Schematic illustrating the mechanism of increased packing density of a self-assembled monolayer after mechanically stretching the substrate. Copyright © 2000 American Association for the Advancement of Science. All Rights Reserved. B) Representation showing the higher water contact angle for MAMs on PDMS versus SAMs on PDMS[2].

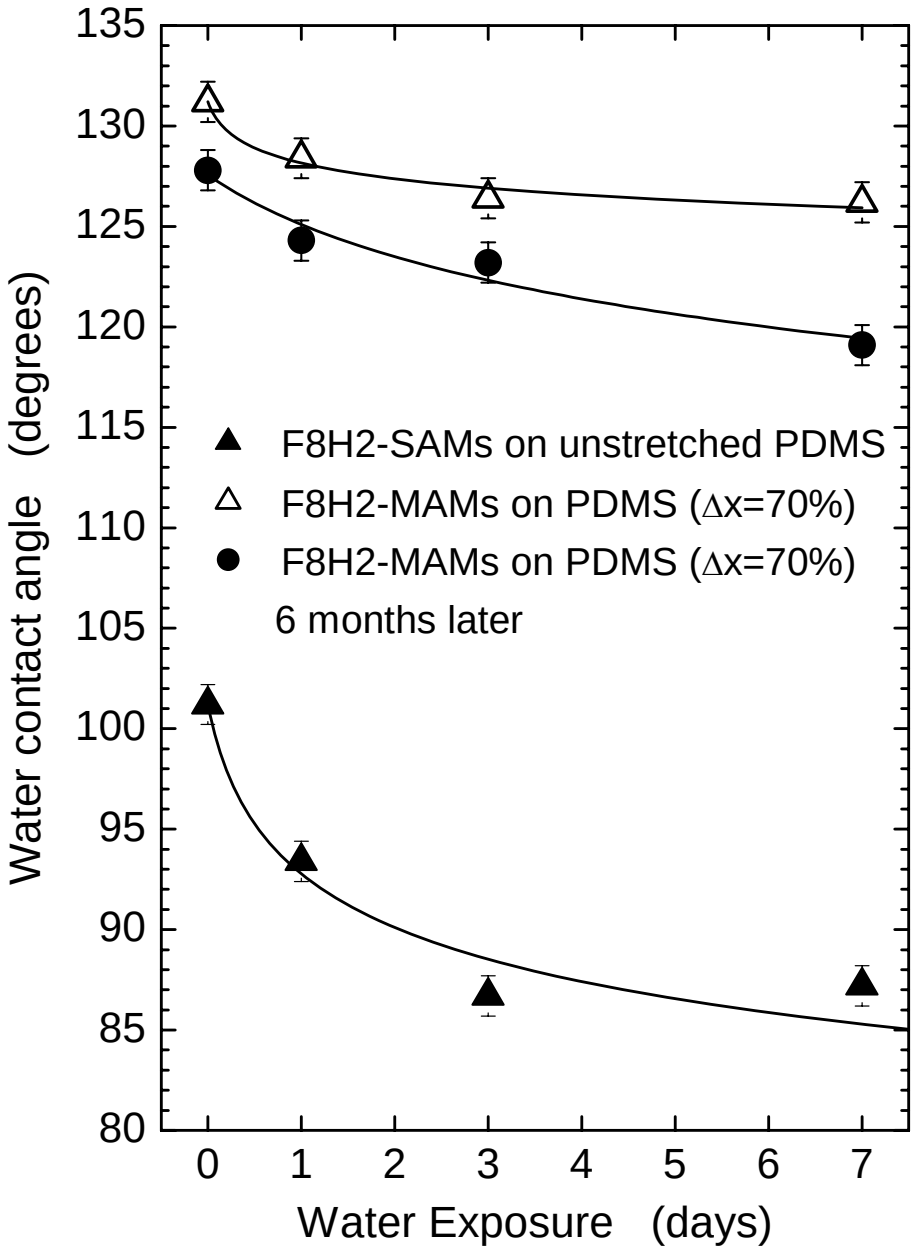

Figure 2.5: Water contact angles for mechanically-assembled monolayers made of semifluorinated alkanes on siloxane elastomers. Copyright © 2000 American Association for the Advancement of Science. All rights reserved[2].

The data in Figure 2.6 depict the dependence of the contact angles of deionized (DI) water on H8-MAM substrates as a function of the deposition time (τ) of n-octyltrichlorosilane (OTS) and the substrate stretch, Δx[29]. Both advancing (solid circles) and receding (open circles) contact angles are shown for each OTS treatment time. As with previous results for the H16-MAMs, where crystalline behavior is expected due to the van der Waals forces between neighboring methylene groups, we measure an increase in the contact angle with increasing τ and Δx for the H8-MAMs. We also detect the same decrease in contact angle hysteresis until a minimum is reached; after this point the hysteresis starts to increase ($\Delta x > 70\%$), which is contributed to increased roughening of the surface due to overcrowding of the alkane chain moieties.

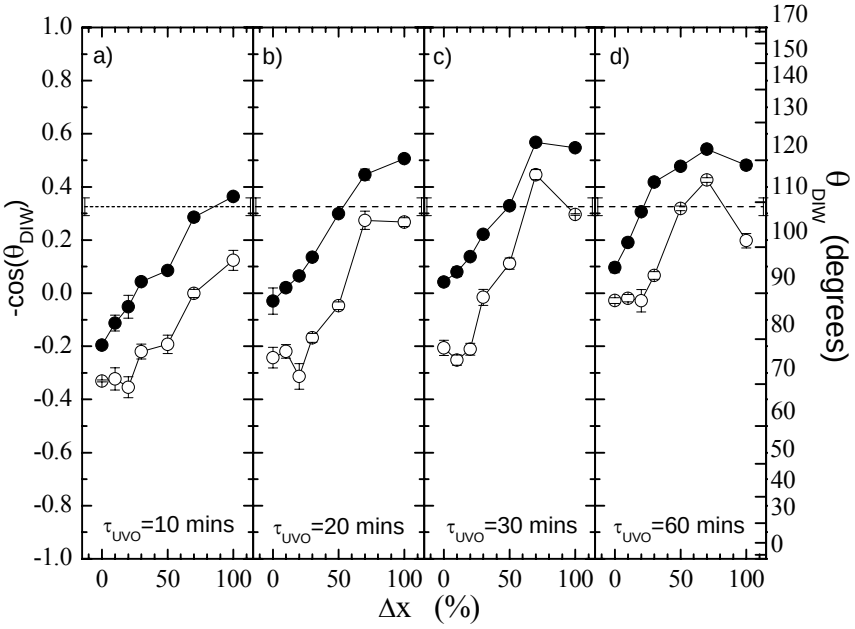

Figure 2.6. Advancing (●) and receding (○) contact angles of DI water, θ_{DIW}, on H8-MAMs prepared by vapor deposition of OTS as a function of the stretching of the PDMS substrate, Δx. The dashed line denotes the value of θ_{DIW} for a crystalline array of $-CH_3$ groups. Copyright © 2002 Materials Research Society Symposium Proceedings[29].

NEXAFS experiments on the H8-MAM samples reveal very interesting information. Namely, while no chain orientation was detected at $\Delta x = 0\%$ and $\Delta x > 30\%$ for all deposition times, several H8-MAM samples prepared on PDMS-UVO pre-stretched to $0\% < \Delta x < 30\%$ and exposed to OTS molecules for $\tau < 30$ minutes exhibited a non-negligible orientation order within the H8-MAM. Detailed analysis of the NEXAFS data revealed that the chains were tilted on average ≈35-45° away from the sample normal. This observation provides important evidence that the liquid-to-solid transition in substrate-anchored alkanes can be fine-tuned by tailoring the molecules packing density.

In our previous work we have established that when exposed to water, SAMs that contain structural defects usually lose their structural order[2]. In contrast, we have demonstrated that MAMs possess excellent barrier properties since after their exposure to polar environments (*i.e.*, water), contact angles do not deteriorate dramatically with time. We have also shown that the high stability of the MAMs resulted from close chain packing. Thus we performed similar stability experiments on the Hn-MAMs. In Figure 2.7, we present the results of the contact angle measurements from "dry" samples and samples exposed to water for 3 and 5 days. Data for both H8-MAM and H16-MAM are shown. For comparison we also include the results obtained from the F8H2-MAM specimens[2]. It is apparent that the surface properties of Hn-MAMs remain very stable even after prolonged exposures to water with values similar to those as obtained by mechanically assembling semi-fluorinated moieties. In addition, the stability of the MAMs is much higher than those of SAMs. This work demonstrates that hydrophobic surfaces with long-lasting barrier properties can be prepared by fabricating hydrocarbon-based MAMs. Adjusting the strain on the elastic substrate

ultimately controls the packing density of Hn-MAMs. Finally, we have shown that increasing Δx can induce a liquid-to-solid transition in surface-anchored alkanes producing excellent surface stability. Considering that hydrocarbon-based moieties are much cheaper than fluorocarbons, the hydrocarbon-based MAMs may provide convenient routes for generating stable, water resistant surfaces in various industrial applications.

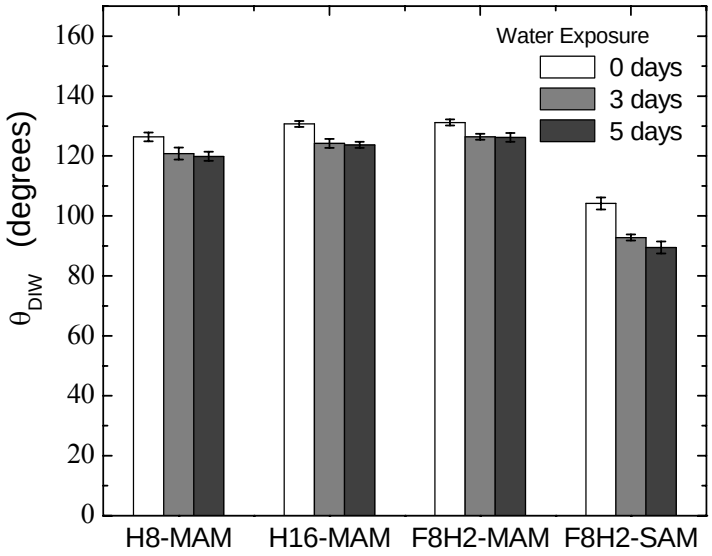

Figure 2.7: Water stability data for H8-MAM, H16-MAM, F8H2-MAM, structures, all stretched to Δx=70 %. Also included are data for F8H2-SAM. Copyright © 2002 Materials Research Society Symposium Proceedings[29].

2.3 Conclusion

The surface mobility of PDMS can be dramatically reduced by the creation of mechanically assembled monolayers (MAMs). By utilizing the elasticity of siloxanes, PDMS substrates were stretched and subsequently modified with UVO/exposure and chemical deposition of hydrophobic organosilanes. The degree of hydrophobicity and

stability correlates to the packing density of the formed monolayers. If the monolayers are dense, random chain conformation is prevented and the hydrophobic substituents both shield the more hydrophilic Si-O backbone and reduce its flexibility. The flexibility reduction prevents reorientation of more hydrophilic moieties when the modified substrates are placed in an aqueous environment.

In parallel to the studies involving PDMS, we were also interested in finding a siloxane surface capable of retaining its elasticity during modification. As the UVO/exposure treatment depends on the generation of radicals, we expected that a chemical moiety requiring lower activation energy than the methyl groups of PDMS would be more efficient in generating radicals that result in the formation of hydrophilic groups on surfaces. Evaluating poly(vinylmethylsiloxane) (PVMS) was a logical choice. An intermediate was available for synthesizing PVMS of varying molecular weights and the vinyl moiety provides a convenient route for preparing a wide variety of functionalized silicone elastomers using simple chemical methods [4,33,34]. Besides the physical surface treatments, *i.e.*, ultraviolet oxidation, radiation, plasma or corona exposure, direct covalent attachment of the desired functionality through addition reactions such as hydrosilation, hydrosulfidation, hydrophosphination, epoxidation, and alkyl halide addition reactions allows for a myriad of possibilities[35-38]. Chapters 3 and 4 in this Ph.D. thesis describe our work on modifying PVMS and its resultant properties. Most notable is the generation of controlled wettability and the ability to switch surface composition states by changing the external environment.

2.4 **References**

1. Clarson, S. J. in *Siloxane Polymers* (eds. Clarson, S. J. & Semlyen, J. A.) 216-244 (PTR Prentice Hall, Englewood Cliffs, New Jersey, 1993).

2. Genzer, J. & Efimenko, K. Creating long-lived superhydrophobic polymer surfaces through mechanically assembled monolayers. *Science* **290**, 2130-2133 (2000).

3. Herczynska, L., Lestel, L., Boileau, S., Chojnowski, J. & Polowinski, S. Modification of polysiloxanes by free-radical addition of pyridylthiols to the vinyl groups of the polymer. *European Polymer Journal* **35**, 1115-1122 (1999).

4. Holmes-Farley, S. R., Reamey, R. H., Nuzzo, R., McCarthy, T. J. & Whitesides, G. M. Reconstruction of the Interface of Oxidatively Functionalized Polyethylene and Derivatives on Heating. *Langmuir* **3**, 799-815 (1987).

5. Jalbert, C., Koberstein, J. T., Hariharan, A. & Kumar, S. K. End group effects on surface properties of polymers: Semiempirical calculations and comparison to experimental surface tensions for alpha,omega-functional poly(dimethylsiloxanes). *Macromolecules* **30**, 4481-4490 (1997).

6. Jin, M. et al. Super-Hydrophobic PDMS Surface with Ultra-Low Adhesive Force. *Macromolecular Rapid Communications* **26**, 1805-1809 (2005).

7. Koberstein, J. T. Molecular design of functional polymer surfaces. *Journal of Polymer Science Part B-Polymer Physics* **42**, 2942-2956 (2004).

8. Gordon, G. V. et al. Silicone release coatings: An examination of the release mechanism. *Adhesives Age* **41**, 35-+ (1998).

9. Chen, H., Brook, M. A. & Sheardown, H. Silicone elastomers for reduced protein adsorption. *Biomaterials* **25**, 2273-2282 (2004).

10. Ratner, B., Hoffman, A., Schoen, F. & Lemons, J. (eds.) *Biomaterials Science: An Introduction to Materials in Medicine.* (Academic Press, San Diego, 1996).

11. Brash, J. L. Exploiting the current paradigm of blood--material interactions for the rational design of blood-compatible materials. *Journal of Biomaterials Science -- Polymer Edition* **11**, 1135 (2000).

12. Ratner, B. R. Blood compatibility--a perspective. *Journal of Biomaterials Science -- Polymer Edition* **11**, 1107 (2000).

13. Rouse, J. H., Twaddle, P. L. & Ferguson, G. S. Frustrated reconstruction at the surface of a glassy polymer. *Macromolecules* **32**, 1665-1671 (1999).

14. Owen, M. J. Plasma/Corona Treatment of Silicones. *Australian Journal of Chemistry* **58**, 433-436 (2005).

15. Ferguson, G. S., Chaudhury, M. K., Biebuyck, H. A., and Whitesides, G. M. Monolayers on Disordered Substrates - Self-Assembly of Alkyltrichlorosilanes on Surface-Modified Polyethylene and Poly(Dimethylsiloxane). *Macromolecules* **26**, 5870-5875 (1993).

16. Hillborg, H. et al. Crosslinked polydimethylsiloxane exposed to oxygen plasma studied by neutron reflectometry and other surface specific techniques. *Polymer* **41**, 6851-6863 (2000).

17. Hillborg, H. & Gedde, U. W. Hydrophobicity changes in silicone rubbers. *Ieee Transactions on Dielectrics and Electrical Insulation* **6**, 703-717 (1999).

18. Hillborg, H. & Gedde, U. W. Hydrophobicity recovery of polydimethylsiloxane after exposure to corona discharges. *Polymer* **39**, 1991-1998 (1998).

19. Owen, M. J. & Smith, P. J. Plasma Treatment of Polydimethylsiloxane. *Journal of Adhesion Science and Technology* **8**, 1063-1075 (1994).

20. Williams, R. L., Wilson, D. J. & Rhodes, N. P. Stability of plasma-treated silicone rubber and its influence on the interfacial aspects of blood compatibility. *Biomaterials* **25**, 4659-4673 (2004).

21. Efimenko, K., Wallace, W. E. & Genzer, J. Surface modification of Sylgard-184 poly(dimethyl siloxane) networks by ultraviolet and ultraviolet/ozone treatment. *Journal of Colloid and Interface Science* **254**, 306-315 (2002).

22. Huck, W. T. S. et al. Ordering of spontaneously formed buckles on planar surfaces. *Langmuir* **16**, 3497-3501 (2000).

23. Ouyang, M., Yuan, C., Muisener, R. J., Boulares, A. & Koberstein, J. T. Conversion of some siloxane polymers to silicon oxide by UV/ozone photochemical processes. *Chemistry of Materials* **12**, 1591-1596 (2000).

24. Meincken, M., Berhane, T. A. & Mallon, P. E. Tracking the hydrophobicity recovery of PDMS compounds using the adhesive force determined by AFM force distance measurements. *Polymer* **46**, 203-208 (2005).

25. Genzer, J. & Efimenko, K. Recent developments in superhydrophobic surfaces and their relevance to marine fouling: a review. *Biofouling* **22**, 339-360 (2006).

26. Sun, T. L. et al. Reversible switching between superhydrophilicity and superhydrophobicity. *Angewandte Chemie-International Edition* **43**, 357-360 (2004).

27. Chaudhury, M. K. *Materials Science & Engineering Reports* **16**, 97 (1996).

28. Ulman, A. *An Introduction to Ultrathin Organic Films from Langmuir-Blodgett to Self Assembly* (Academic Press, New York, 1991).

29. Efimenko, K. & Genzer, J. Tuning the surface properties of elastomers using hydrocarbon-based mechanically assembled monolayers. *Materials Research Society Symposium Proceedings* **DD10.3.1**, 710 (2002).

30. Allara, D. L., Parikh, A. N. & Judge, E. The existence of structure progressions and wetting transitions in intermediately disordered monolayer alkyl chain assemblies. *Journal of Chemical Physics* **100**, 1767-1764 (1994).

31. Chaudhury, M. K. & Owen, M. J. Correlation between Adhesion Hysteresis and Phase State of Monolayer Films. *The Journal of Physical Chemistry* **97**, 5722-5726 (1993).

32. Snyder, R. G., Strauss, H. L. & Elliger, C. A. C-H Stretching Modes and the Structure of *n*-Alkyl Chains. 1. Long, Disordered Chains. *The Journal of Physical Chemistry* **90**, 5623-5630 (1982).

33. Carey, D. H. & Ferguson, G. S. Synthesis and Characterization of Surface-Functionalized 1,2-Polybutadiene Bearing Hydroxyl or Carboxylic-Acid Groups. *Macromolecules* **27**, 7254-7266 (1994).

34. Holmes-Farley, S. R. & Whitesides, G. M. Fluorescence Properties of Dansyl Groups Covalently Bonded to the Surface of Oxidatively Functionalized Low-Density Polyethylene Film. *Langmuir* **2**, 266-281 (1986).

35. Cai, G. P. a. W., W. P. Synthesis and chemical modification of poly(divinylsiloxane). *Polymer* **43**, 1753-1759 (2002).

36. Bauer, J., Husing, N., and Kickelbick, G. Synthesis of new types of polysiloxane based surfactants. *Chemical Communications* **01**, 137-138 (2001).

37. Bauer, J., Husing, N., and Kickelbick, G.,. Preparation of functional block copolymers based on a polysiloxane backbone by anionic ring-opening polymerization. *Journal of Polymer Science Part a-Polymer Chemistry* **40**, 1539-1551 (2002).

38. Boutevin, B., F. Guida-Pietrsanta, and A. Ratsimihety'. in *Silicone-Containing Polymers* 79-112 (Kluwer Academic Publishers, Dordrecht, 2000).

CHAPTER 3: Responsive Siloxane-Based Polymeric Surfaces

3.1 Introduction

A responsive surface adapts its physico-chemical characteristics in response to an external stimulus, *i.e.*, chemical, electrical, or mechanical [1,2]. A responsive surface can entail a recognition event that triggers a conditional response, such as a pH responsive polymer conjugated with glucose oxidase and embedded with insulin. For example, when sufficient levels of glucose are present in the contacting media, a decrease in pH causes a matrix pore size change due to polymer collapse thereby releasing insulin [3]. Such materials are often described as biomimetic [4] due to their ability "to mimic the efficient conversion of chemical energy into mechanical energy in living organisms" and have been demonstrated in artificial muscles [3]. In many cases, surface responsiveness is a result of the rearrangement of various chemical functionalities present close to or directly at the surface. The two key parameters that define the functionality (and ultimately application) of any responsive surface are: 1) the degree of change of the surface properties after the external trigger was applied, and 2) the rate at which these variations occur. Hence a "supreme" responsive surface is one that instantaneously responds to changes in its environment with a measurable property change.

Polymeric materials represent suitable candidates for creating responsive surfaces. Tailoring the surface could encompass involving a hydrophobic, hydrophilic, or specific recognition receptor moiety. Local molecular heterogeneities along the polymer backbone provide the driving force for the response of the polymer backbone to changes in the environment. Polymers have to be mobile in order to respond to external stimuli. Polymer mobility in the bulk and at the surface depends on the polymer's glass transition temperature,

creating a convenient means of adjusting response time through the solid-liquid duality of polymers. Recent results have shown that the glass transition temperature is lower in the surface region than in the bulk enhancing surface reconstruction rates [5-7].

Several research groups have studied the dynamic nature of polymer surfaces, reconstruction dynamics associated with switching the external medium, and changing the chemical make-up of the surface itself. Pioneering work in this area includes the studies by Whitesides and coworkers, who evaluated the wettability of oxidized polyethylene after various environmental exposures and temperature variations [8]. Another series of adaptable polymeric surfaces with broad lyophobicity was created by Koberstein and coworkers, who utilized synthetic polymers tailored with various end-groups ranging from carboxylic acid to fluorine-containing moieties[9]. Utilizing these principles, Ferguson and coworkers varied substrate elasticity and composition of oxidized butadienes to create a system with a controlled rate of surface reconstruction. The surface reconstruction was dictated by shifts in enthalpic and entropic driving forces on the surface free energy[10-12].

In this chapter, we define polymer surface dynamics in regard to our work and describe how to generate responsive polymer surfaces made of flexible substrates comprising functional siloxane elastomers. We will demonstrate that these surfaces possess very fast reconstruction kinetics and can be chemically tailored to adjust the responsiveness to various external media.

3.2 Modes of Polymeric Surface Dynamics

Surfaces may respond to the changes in the outside environment in several ways. Various chain constituents can either be delivered to the surface from the bulk or, when

already present at or close to the surface, they can locally rearrange. In the former case, surface segregation occurs due to disparities between the surface energy of the monomers (or parts of the polymers such as end-groups), polymer flexibility, tacticity, and molecular weight. Presence of a chemical moiety, different from the rest of the chain, may influence local chain rearrangements in the latter case.

3.2.1 Wettability Studies

In order to study surface segregation, a technique is needed that is sensitive only to the surface's first few angstroms from the interface. Through contact angle measurements,

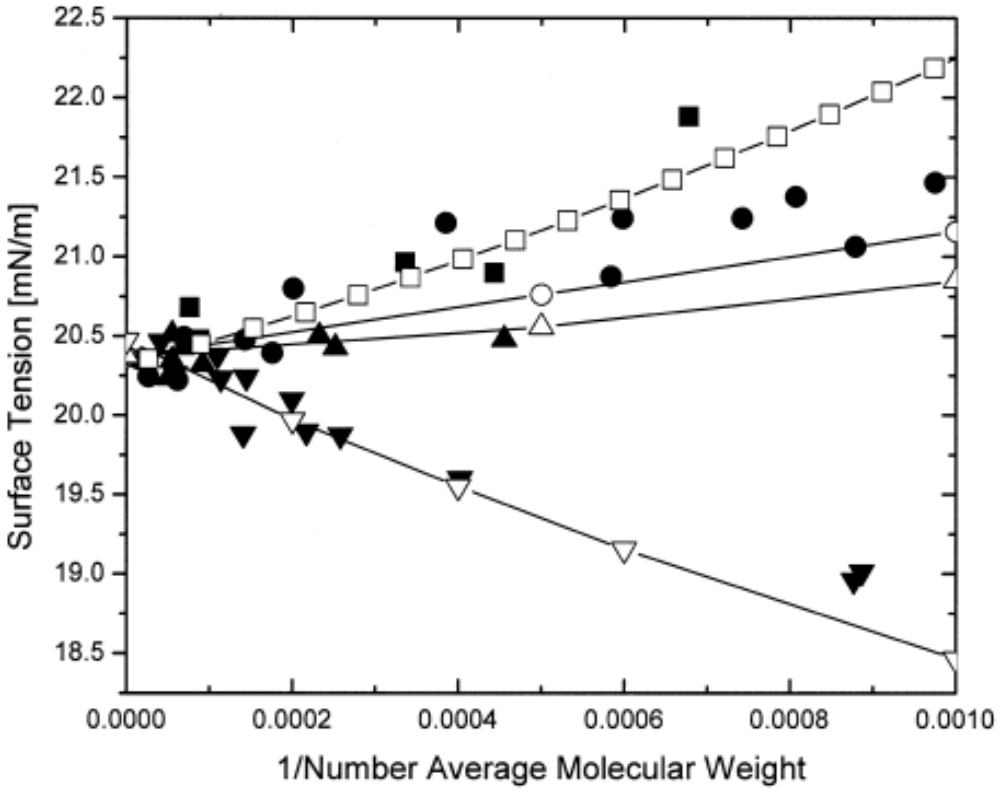

Figure 3.1: Comparison of (■, ●, ▲,▼) experimental and (□, ○, Δ, ∇, —) calculated surface tensions for α, ω-terminated PDMS: (■,□) carboxypropyl-terminated, (●,○) aminopropyl-terminated, (▲, Δ) hydroxypropyl-terminated, and (▼,∇) methyl-terminated[9].

Whitesides et al. determined the depth sensitivity of wetting by evaluating ω-mercapto ethers on gold surfaces[13]. Methyl ether surfaces had advancing water contact angles of ≈75º. As the polar ether placement was varied along the length of the alkyl chain, the contact angle reached a limiting value of ≈110º for ether depths greater than 5 Å (or in excess of a butyl linkage). While contact angles for surfaces with $HS(CH_2)_{16}O(CH_2)_{n\geq4}CH_3$ were identical to the C21-thiol (*i.e.*, having 21 methylene, $-(CH_2)-$, units), deeper surface probing with X-ray photoelectron spectroscopy (XPS) and external reflection infrared spectroscopy confirmed the presence of ether groups absent in the C21 surface. This finding verified that ethers groups "buried" below the alkane-chain surface had little impact on the contact angle, making it a sensitive technique to study changes in surface behavior. While the technique's sensitivity was proven on a rigid gold surface, contact angle has been set as a precedent for characterizing polymeric surface behavior.

3.2.2 Surface Segregation

By combining two factors that drive surface segregation, namely, polymer molecular weight and end-group surface interactions, Koberstein's group evaluated the resulting surface energy variations in α,ω-terminated PDMS fluids[9,14]. Four end-groups on siloxane backbones of various molecular weights were studied, including, carboxypropyl, aminopropyl, hydroxypropyl, and methyl groups. As shown in Figure 3.1, the slope in the surface energy *vs.* molecular weight plot differs for each functional group. In the case of methyl-terminated fluids, the surface energy decreases with decreasing molecular weight. The carboxypropyl- and aminopropyl-terminated fluids, however, cause an increase in the

surface energy with decreasing molecular weight. Finally, the hydroxypropyl-terminated fluid exhibits only slight variations in surface energy in the defined molecular weight range.

Koberstein and coworkers considered four possible effects to explain the observed surface energy differences: 1) polymer polydispersity, 2) fluid density and molecular weight, 3) change in surface entropy, and 4) preferential surface adsorption or depletion of the functional group. Polydisperse polymers could cause preferential adsorption at the surface due to molecular weight disparity. By evaluating methyl-terminated poly(dimethyl-siloxane) (PDMS) with molecular weights around 6.5 kDa and with polydispersities between 1.7-8.7, Koberstein et al. found the surface tension to be constant. The molecular weight, M_n, scaled with surface tension as a function of M_n^{-1}, a result that was consistent with lattice model predictions[15]. Molecular weight (and density) variation alone did not account for the positive and negative $d\gamma/dM_n^{-1}$ differences in Figure 3.1. The contribution to surface energy among all components evaluated was primarily due to surface enthalpy rather than entropy ($d\gamma/dT \approx$ 0.05 dyn/(cm·^{o}C) for all materials)[14,16]. XPS[17] and neutron reflectivity[18] experiments revealed that a compositional gradient profile existed for the scanned surface depth, indicating that polymers with high-energy or repulsive carboxyl and amino groups were depleted at the air-polymer interface. In contrast, when the functional groups comprised low-energy fluorine or methyl molecules, attractive forces led to preferential adsorption of the chain termini at the surface.

Utilizing end-group surface depletion effects, interfacial tension was reduced by 30% for the immiscible blends of PDMS and polybutadiene (PBD) by incorporating amino-terminated PDMS into the mixture[19]. It was established that interfacial tension depended

linearly on the amino-concentration. As a deviation in interfacial tension should occur at the critical concentration for a system surfactant, the amino-terminated PDMS did not follow this behavior. Instead the interfacial tension reduction was explained by a bulk thermodynamic effect of the end-functional groups, as the blend solubility parameter was reduced due to intrachain repulsion between the PDMS repeat groups and its amine-functional end groups. It was concluded that higher repulsion (or interaction) between a chain and its end-groups led to higher blend solubility between components[19,20].

3.2.3 Surface Reorientation

Wong and coworkers evaluated the responsiveness or reconstruction of end-functional homopolymers[21]. The surface behavior of fluorine-terminated polystyrene (PS-F) with molecular weights ranging from 5 to 25 kDa was probed between temperatures of 30-70^{o}C in a humid environment. Monitoring changes in contact angle values followed surface reconstruction of the film. For instance, 10 kDa PS-F was equilibrated at a saturated water vapor temperature of 30^{o}C. The initial contact angle of 95^{o} was reduced to ≈85^{o} after 10 days. This change was attributed to surface reconstruction of the fluorine end-groups, which "dived" below the polymer's surface upon exposing the polymer film to water.

Studies by Whitesides et al. demonstrated the dynamic nature of surfaces through experiments involving surface stability of functionalized polyethylene[8]. Low-density polyethylene (LDPE) was oxidized above its glass transition temperature to yield a hydrophilic surface comprising carboxylic acid (PE-COOH) and aldehyde groups. Wettability studies proved the films stable until exposed to heat-treatment in vacuum or

argon (*cf.* Figure 3.2). Although the reconstruction rate was found to be temperature-dependent, high surface energy films (starting water contact angles of ≈50°) resembled an unmodified polyethylene surface (water contact angle of 103°) in less than 5 minutes of heat-treatment at 100°C in vacuum. In contrast, identical studies on low-energy films (starting water contact angle of 141° for $PE(CH_2OCO(CF_2)_6CF_3)$ reconstructed either slowly or not at all with equilibrium contact angle values being reached after about one hour. Similar reconstruction behavior was seen with heat-treatment against water (polar) or perfluorodecalin (non-polar) (*cf.* Figure 3.2). The polar PE-COOH surface was stable in a polar media at high temperatures but reconstructed when exposed to a nonpolar liquid medium.

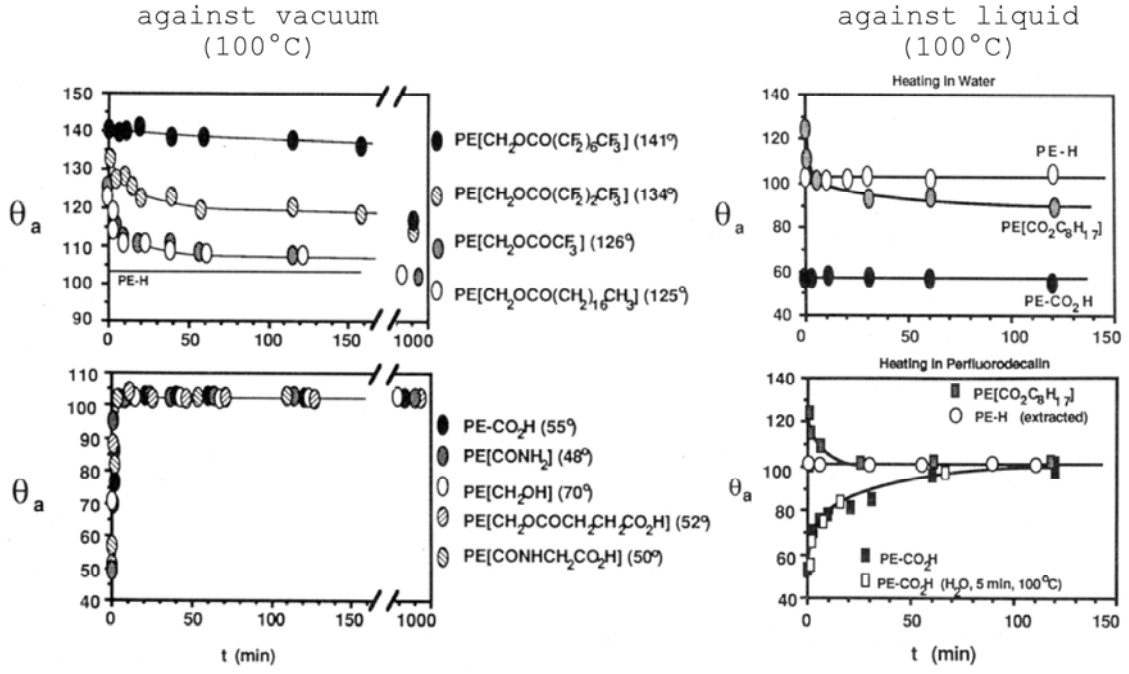

Figure 3.2: (Left) Dependence of advancing contact angle of water on heating time against vacuum at 100°C for low energy (top left) and high-energy (bottom left) groups. (Right) Dependence on contacting media for various reconstructive behaviors. Data reconfigured from reference 8.

While the PE-COOH surfaces after reconstruction are inaccessible for van der Waals interactions, their carboxylic acid groups could still undergo deprotonation or be reacted with a fluorescent probe. Both reactive techniques demonstrated that while the carboxy groups were no longer "surface" active, they still responded under certain experimental conditions. Finally, once the polar groups were buried in the bulk phase, they could be regenerated to a limited extent by exposing the reconstructed film to water. The carboxy-group regeneration efficiency was found to depend on the extent of reconstruction to its original hydrophobic state as shown in Figure 3.3 for various environmental treatments [8].

3.2.4 Dynamic Interplay Between Segregation and Reorientation

The two modes of surface dynamics, namely, surface segregation and chain reorientation, often act in accord and contribute simultaneously to variations in surface activity. First, polymer mobility in the bulk and at the surface depends on system temperature. While polymer motion in a glassy state is very slow, it increases dramatically when the temperature of the system is raised above the glass transition temperature (T_g). At temperatures above the T_g polymer chains can restore their preferred random flight conformations if an entropic gain exceeds enthalpic interactions between the polymer and the surface, unless there is an additional constraint, such as the presence of crystalline or cross-linked regions. Koberstein showed that some reorientation still occurs even below the glass transition temperature for end-functionalized PS[9]. Secondly, the time scales needed for the surface reorganization depends on the chemical and physical nature of the polymeric constituents. The interplay between segregation and reorientation has been discussed by Koberstein[9] and demonstrated elegantly in Anastasiadis' work with a blend of polystyrene (PS) and dimethylamine-

terminated poly(isoprene-b-styrene) copolymers [22]. The low-energy polyisoprene block first segregated to the PS matrix-air interface, dragging the rest of the copolymer chain along. This process was characterized by a rather long equilibration time. After exposure to a humid environment, rearrangement of the higher-energy dimethylamine end-group

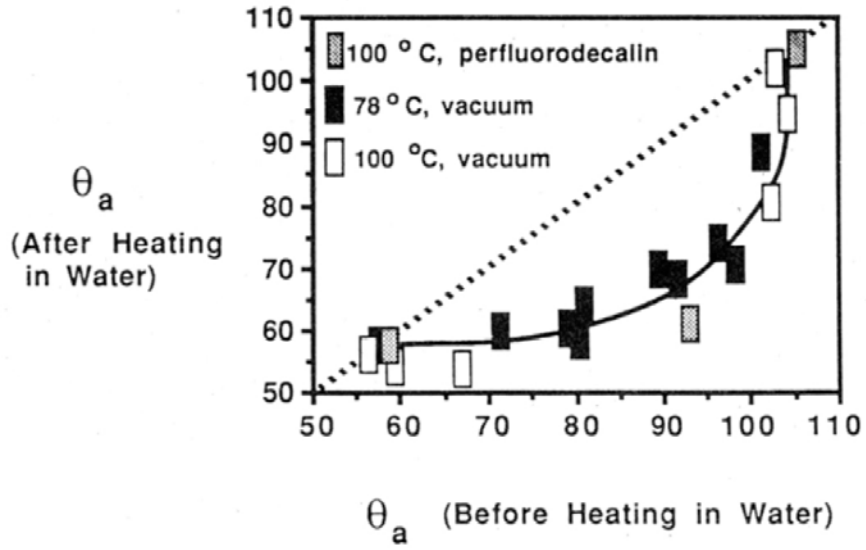

Figure 3.3: Contact angle of water (pH 1) on samples of PE-COOH after treatment in hot distilled water (pH 6-7, 100°C, 30 s) as a function of the contact angle prior to heating in water. Prior to the treatment in water, samples were partially reconstructed by heating under vacuum at 78 or 100°C or by heating in perfluorodecalin (100°C), to attain the various values of θ_a [8].

dominated the surface make-up as indicated by a drop in contact angle. The later process was found to take place more rapidly because the reorganization involved only local chain rearrangements rather than motion of the entire chain.

As described in Chapter 2 in this Ph.D. Thesis, there are applications where surface stability is desired; the MAMs technique is an example of this surface class[23]. Rouse et al.'s work on "frustrated" glassy surfaces also accentuated entropic control at a polymer interface

by manipulating the reconstruction temperature[24]. Using poly(4-methyl styrene) as a model glassy polymer, Rouse et al. oxidized its surface below the polymer's T_g of 110°C. The resulting functionalized surface was "locked" and remained hydrophilic when exposed to air below its bulk T_g. Upon exposure to temperatures higher than the glass transition, the chain could fully reconstruct to its unmodified state of hydrophobicity, as illustrated by the data in Figure 3.4.[24]

3.3 Switchable Surfaces

Defining the optimum response of a switchable surface involves understanding the characteristics responsible for the change in surface properties. Creating a surface that turns "on" or "off" within an optimum timeframe first requires a measurable magnitude change in response to environmental changes such as temperature, pH, and chemical composition. In addition, the reversibility of a "true" switchable surface should not deteriorate over time. Both rigid inorganic surfaces and polymeric surfaces have been studied to demonstrate stimuli-responsive behavior.

3.3.1 Polymers on "Hard" Surfaces

Recent studies involving poly(N-isopropyl acrylamide) (PNIPAAm) polymers grafted onto silicon surfaces demonstrated "reversible switching between superhydrophilicity and superhydrophobicity" [25]. PNIPAAm surfaces have been studied extensively for their reversible thermoresponsive properties due to the lower critical solution temperature (LCST) of PNIPAAm in water. At temperatures below the LCST, intermolecular forces between the water molecules and polymer are energetically favored resulting in a hydrophilic surface.

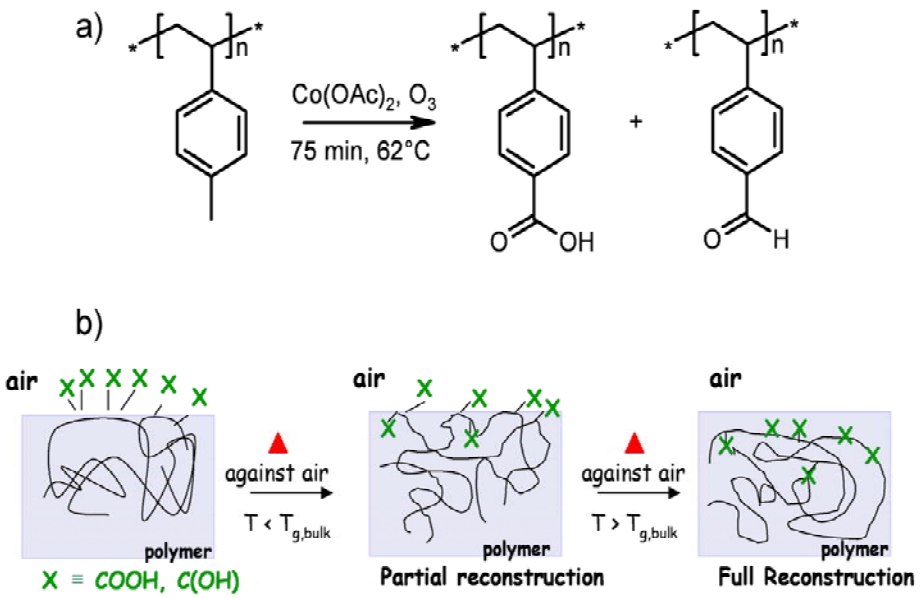

Figure 3.4: (a) Chemical oxidation of poly(4-methyl styrene) with cobalt (II) acetate. (b) Schematic representation of the surface reconstruction of a chemically modified glassy polymer below and above its bulk glass-transition temperature. Redrawn from reference 9.

Above the LCST, the intramolecular hydrogen bonding among NIPAAm monomers dominates causing chain collapse and a more hydrophobic surface. Sun and coworkers enhanced the hydrophilic-hydrophobic effect from 63.4 to 93.2° water contact angle for a smooth PNIPAAm surface-polymerized silicon substrate to a superhydrophilic-superhydrophobic effect from ≈0° to greater than ≈145° water contact angle for PNIPAAm on a rough silicon surface. The switch between the hydrophilic and hydrophobic states was reported to occur within minutes of the temperature transition and could be repeated for over 20 temperature cycles.

3.3.2 Polymers on "Soft" Surfaces

The ability of polymer surfaces to respond to changes in outside environment depends on the structure of polymeric constituents. Ferguson classified the surface responsiveness in relation to the polymer structure into the groups: (I) free chains, (II) lightly cross-linked chains, and (III) highly cross-linked chains[12]. The distinction between Regions II and III is defined as a change in the surface's rubber elasticity that can be experimentally varied by the cross-linker concentration. Ferguson and coworkers demonstrated the reconstruction differences between amorphous or crystalline polymers utilizing semi-crystalline poly(1,2-butadiene) (1,2-PBD) and completely amorphous 1,4-PBD films at various cross-link densities. The films were chemically oxidized to generate –COOH and –OH moieties along the PBD backbone (PBD-ox)[10]. Initial advancing water contact angles θ_a were $\approx 60^o$ but the oxidized surfaces would reconstruct to a hydrophobic state ($\approx 90^o$) if left in air for an extended time (8.5 hours). Rearrangement of the hydrophilic groups occurred when 1,2-PBD-ox was exposed to water, reaching original θ_a values after 6 hours[10,11]. The rearrangement to the more hydrophilic surface was associated with an enthalpy-driven equilibrium involving hydrogen bonding, Lewis acid-based interactions and van der Waals forces of the hydroxyl and carboxylic acid moieties along the polymer chain. Upon heating the substrate in water, the exposed side of PBD-ox became hydrophobic within minutes. This switch from hydrophilic to hydrophobic state triggered by heat was attributed to an entropy change in the system allowing the chains to assume their random coil conformations thereby pulling out the hydrophilic moieties from the surface to the bulk. The hydrophobic-

hydrophilic switch occurred with system temperature oscillating between 80 and 43°C but dampened after a few cycles (*cf.* Figure 3.5). At this point the surface reached an equilibrium value almost equal to its original contact angle.

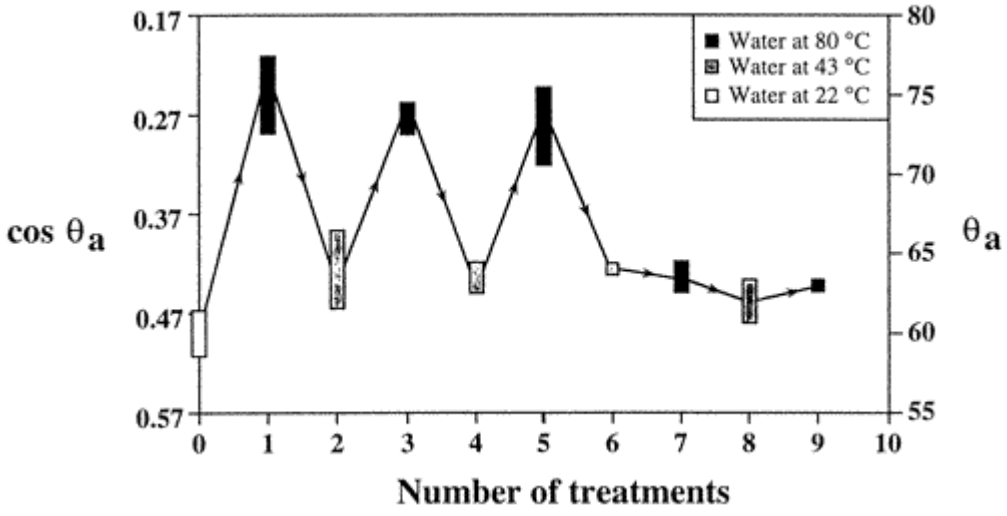

Figure 3.5: Contact angles of water (pH=1) for two separate samples of PBD-ox cycled repeatedly against deionized water at 80°C and at 43°C. The error bars one standard deviation above and below the mean of the contact angle measurements[11].

3.4 Rubber Elasticity and the Siloxane Bond

From the previous description it is apparent that a direct correlation exists between polymer elasticity and surface response. Starting with a very flexible substrate, such as a silicone elastomer, one should increase the likelihood of generating prompt responses to external stimuli. As eluded in Chapter 2 in this Ph.D. Thesis, however, the relatively inert PDMS does not lend itself to a dual-characteristic surface. With poly(vinylmethylsiloxane) (PVMS), however, one of the methyl groups is replaced with a vinyl functionality increasing

its chemical tailorability. PVMS is a unique polymer providing multiple functions: 1) the low surface energy methyl group, 2) the highly flexible siloxane backbone, and 3) the vinyl moiety that can be used as an attachment point for various chemistries (*cf.* Chapter 4). We incorporated this design flexibility into our research by: 1) synthesizing various molecular weight PVMS with reactive end-groups for subsequent network formation, 2) utilizing alkoxy-condensation cure chemistry for network formation that would allow us to later react the vinyl moieties, and 3) modifying PVMS with hydrophilic and hydrophobic functionalities.

3.5 Surface Reconstruction and Reversibility

Our initial observations of reversible PVMS siloxane surfaces was demonstrated with deionized water contact angle (θ_{DIW}) measurements[26]. As the vinyl group has a slightly higher surface energy than methyl group, it hides beneath the surface when exposed to hydrophobic environments, such as air. Exposure to water leads to a rearrangement of the surface moiety make-up as the preferred state is orientation of the vinyl groups at the surface, as illustrated in Figure 3.6. As contact angle measurements are sensitive to just the first ≈5 Å of the polymer surface[13], the composition rearrangement can be observed by time-dependent contact angle measurements and utilized to characterize response kinetics of modified and unmodified PDMS and PVMS surfaces. In Figure 3.7 we plot the water contact angle ($d\theta_{DIW}$) on model PDMS network (■), Sylgard-184 (□) and PVMS (●) as a function of exposure time to a water droplet. In all three cases, there is a linear decrease in the contact angle with increasing time. We noticed that the volume drop size was changing throughout

the experiment. Detailed analysis of the data revealed that while the drop diameter remained essentially unchanged, there was a steady decrease in the height of the drop. We thus attributed this behavior to the evaporation of water from the probing droplet. Although this drop in contact angle is a common factor with the 3 substrates, the PVMS surface behavior is noticeably different from the two PDMS networks. The data in Figure 3.7 reveal that contact angle decreases very rapidly in first 20 seconds from the moment of drop application time for PVMS and then continues to decrease much more slowly in the common linear fashion. The rate of change of contact angle with time ($d\theta_{DIW}/dt$) plotted in Figure 3.8 as a function of water exposure time was found to be constant for both model PDMS and Sylgard-184 networks. In contrast, the PVMS data clearly indicate the existence of two wettability regions. Initially, $d\theta_{DIW}/dt$ changes very rapidly and then saturates. We attribute the

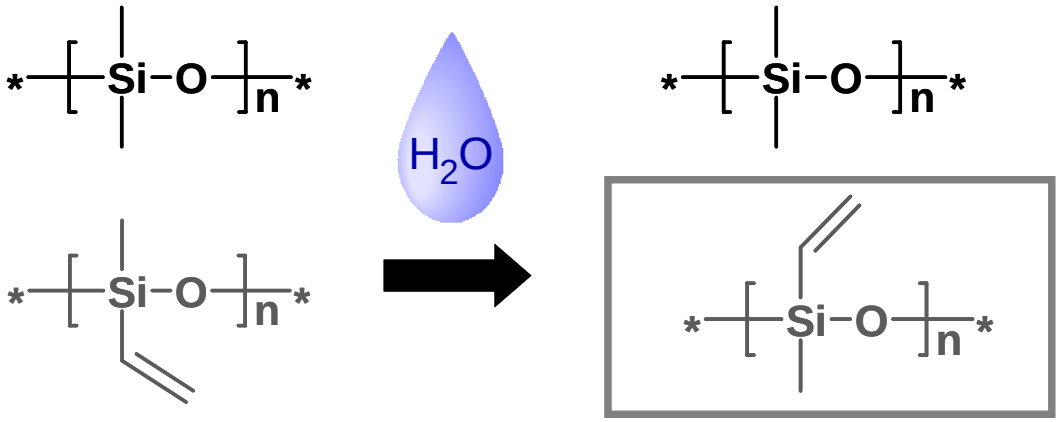

Figure 3.6: Illustration of the differences in surface rearrangement between PDMS and PVMS elastomers. The vinyl moiety has a higher affinity for water relative to the methyl group thus "flipping" to the surface after water exposure.

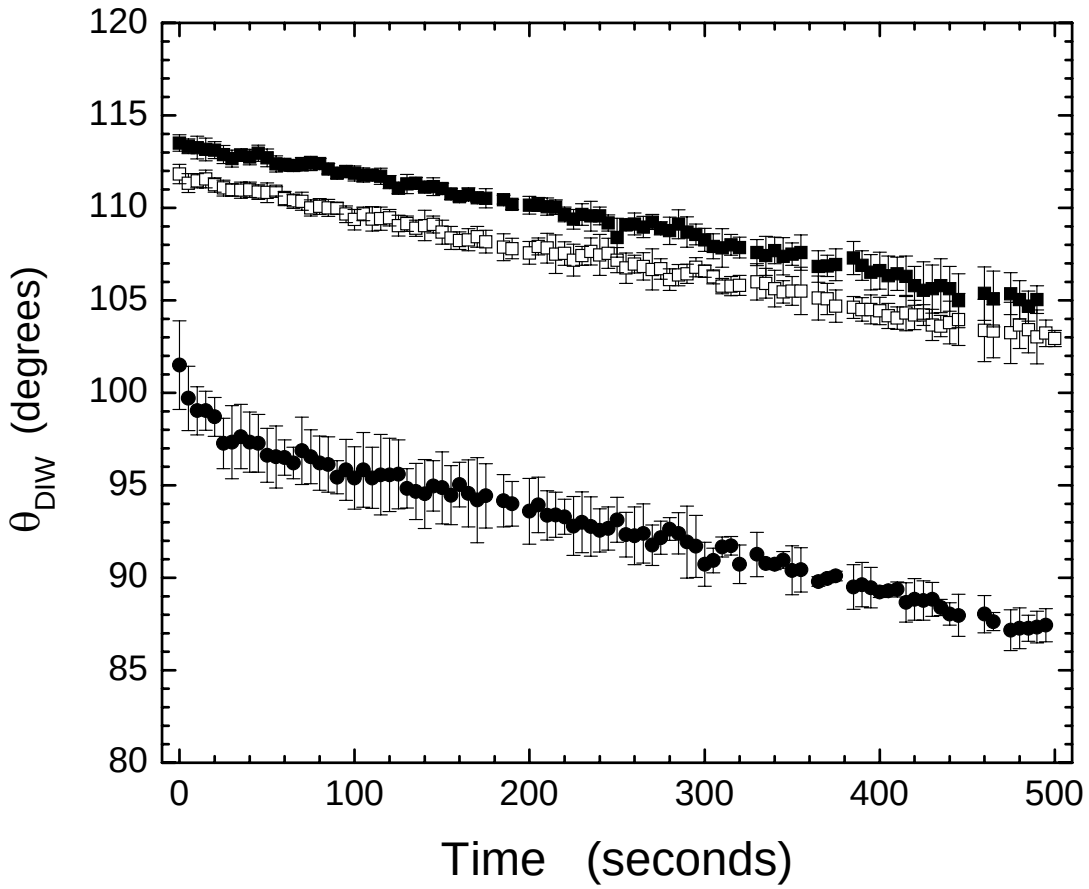

Figure 3.7: Time dependence of water contact angle measured on model PDMS networks (■), Sylgard-184 networks (□), and bare PVMS networks (●). The error bars represent an average over 3 measurements performed on three different areas of the same sample.

observed effects to the following behavior. As water comes into contact with the PVMS surface, the system minimizes its free energy by replacing the hydrophobic methyl groups with higher-surface energy vinyl moieties at the PVMS/water interface. The rapid decrease in the contact angle recorded at the short exposure times can thus be associated with the aforementioned rearrangements of the functionalities on the surface; the rapid rate of the response is a consequence of the high flexibility of the Si-O backbone.

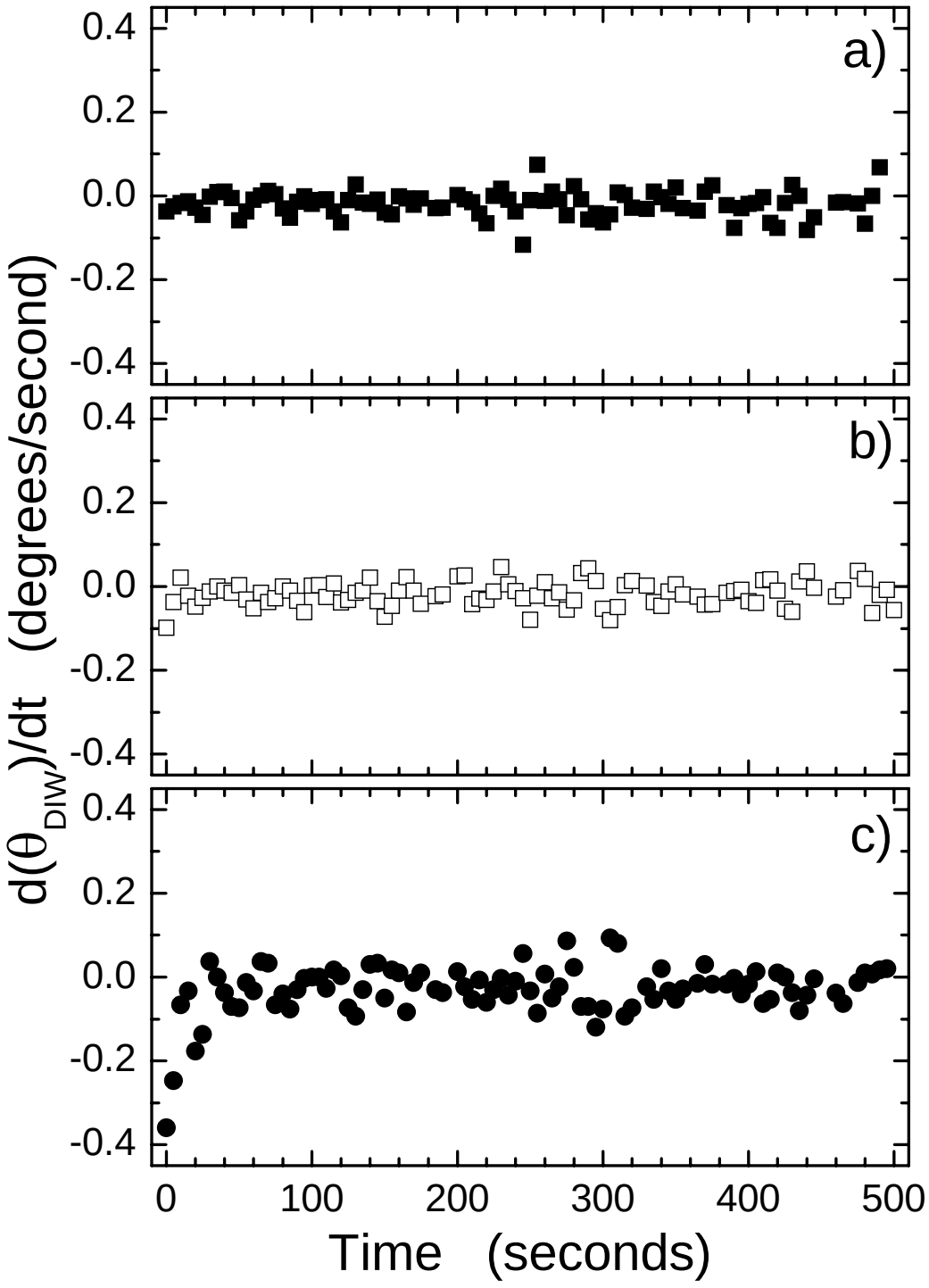

Figure 3.8: Change of the contact angle with increasing time for model PDMS networks (a, ■), Sylgard-184 networks (b, □), and bare PVMS networks (c, ●).

3.6 Rapid Formation of Hydrophilic Surfaces

To further accentuate the difference in surface energy effects, we modified the vinyl moiety on the PVMS substrate by two separate methods; 1) UVO exposure (PVMS-UVO) and 2) through a thiol-ene addition reaction (*cf*. Chapter 4). Similar to our work with Sylgard-184, we studied the mechanism of surface modification of PVMS-UVO via static contact angle, FTIR-ATR, NEXAFS, and AFM[26]. As mentioned earlier, modification to PVMS with UVO would be much more efficient as the strained vinyl functionality is activated more easily than the more stable Si-O and Si-C bonds[26,27]. We confirmed this with the FTIR-ATR experiments, as the signature Si-O-Si peak (1055-1090 cm^{-1}) remained unchanged after UVO exposure. In contrast, the PDMS UVO-exposed samples showed a distinct decrease in the Si-O-Si peak intensity indicative of chain scission. Comparing the wettability of the treated samples as a function of UVO exposure time (*cf.* Figure 3.8), revealed that treatment times of 300 seconds resulted in water contact angles of 62˚. In addition, comparisons of surface and bulk modulus measurements revealed that the PVMS elasticity was essentially unchanged after 2 minutes of UVO treatment[26]. As the resulting shorter UVO treatment times for PVMS (an order of magnitude lower as compared to PDMS) give rise to a considerably reduced modification to the bulk modulus, we could produce very flexible networks capable of rapid surface rearrangement under appropriate conditions. This is demonstrated in Figure 3.9; the water contact angle was seen to decrease between 20-50˚ per given substrate. Although not completely evaluated, the variation in the rate of change between these substrates was attributed to differences in surface modulus of the substrate under evaluation. Hence, if we could keep the flexibility of the PVMS

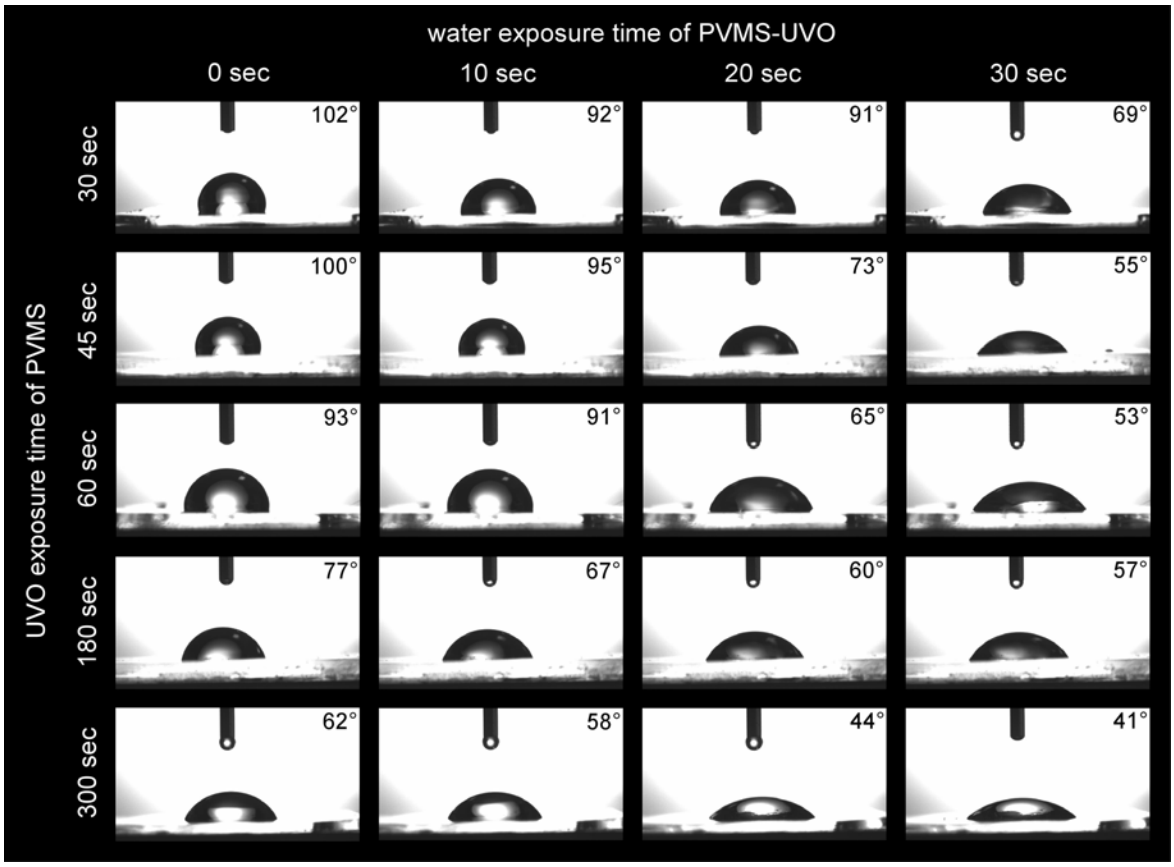

Figure 3.9: Images of water droplet spreading on PVMS-UVO surfaces treated for various UVO times (ordinate) collected at various time intervals after depositing the droplet (abscissa). The numbers indicate the water contact angle that was evaluated from the images of the water droplets. Copyright © 2005 Elsevier Ltd All rights reserved[26].

backbone intact during modification, then obtaining rapid reorientation of the surface to its preferred configuration is possible. By investigating the kinetics of surface restructuring utilizing the capability to functionalize PVMS, we gained an understanding of the transition between a repeatable responsive surface and a surface with an inferred stable chemistry.[28]

3.7 Conclusion

In this chapter we have provided an overview on responsive surfaces, and discussed how the surface reorganization can be dependent on the bulk polymer as well as the surface polymer's glass transition temperature, and the preferred orientation of hydrophilic versus hydrophobic functional groups. We introduce siloxane networks as a novel platform of substrates capable of rapidly reorganizing in the presence of polar media. In Appendix 3.1, we provide the details of our polymer synthesis and how we quantified it overall molecular weight. In comparison to PDMS networks, our results indicate that PVMS has great potential for creating smart and responsive surfaces.

3.7 References

1. Luzinov, I., Minko, S. & Tsukruk, V. V. Adaptive and responsive surfaces through controlled reorganization of interfacial polymer layers. *Progress in Polymer Science* **29**, 635-698 (2004).

2. Russell, T. P. Surface-responsive materials. *Science* **297**, 964-967 (2002).

3. Galaev, I. Y. & Mattiasson, B. 'Smart' polymers and what they could do in biotechnology and medicine. *Trends in Biotechnology* **17**, 335-340 (1999).

4. Kasemo, B. Biological surface science. *Surface Science* **500**, 656-677 (2002).

5. Ellison, C. J. & Torkelson, J. M. The distribution of glass-transition temperatures in nanoscopically confined glass formers. *Nature Materials* **2**, 695-700 (2003).

6. Schwab, A. D., Agra, D. M. G., Kim, J. H., Kumar, S. & Dhinojwala, A. Surface dynamics in rubbed polymer thin films probed with optical birefringence measurements. *Macromolecules* **33**, 4903-4909 (2000).

7. Wallace, W. E., Fischer, D. A., Efimenko, K., Wu, W. L. & Genzer, J. Polymer chain relaxation: Surface outpaces bulk. *Macromolecules* **34**, 5081-5082 (2001).

8. Holmesfarley, S. R., Reamey, R. H., Nuzzo, R., McCarthy, T. J. & Whitesides, G. M. Reconstruction of the Interface of Oxidatively Functionalized Polyethylene and Derivatives on Heating. *Langmuir* **3**, 799-815 (1987).

9. Koberstein, J. T. Molecular design of functional polymer surfaces. *Journal of Polymer Science Part B-Polymer Physics* **42**, 2942-2956 (2004).

10. Carey, D. H. & Ferguson, G. S. Synthesis and Characterization of Surface-Functionalized 1,2-Polybutadiene Bearing Hydroxyl or Carboxylic-Acid Groups. *Macromolecules* **27**, 7254-7266 (1994).

11. Carey, D. H. & Ferguson, G. S. A smart surface: Entropic control of composition at a polymer/water interface. *Journal of the American Chemical Society* **118**, 9780-9781 (1996).

12. Carey, D. H., Grunzinger, S. J. & Ferguson, G. S. Entropically influenced reconstruction at the PBD-ox/water interface: The role of physical cross-linking and rubber elasticity. *Macromolecules* **33**, 8802-8812 (2000).

13. Bain, C. D. & Whitesides, G. M. Depth Sensitivity of Wetting - Monolayers of Omega-Mercapto Ethers on Gold. *Journal of the American Chemical Society* **110**, 5897-5898 (1988).

14. Jalbert, C., Koberstein, J. T., Yilgor, I., Gallagher, P. & Krukonis, V. Molecular-Weight Dependence and End-Group Effects on the Surface-Tension of Poly(Dimethylsiloxane). *Macromolecules* **26**, 3069-3074 (1993).

15. O'Rourke-Muisener, P. A. V., Koberstein, J. T. & Kumar, S. Optimal chain architectures for the molecular design of functional polymer surfaces. *Macromolecules* **36**, 771-781 (2003).

16. Dee, G. T., Ougizawa, T. & Walsh, D. J. The Pressure Volume Temperature Properties of Polyethylene, Poly(Dimethyl Siloxane), Poly(Ethylene Glycol) and Poly(Propylene Glycol) as a Function of Molecular-Weight. *Polymer* **33**, 3462-3469 (1992).

17. Jalbert, C. J. et al. Surface Depletion of End-Groups in Amine-Terminated Poly(Dimethylsiloxane). *Macromolecules* **27**, 2409-2413 (1994).

18. Elman, J. F., Johs, B. D., Long, T. E. & Koberstein, J. T. A Neutron Reflectivity Investigation of Surface and Interface Segregation of Polymer Functional End-Groups. *Macromolecules* **27**, 5341-5349 (1994).

19. Fleischer, C. A., Koberstein, J. T., Krukonis, V. & Wetmore, P. A. The Effect of End-Groups on Thermodynamics of Immiscible Polymer Blends .1. Interfacial-Tension. *Macromolecules* **26**, 4172-4178 (1993).

20. Lee, M. H., Fleischer, C. A., Morales, A. R., Koberstein, J. T. & Koningsveld, R. The effect of end groups on thermodynamics of immiscible polymer blends. 2. Cloud point curves. *Polymer* **42**, 9163-9172 (2001).

21. Wong, D., Jalbert, C. & Koberstein, J. T. Surface Reorganiztion Kinetics of a Model End-Funtionalized Polymer System. *Polymer Preprints* **39**, 901-902 (1998).

22. Anastasiadis, S. H., Retsos, H., Pispas, S., Hadjichristidis, N. & Neophytides, S. Smart polymer surfaces. *Macromolecules* **36**, 1994-1999 (2003).

23. Genzer, J. & Efimenko, K. Creating long-lived superhydrophobic polymer surfaces through mechanically assembled monolayers. *Science* **290**, 2130-2133 (2000).

24. Rouse, J. H., Twaddle, P. L. & Ferguson, G. S. Frustrated reconstruction at the surface of a glassy polymer. *Macromolecules* **32**, 1665-1671 (1999).

25. Sun, T. L. et al. Reversible switching between superhydrophilicity and superhydrophobicity. *Angewandte Chemie-International Edition* **43**, 357-360 (2004).

26. Efimenko, K. et al. Rapid formation of soft hydrophilic silicone elastomer surfaces. *Polymer* **46**, 9329-9341 (2005).

27. Efimenko, K., Wallace, W. E. & Genzer, J. Surface modification of Sylgard-184 poly(dimethyl siloxane) networks by ultraviolet and ultraviolet/ozone treatment. *Journal of Colloid and Interface Science* **254**, 306-315 (2002).

28. Crowe, J. A. & Genzer, J. Creating responsive surfaces with tailored wettability switching kinetics and reconstruction reversibility. *Journal of the American Chemical Society* **127**, 17610-17611 (2005).

Appendix 3.1 Generating PVMS networks—Materials and Methods.

A3.1 PVMS Synthesis

PVMS can be synthesized using either 1) ring opening polymerization (ROP); either thermodynamic equilibration or kinetically controlled, or 2) step-growth polymerization methods[1,2]. Equilibrium controlled ring opening polymerization is a common commercial route for synthesizing PDMS. It is a well-established process, in which the molecular weight of the resulting polymer is determined by the amount of chain end-terminators included in the starting formulation. Equilibrium yield of the siloxane linears depends on the substituents attached to the silicon atom (with the bulkier groups producing more cyclic monomer than polymer)[1]. Therefore, after equilibration it is necessary to remove the cyclics under reduced pressure and high temperature. Replacing a methyl group with a vinyl moiety on the silicon atom, however, increases susceptibility to high temperature oxidation that results in a cumbersome linear/cyclic separation[3]. While this limitation restricts commercial availability of higher molecular weight PVMS homopolymers, it still allows for limited production of such species on laboratory scale [4-6] via the steps illustrated in Scheme 3.1.

Our route to producing hydroxy-terminated PVMS utilizes the step-growth polymerization (Scheme 3.1, Method A). Short-chain silanols are condensed until reaching the desired polymer chain length. A typical reaction consisted of charging 500 grams of linear VMS silanols (Dow Corning PJ Fluid®) catalyzed with 10 ppm of lithium hydroxide (added as a 1% aqueous solution). Polymerization takes place at elevated temperatures (>100^{o}C), which facilitates the removal of water from the mixture. The lithium hydroxide is neutralized with glacial acetic acid at 1:1 molar basis or excess carbon dioxide and filtered

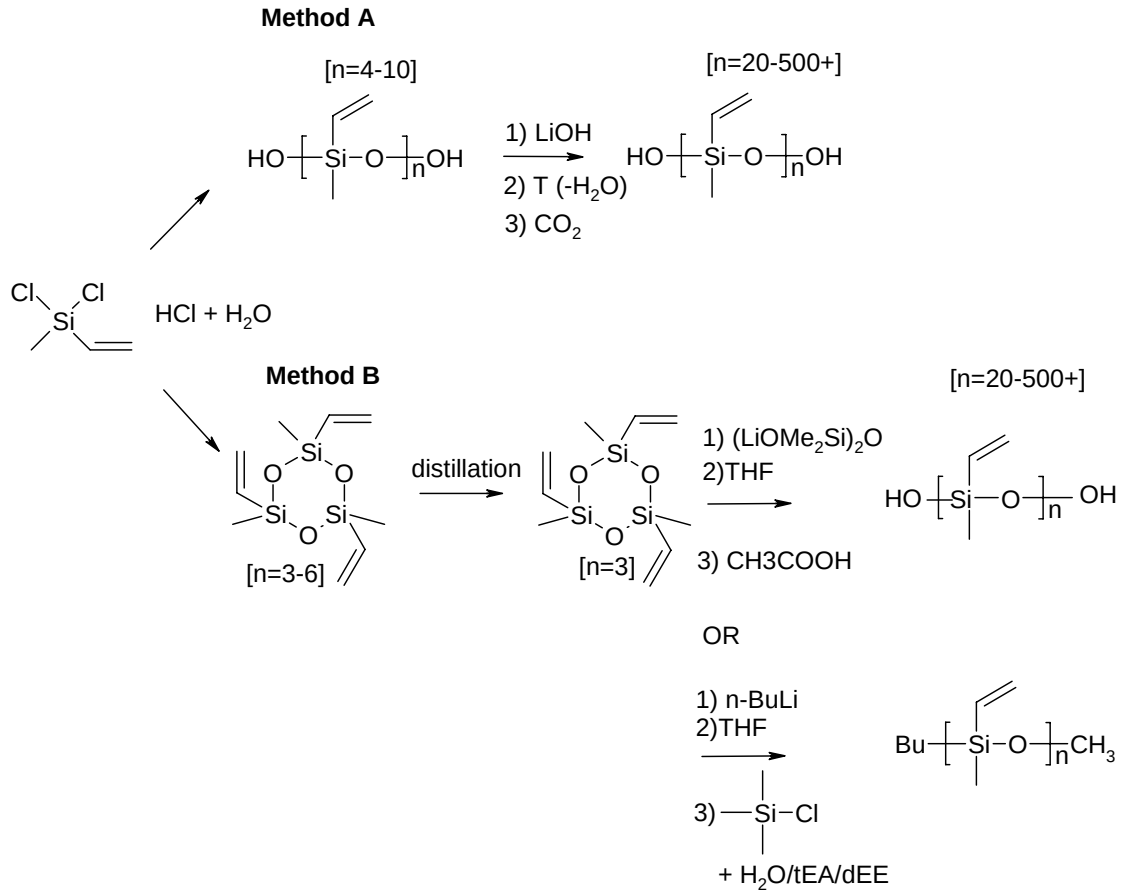

Scheme A3.1: Synthesis routes for poly(vinylmethylsiloxane). Method (A) is step-condensation polymerization and Method (B) is kinetically controlled anionic ring opening polymerization.

through a Superlite® filter cake. The advantages of this route include an available source of the short-chain silanols, almost a 98% yield of polymer, and the flexibility to obtain PVMS with different molecular weights.

The molecular weights of the synthesized PVMS ranged between 4.9-78.7 kDa with M_w/M_n of 1.5-3.0. Molecular weights were determined using gel permeation chromatography (GPC) with HPLC-grade toluene as a mobile phase. The GPC system was

equipped with three Styragel® 4.6 × 300 mm columns (models HR3, HR4, and HR4E, Waters Corporation, Milford, MA) for the polymer separation. The Optilab rEX (refractometer with EXtended range, Wyatt Technology, Santa Barbara, CA) was used as the concentration detector and a miniDAWN Tristar as the light scattering detector (Model WTR-02, Wyatt Technology, Santa Barbara, CA). With the intensity of light scattered and the absolute concentration measured, the molar mass is obtained. Polymer solutions with concentration of ≈2 mg/ml were prepared. The solutions were filtered to GPC sampling vials with 0.2 μm PTFE syringe filters. The GPC data was processed with ASTRA software

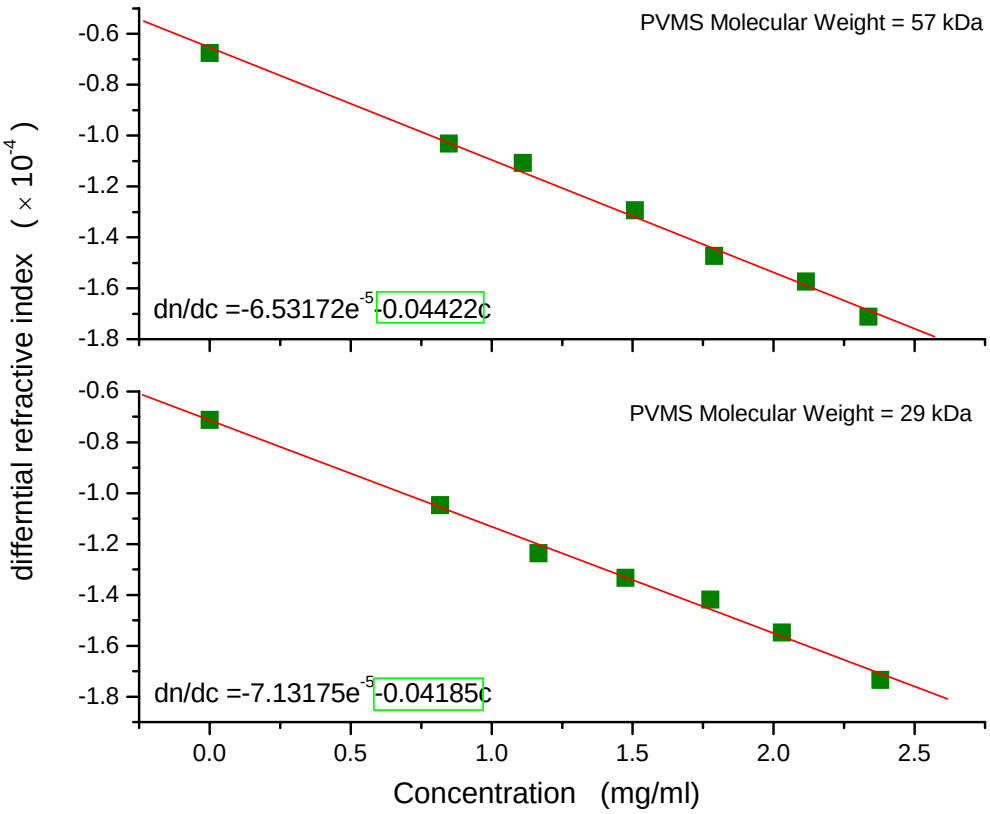

Figure A3.1: Differential refractive index (dn/dc) values for PVMS in HPLC-grade toluene.

(version 5.1.9.1, Wyatt Technology, Santa Barbara, CA).

As the dn/dc of PVMS was not available in the literature, we determined it by preparing exact solutions with concentrations ranging from 0-2.5 mg/ml of polymer in HPLC-grade toluene. Two different batches of PVMS were selected for testing with the defractometer. The dn/dc value is the slope of the DRI versus concentration as shown in Figure A3.1. As there appears to be a slight molecular weight dependence on the dn/dc value, samples were analyzed as deemed appropriate in ASTRA.

An example PVMS run with changing molecular weights is shown in Figure A3.2 where the final molecular weight of the polymer was determined to be ≈45 kDa after 6 hours at ≈110^{o}C (*cf.* Table A3.1). The kinetics of the reaction depends on the lithium hydroxide concentration and activity as well as the starting material (Dow Corning PJ Fluid®) quality. Light scattering indicates a higher molecular weight peak in the final sample; this is a signature of an agglomerate/gel that occurs with long reactions times and does not contribute greatly to a an overall higher molecular weight as the reaction rates slow down with time.

Table A3.1 Properties of PVMS polymers whose trace scans are show in Figure A3.2

Trace	Reaction Time (hours)	M_w (kDa)
A	1	1.50
B	2	17.00
C	2.5	23.40
D	3	29.34
E	3.5	38.60
F	6	45.37

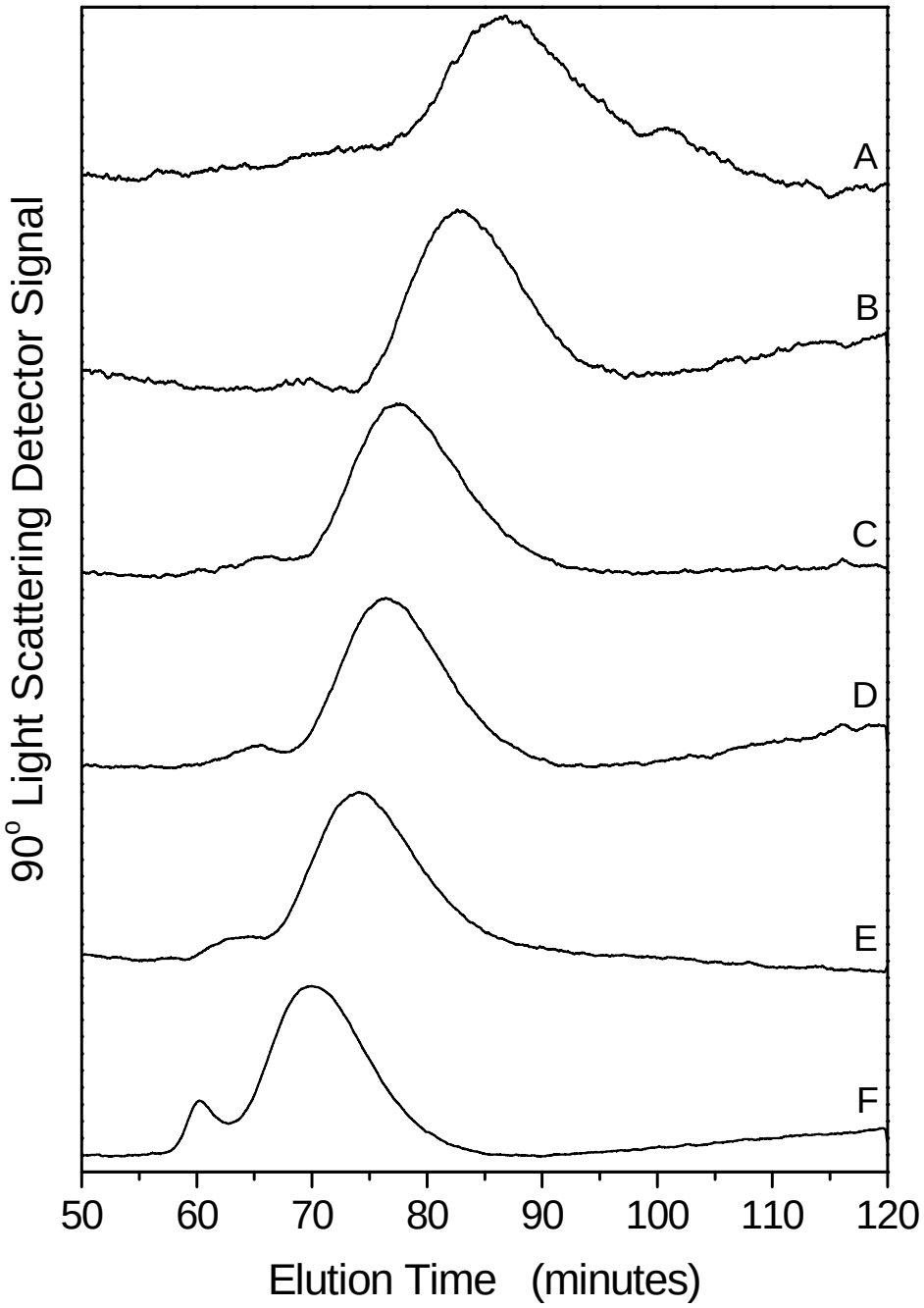

Figure A3.2: GPC traces for the 90° light scattering detector for a typical run of PVMS during the step-condensation process of vinyl methyl silanols. Molecular weight for each trace is listed in Table 3.1. Average polydispersity index is 3.0.

A3.2 PVMS Network Formation

Chemical cross-linking of siloxanes can be accomplished with four types of common commercial reactions[7]: 1) peroxide-induced free radical, 2) condensation reactions, 3) hydrosilylation addition reactions, and 4) hydridosilane/silanol reactions. In order to gain control over the cross-link densities and preserve the active vinyl group along the PVMS backbone, we utilize the condensation (or alkoxy-cure) reaction route that entails linking hydroxyl-terminated siloxanes with tetraethoxysilane (TEOS) in the presence of tin catalyst. This procedure results in a model tetrafunctional network, where the "liquid" nature of the siloxane backbone between junction points remains intact[8].

Our PVMS networks were formulated as previously described with the 36.3 kDa (M_w/M_n=2.25) polymer[9]. In addition, PDMS networks were prepared by cross-linking 1) monodisperse PDMS chains by following reported procedures[8,10] and by utilizing the commercial Sylgard-184 kit (Dow Corning). All other chemicals were obtained from Sigma-Aldrich Chemicals and used as received.

A3.3 Surface Reorientation

Advancing contact angles were monitored as a function of time to access the chain reorientation at the PVMS film surfaces. The contact angle (sessile drop technique) experiments were performed with deionized (DI) water (R>15 MΩ·cm) using a Ramé-Hart contact angle goniometer (model 100-00) equipped with a CCD camera, and analyzed with the Ramé-Hart Imaging 2001 software. The advancing contact angles θ_a were recorded as a

function of time (with 5 second increments for 5 minutes) after depositing 8 μL of the probe liquid on the substrate (the error in $\theta = \pm 1.5°$).

A3.4 References

1. Chojnowski, J. in *Siloxane Polymers* (ed. Semlyen, J. A.) 216-244 (PTR Prentice Hall, Englewood Cliffs, New Jersey, 1993).

2. Brook, M. A. in *Silicon in Organic, Organometallic, and Polymer Chemistry* 261-273 (John Wiley & Sons, Inc., New York, 2000).

3. Ziemelis, M. J. & Saam, J. C. Sequence Distribution in Poly(Dimethylsiloxane-Co-Methylvinylsiloxanes). *Macromolecules* **22**, 2111-2116 (1989).

4. Suzuki, T. & Okawa, T. Poly(dimethylsiloxane) macromonomers having both alkenyl and polymerizable groups. Application to crosslinkable copolymers. *Polymer* **29**, 2095-2099 (1988).

5. Chojnowski, J., Cypryk, M., Fortuniak, W., Rozga-Wijas, K. & Scibiorek, M. Controlled synthesis of vinylmethylsiloxane-dimethylsiloxane gradient, block and alternate copolymers by anionic ROP of cyclotrisiloxanes. *Polymer* **43**, 1993-2001 (2002).

6. Cai, G. P. & Weber, W. P. Synthesis and chemical modification of poly(divinylsiloxane). *Polymer* **43**, 1753-1759 (2002).

7. Clarson, S. J. in *Siloxane Polymers* (ed. Semlyen, J. A.) 567-517 (PTR Prentice Hall, Englewood Cliffs, New Jersey, 1993).

8. Clarson, S. J. in *Silicon-Containing Polymers* (ed. Chojnowski, J.) 185-212 (Kluwar Academic Publishers, Dordrecht, 2000).

9. Efimenko, K. et al. Rapid formation of soft hydrophilic silicone elastomer surfaces. *Polymer* **46**, 9329-9341 (2005).

10. Efimenko, K., Wallace, W. E. & Genzer, J. Surface modification of Sylgard-184 poly(dimethyl siloxane) networks by ultraviolet and ultraviolet/ozone treatment. *Journal of Colloid and Interface Science* **254**, 306-315 (2002).

CHAPTER 4: Modified PVMS Surfaces

4.1 Introduction

In Chapter 3 of this Ph.D. Thesis we introduced the definition of responsive surfaces, outlined the inherent advantages of a siloxane network with regards to responsiveness, and described how the different surface energies of the methyl compared to the vinyl substituent in poly(vinylmethylsiloxane) (PVMS) gave rise to unusual time-dependent behavior of the water contact angle on PVMS surface. Although it was apparent that surface reorganization occurred with respect to the changing slope of $d\theta_{water}/dt$, it constituted only a small change in surface energy. Here we improve on the responsive nature of PVMS surfaces by grafting amphiphilic moieties on the silicone elastomer backbone. We provide evidence that the combination of the high flexibility of the silicone elastomer chain and the amphiphilic nature of the side groups endows these materials with exceptionally fast surface reconstruction kinetics and a high degree of repeatability. In particular, we show that the advantage of utilizing the PVMS network is that the vinyl ($-CH=CH_2$) group present on the siloxane backbone can be chemically modified in various ways, including:

- Chemical oxidization to form either alcohol or carboxylic acid moieties with subsequent chemical grafting of organosilanes at the generated hydroxyl sites [1,2].
- Direct attachment of the desired functionality through addition reactions such as hydrosilation, hydrosulfidation, hydrophosphination, epoxidation, and alkyl halide addition reactions [3-6].

In the past, the modification of a vinyl substituent on the siloxane backbone via a thiol-

ene reaction had been successfully carried out by both by Ferguson's and Chojnowski's groups [1,7]. Bulk modification allowed for detailed characterization of the synthesized polymer, a process that is critical for understanding the attachment mechanism [8-11]. Amphiphilic block siloxane copolymers synthesized by Chojnowski et al. transformed >90% of the pendant vinyl groups with the free radical addition of mercaptoacetic acid. It has been demonstrated that the reaction follows the anti-Markovnikov rule resulting in the β-adduct copolymers [8,11]. We used this modification process for modifying our PVMS networks and carrying out subsequent physico-chemical analysis.

4.2 Thiol-ene Addition Reaction on PVMS networks

Implementing a route similar to Chojnowski's method[12], we modified PVMS substrates with 11-dodecanethiol ($HS(CH_2)_{11}CH_3$) and 3-mercaptopropionic acid ($HS(CH_2)_2COOH$). The addition to the vinyl bond was confirmed via the elimination of the C=C peaks at 960, 1407, and 1587 cm^{-1} in ATR-FTIR spectroscopy. In Figure 4.1 we plot the FTIR-ATR data for the 11-dodecanethiol addition to PVMS. The results indicate a high conversion to the alkane groups; the peaks corresponding to the vinyl group in the modified samples were absent after the thiol-ene reaction. The surface composition variation in thiol-ene modified-PVMS samples was also confirmed by a change in the water contact angle. The dodecane group is more hydrophobic than the methyl group, as is apparent in the water contact angle shift of $\approx 105^{o}$ before modification to $\approx 125^{o}$ after modification (*cf.* Figure 4.1). Note that the thiol-ene reaction with 11-dodecanethiol took place in the bulk siloxane fluid. This modified PVMS fluid was subsequently cross-linked through its hydroxyl end-groups. The high water

contact angle (≈125˚) of the PVMS-S-$(CH_2)_{11}CH_3$ substrate is likely due to both the hydrophobicity of 11-dodecane thiol and the inherent roughness of cross-linking such a heavy substituted siloxane chain.

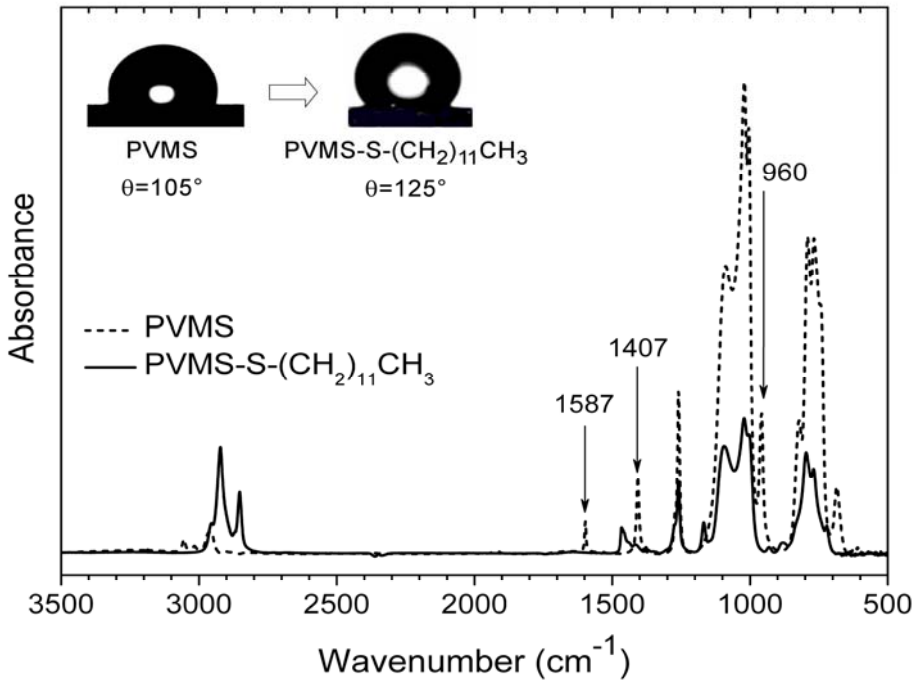

Figure 4.1: ATR-FTIR spectra of bare PVMS (dashed line) and PVMS after thiol-ene addition of 1-dodecanethiol, PVMS-S-$(CH_2)_{11}CH_3$ (solid line). The PVMS network was prepared by cross-linking PVMS chains (MW = 39 kDa) with a 70% excess of TEOS cross-linker. Vinyl peaks at 960, 1407, and 1587 cm^{-1} in the thiol-ene modified sample are not present. The inset shows photographs of water droplets on PVMS and PVMS-S-$(CH_2)_{11}CH_3$ samples.

Obtaining dual-responsiveness of the opposing substituent groups requires a situation as illustrated in Figure 4.2 for the carboxy-functionalized siloxane substrate. When the surface is exposed to air, the methyl groups populate the air-siloxane interface. Exposing the substrate to water repels the methyl groups from the surface and attracts the carboxy-groups in their stead to maximize the polar interactions. To confirm that the thiol-ene addition

modification resulted in a dual-energy surface, time-dependent water contact angle measurements were performed at room temperature. The results are presented in Figure 4.3 for PVMS, PVMS-S-$(CH_2)_{11}CH_3$, and PVMS-S-$(CH_2)_2COOH$. After three minutes of exposure to the probing water droplet, the PVMS-S-$(CH_2)_{11}CH_3$ substrate became less hydrophobic; the contact angle changed from ≈125° to ≈115°. In contrast, the high energy PVMS-S-$(CH_2)_2COOH$ substrate responded almost instantaneously to water exposure with a 2° per second drop in contact angle. This very fast response is attributed to both the high flexibility of the polymer backbone and the large chemical disparity between the methyl and

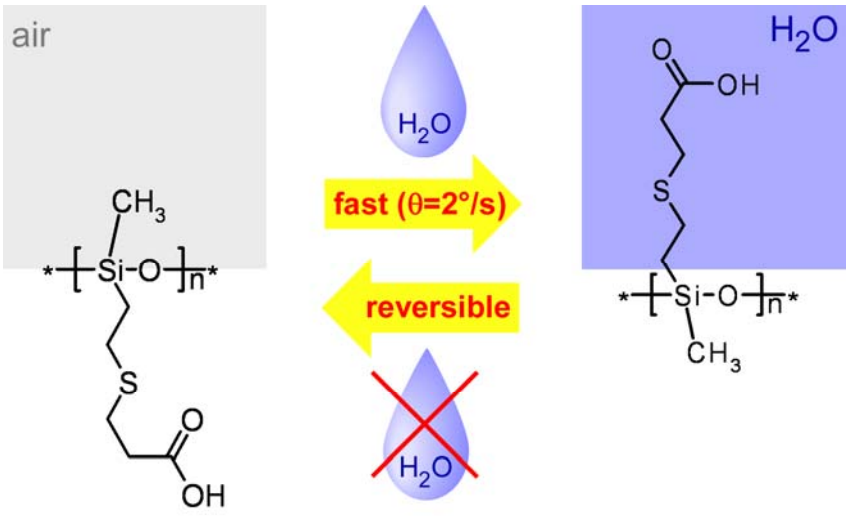

Figure 4.2: Illustration of the reversible nature of a dual-energy siloxane substrate. When the –COOH functionalized surface is exposed to water, the –COOH reorient to the surface to maximize their contact with water. Removal from the aqueous environment returns the substrate to the original state.

carboxylic acid groups.

Surfaces with fast and reversible reconstruction are needed for designing materials with real-time switchable behavior. Other researchers observed that reversibility disappeared after

several switching cycles [13-17]. In order to return the material to the original surface composition, another stimulus, such as temperature, has to be applied [2]. We postulated that as barriers to rotation for the siloxane backbone are very low, the PVMS network would easily reorient in a new media to favor the lowest energy state. We observed this behavior during a reversibility study with the PVMS-S-$(CH_2)_2$COOH surface in contact with the water droplet. After the first cycle of rapid surface reorientation, we removed the water droplet via adsorption by a Kim-wipe®. The surface was dried with a stream of nitrogen and allowed to

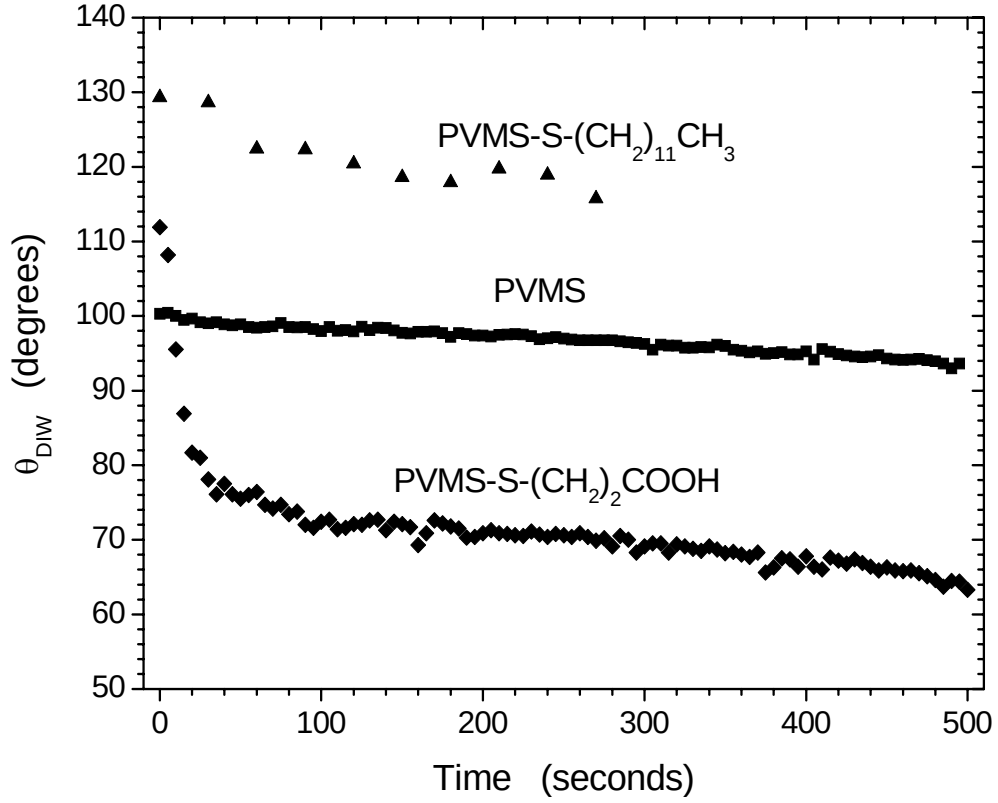

Figure 4.3: Time-dependent water contact data for PVMS substrates (Molecular weight is 39 kDa, *R*=1.7 moles of cross-linker/moles of polymer): bare PVMS (■), 1-dodecanethiol-modified PVMS (PVMS-S-$(CH_2)_{11}CH_3$, ▲), and 3-mercaptopropionic acid modified PVMS (PVMS-S-$(CH_2)_2$COOH, ◆). Average error in contact angle measurement is ±1.5 degrees.

rest in ambient conditions for 3-5 minutes. At this point we applied another water droplet to the same location on the surface. Excellent reversibility was observed (*cf.* Figure 4.4) as the surface was able to return to its original hydrophobic state, indicating that: 1) residual water was removed from the surface as contact angles exceeding 110^{o} would be difficult to obtain otherwise, 2) the -S-$(CH_2)_2$COOH moieties easily reoriented beneath the surface upon removal of the water drop, and 3) returned to the surface when exposed to additional water. The data in Figure 4.4 indicate that the reversible behavior may be dampening as the third cycle's starting contact angle was 1-2^{o} less and ended with the lowest contact angle of the three sets (≈55^{o}). We note that the wait-time between cycling was 3 minutes versus 5 minutes for this set and planned additional systematic reconstruction studies to more thoroughly characterize the reversibility behavior.

We now compare the reorientation kinetics detected in our PVMS-based materials to that reported previously for other systems. For example, oxidized polyethylene reoriented only at elevated temperatures due to its high T_g. While it restructured to its hydrophobic state in vacuum at 100ºC within a few minutes, our PVMS-S$(CH_2)_2$COOH responded in seconds at room temperature [2]. Fluorine-terminated polystyrene exposed to a saturated humid environment decreased 10º in water contact angle [18] after ten days of contact time. The surface segregation of polyisoprene in PS-b-PI-$(CH_2)_3N(CH_3)_2$ occurred after annealing the surface for 24 hours at 170º (above the T_g) and the dimethylamine end group reoriented only after 6-10 days of humidity exposure [19]. Oxidized 1,2 polybutadiene took hours to oscillate between hydrophobic and hydrophilic surfaces when relying solely on contacting media effects at room temperature but did respond within minutes to heated water [14]. To our

knowledge, the observed reorientation kinetics of PVMS-S-$(CH_2)_2$COOH thus possesses the fastest responses ever reported for any polymeric surface.

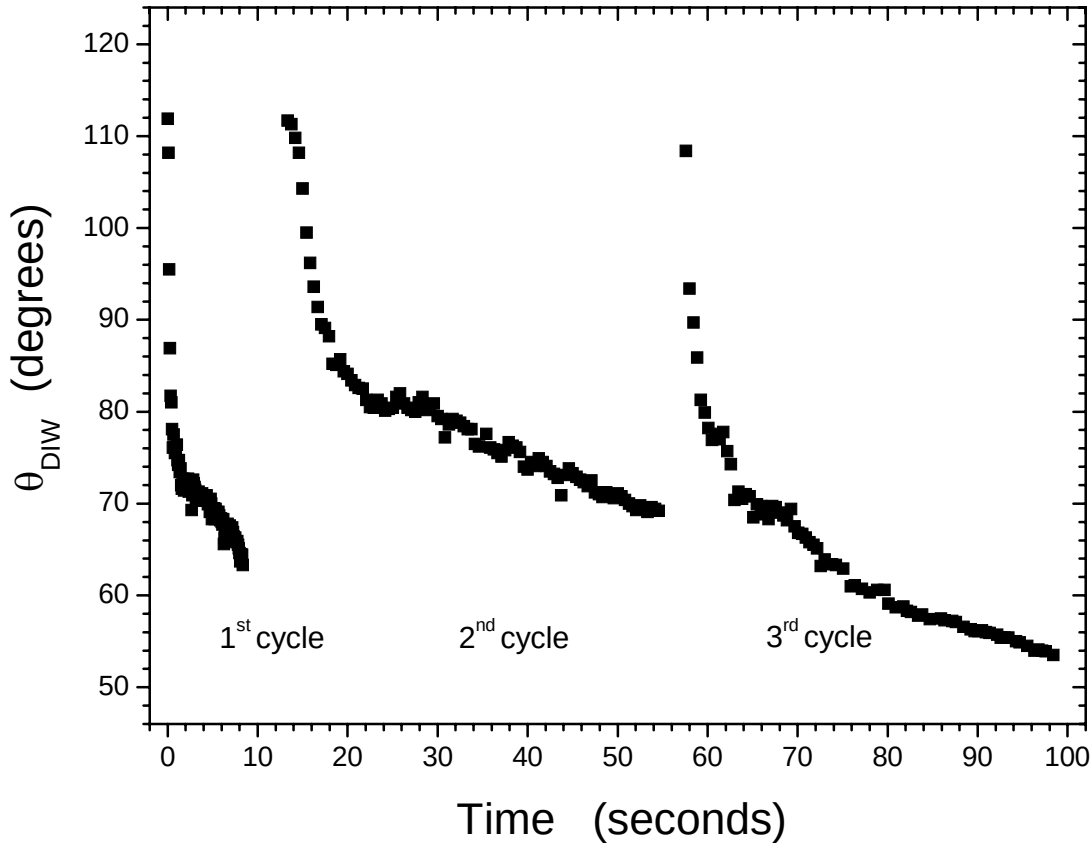

Figure 4.4: Ability of PVMS-S-$(CH_2)_2$COOH to reverse its wettability behavior.

4.3 Tailored Wettability Switching Kinetics and Reconstruction Reversibility

Inspection of the data for the PVMS-S-$(CH_2)_{11}CH_3$ substrate in Figure 4.3, indicates its loss of hydrophobicity after exposure to water as the methyl groups have a higher surface energy compared to the 11-dodecanethiol substituents. While the surface reconstruction occurs, it does so at a slower rate than for the PVMS-S-$(CH_2)_2$COOH substrate. This

behavior was attributed to the difference in the methylene spacers where a -$(CH_2)_{11}$- spacer would be more sluggish to rearrange than a shorter -$(CH_2)_2$- spacer. In order to comprehend the mechanism of surface rearrangement, we chemically grafted mercaptoalkanols with methylene spacers having a variable length[20]. Evaluating the surface response of mercaptoalkanols versus mercaptoalkanoic acids eliminated any possible complications of acid-base interactions due to the carboxy groups [2,21,22]. As done previously, we study the surface rearrangement kinetics by monitoring wettability changes using both static and dynamic contact angle measurements. To further characterize surface reconstruction in the mercaptoalkanol-modified PVMS substrates, we exposed the specimens to alternating wet and dry cycles utilizing dynamic contact angle measurements to study hysteresis in the surface reorganization. As documented below we demonstrate that increasing the number of methylene spacers in the mercaptoalkanols leads to slower reorganization kinetics and eventual loss of surface switching due to the tendency of these side groups to form semi-crystalline domains at the surface[23-25].

4.3.1 Modification of PVMS with Mercaptoalkanols

PVMS sheets were modified with three different mercaptoalkanols: $HS(CH_2)_2OH$, $HS(CH_2)_6OH$, and $HS(CH_2)_{11}OH$. In Figure 4.5 we compare the static contact angle of deionized (DI) water (θ_{DIW}) as a function of time for each mercaptoalkanol-modified PVMS surface. PVMS-S-$(CH_2)_2OH$ exhibited a very fast drop in contact angle upon exposure to water ($\Delta\theta_{DIW} \approx 35^{\circ}$). In contrast, PVMS-S-$(CH_2)_{11}OH$ revealed only a modest change in contact angle ($\Delta\theta_{DIW} \approx 7^{\circ}$). This rather "sluggish response" of PVMS-S-$(CH_2)_{11}OH$ upon

exposure to water is attributed to a reduced mobility of surface-bound $-(CH_2)_{11}-$ side chains due to characteristic semi-crystalline behavior. This behavior is inferred from a ≈10-fold increase in the storage modulus, a transition from a liquid-like to a semi-crystalline-like state established by infrared spectroscopy, and a transition from transparent to opaque state. These results will be discussed in greater detail in section 4.4.

While the PVMS-S-$(CH_2)_2$OH and PVMS-S-$(CH_2)_6$OH surfaces initially displayed fast

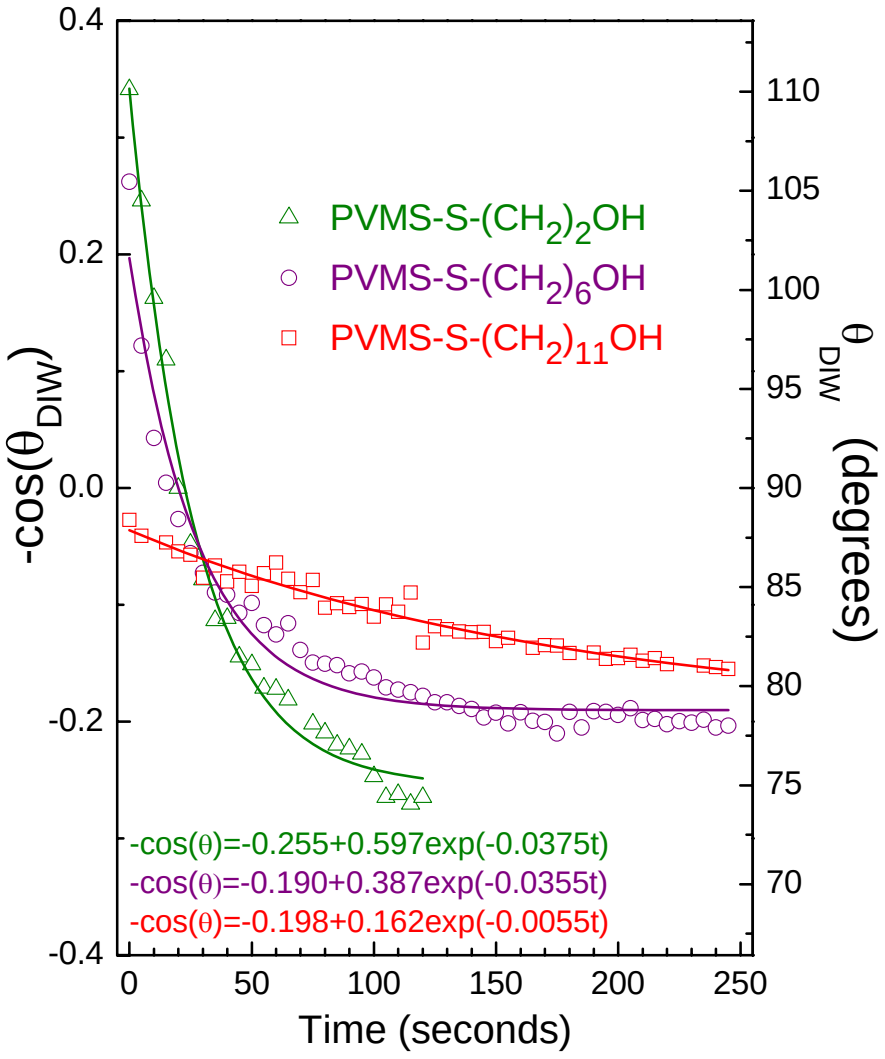

Figure 4.5: Time dependence of the deionized water wettabilities for PVMS-C_n-OH surfaces[20]. The error for θ_{DIW} is ±1.5˚.

surface reorientation kinetics after water exposure, it is the repeatability of the cycling behavior between wet and dry states that critically determines the viability of these surfaces as stimuli-responsive materials. We utilized a Cahn^{TM} Dynamic Contact Analyzer (DCA) to measure wettability cycling with minimal sample handling. As Figure 4.6 illustrates, each cycle consisted of placing a nitrogen-purged rectangular ($\approx 10 \times 10 \times 1$ mm^3) PVMS slab above a beaker containing DI water at room temperature (Stage 1). The DCA stage was raised at a rate of 80 μm/second until the detection of the water-substrate interface (Stage 2). At that point, the stage was advanced for 3 mm, held for 8.5 minutes (Stage 3), and returned to its original position. The total water contact time was 9 minutes for each cycle. During each cycle, the DCA recorded the total force acting on the sample (F_t). F_t is related to contact angle through:

$$F_t = mg + P \cdot \gamma_{DIW} \cdot \cos\theta_{DIW} + V_s \cdot \rho_{DIW} \cdot P \quad , \qquad (4.1)$$

where mg is the gravitational force zeroed out by taring the balance prior to the cycle run, P is the wetted sample perimeter, γ_{DIW} is the surface tension of DI water, V_s is the volume of the solid immersed in water, and ρ_{DIW} is the DI water density. This technique facilitates measurement of advancing and receding contact angles as well as the change in contact angle during the sample hold-time. Since the immersed volume of the sample remains constant during the hold-time, only the wetting force ($P \cdot \gamma_{DIW} \cdot \cos\theta_{DIW}$) changes as a function of time due to the surface reconstruction. After the completion of each cycle, the sample was blow-dried with nitrogen gas and another cycle was commenced. The lapse time between two consecutive cycles was ≈7 minutes; ten wettability cycles were carried out for each sample.

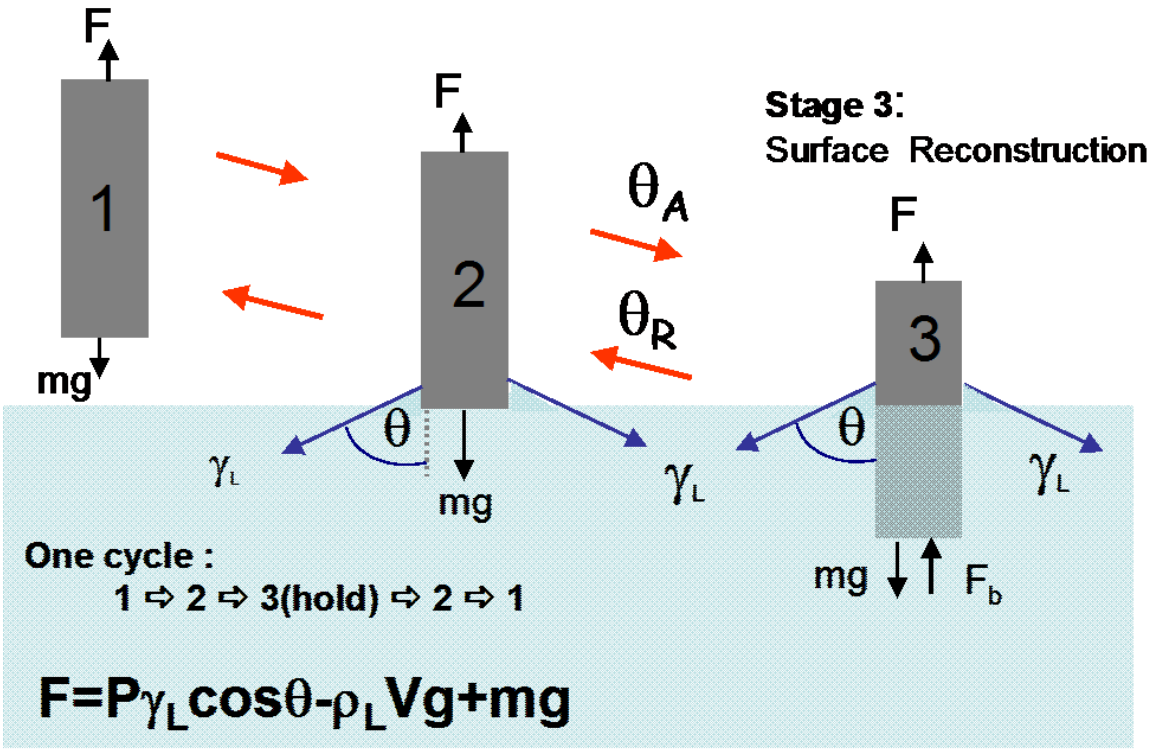

Figure 4.6: Illustration of dynamic contact angle method. The surface reconstruction occurs during stage 3 where the wetting force can be isolated due to negligible volume changes and zeroing the balance to eliminate the gravitational force from the measurement.

Figure 4.7 depicts cycling wettabilities measured for unmodified PVMS and PVMS-S-$(CH_2)_nOH$; one cycle represents an average of all measurements carried out on three separate specimens. For PVMS, the repeated oscillations displayed only minute changes in surface wettability, in agreement with previous findings [12,26,27]. For PVMS-S-$(CH_2)_2OH$ and PVMS-S-$(CH_2)_6OH$, the repeated DCA oscillations demonstrate a close compliance with the static contact angle results. The difference between contact angles of the dry and wet states for PVMS-S-$(CH_2)_6OH$ was consistent through all cycles with only a slight decrease in starting contact angle. PVMS-S-$(CH_2)_2OH$ cycles were even more repeatable with little sign of any

dampening behavior. This substrate exhibited the largest change in contact angle and displayed a greater starting hydrophobic value after the initial cycle. Since this chain possesses the shortest methylene linker, the flexibility of the siloxane backbone remained intact, thus allowing for the restructuring to occur rapidly between the methyl and 3-mercaptoethanol substituents. The behavior of PVMS-S-$(CH_2)_{11}OH$ was more complex. While we observed an initial surface reorientation after the 1st water-dipping cycle, the surface 'froze" in the hydrophobic state during all subsequent cycles. We attempted to recover the original hydrophilic response of PVMS-S-$(CH_2)_{11}OH$ by exposing the specimens to hot water (95˚C) for 60 minutes. After the heat-treatment, the surface reorientation was frozen by immersion in 25˚C water and dried with nitrogen. This surface reoriented to a stable, more hydrophilic surface ($\theta \approx 80^{\circ}$). Continued monitoring of the specimen revealed a slow reconstruction to the hydrophobic state ($\theta \approx 96^{\circ}$) after exposure to air for several days. We note that it was possible to quickly restructure the surface to a starting contact angle of $\approx 105^{\circ}$ if the sample was heated in water and allowed to slowly air-cool in air versus quenching in 25˚C water. This result is consistent with the findings of Carey [1] and Holmes-Farley [2] for surface restructuring of oxidized polybutadiene and oxidized polyethylene, respectively.

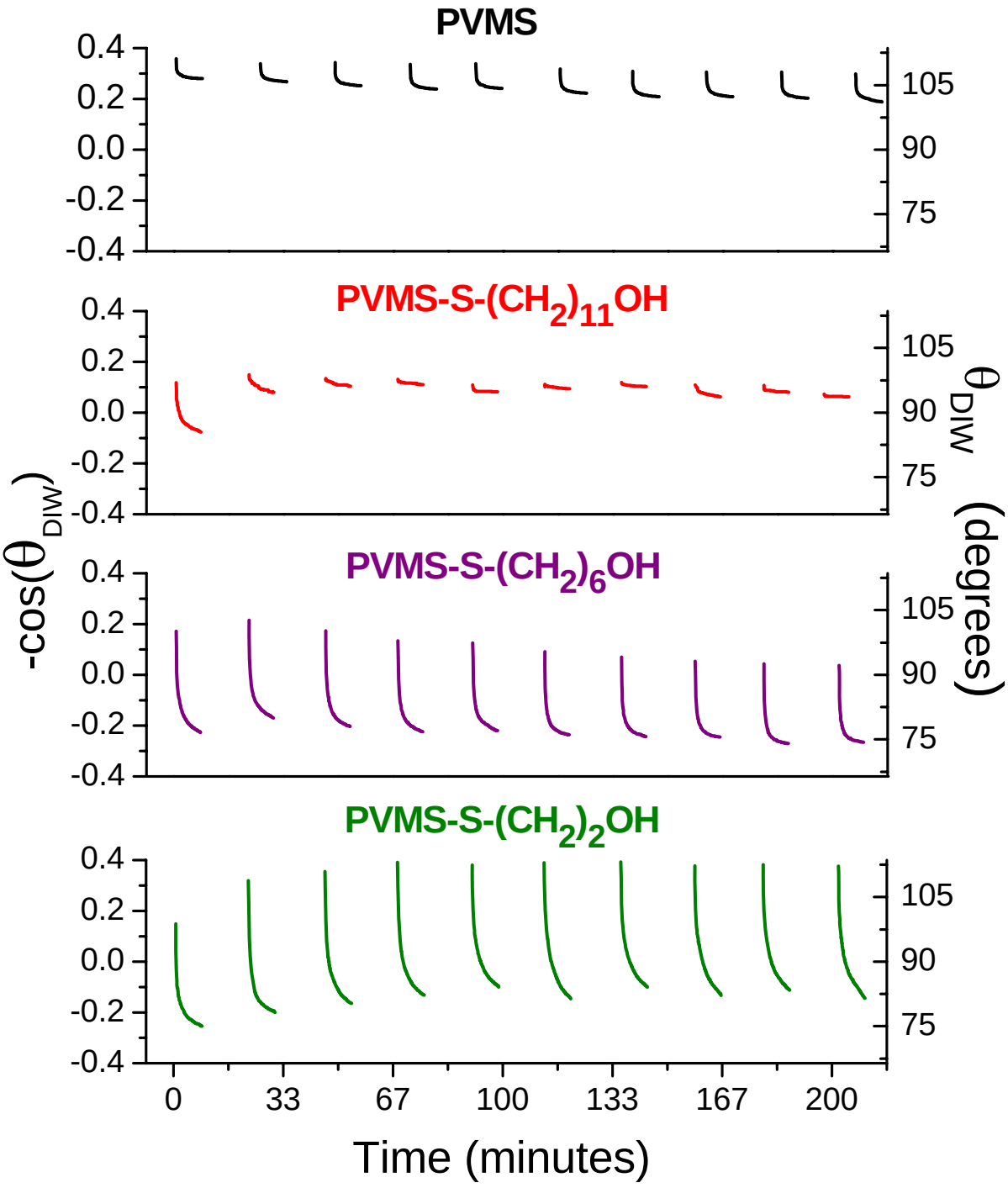

Figure 4.7: Time dependence of the deionized water wettabilities for PVMS-C_n-OH surfaces[20]. The error for θ_{DIW} is ±1.5˚.

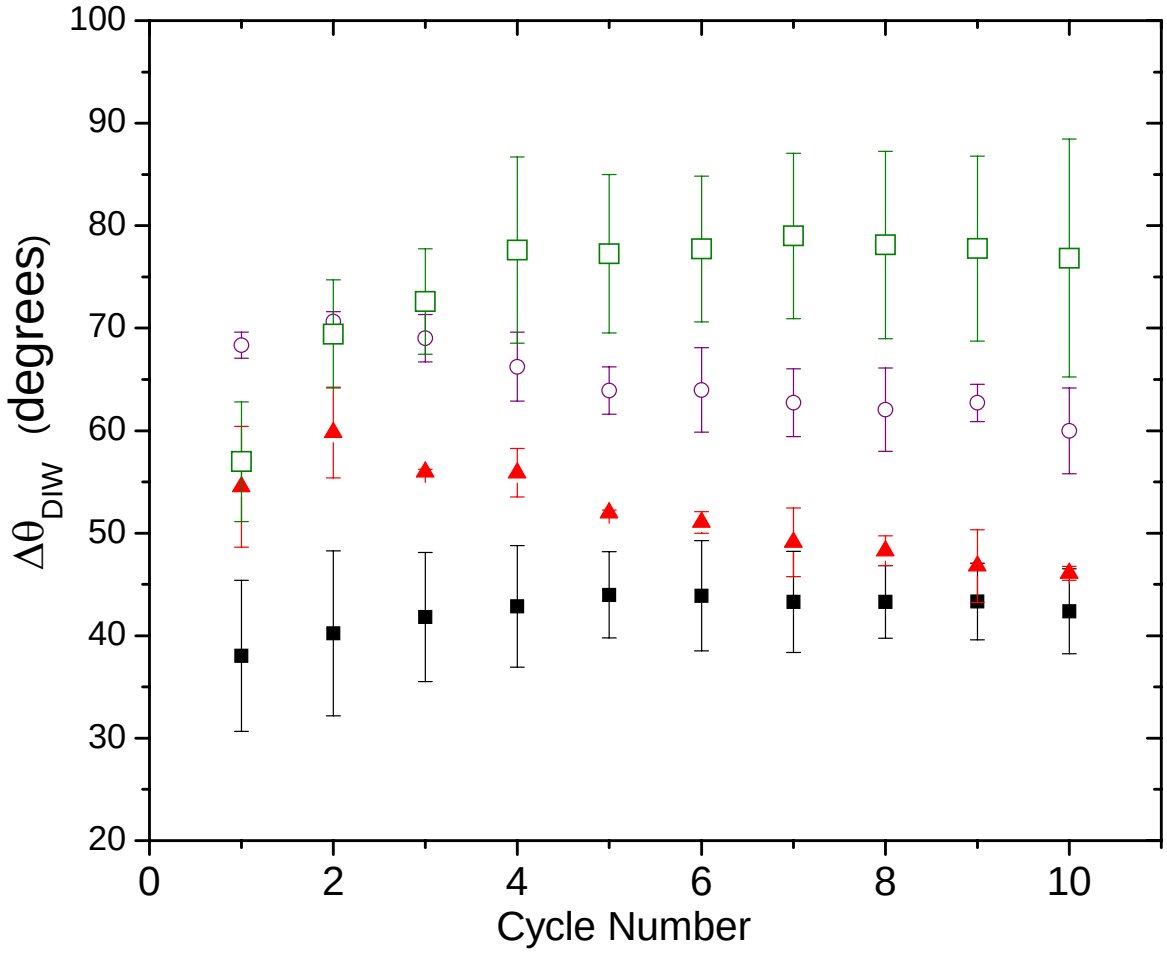

Figure 4.8: Contact angle hysteresis ($\Delta\theta = \theta_{advancing}$-$\theta_{receding}$) for each DCA cycle of the following substrates: PVMS (■), PVMS-S-$(CH_2)_2$OH (□), PVMS-S-$(CH_2)_6$OH(○), and PVMS-S-$(CH_2)_{11}$OH (▲).

We also noted the contact angle hysteresis with the information obtained with the DCA experiments. During the immersion and emersion stages, the advancing and receding contact angles were measured as a function of the exposed substrate. Contact angle hysteresis, $\theta_{advancing}$-$\theta_{receding}$ ($\Delta\theta$), is a measure of several factors, including surface roughness, surface homogeneity, sample swelling or liquid penetration, and surface reorientation[28]. As we are maximizing surface mobility with the siloxane backbone, surface reorientation and

heterogeneity would be the likely contributors to contact angle hysteresis. Figure 4.8 depicts the $\Delta\theta$ for PVMS and the three mercaptoalkanol-modified substrates over the ten cycles. The most responsive surface, PVMS-S-$(CH_2)_2$OH, has the largest observed hysteresis of $\approx 75^o$, consistent with its repeatable and reversible state between a polar and nonpolar environment. Besides PVMS, PVMS-S-$(CH_2)_{11}$OH has the smallest hysteresis, continually decreasing with each wet/dry oscillation. This observation is consistent with the hypothesis that we had formed a stable surface in this sample by inducing crystallinity. We discuss our confirmation of crystallinity in PVMS-S-$(CH_2)_{11}$OH in the following section.

4.4 Determination of Semi-crystallinity

All PVMS, PVMS-S-$(CH_2)_2$OH, and PVMS-S-$(CH_2)_6$OH samples were transparent, elastic and tacky (they adhered well to a polystyrene Petri dish). In contrast, the PVMS-S-$(CH_2)_{11}$OH specimens were opaque, rigid, and non-adhering to polystyrene (*cf.* Figure 4.9). Upon immersion into hot water (temperature $\geq 70^{\circ}$C), PVMS-S-C_{11}-OH became transparent but turned opaque again upon cooling. The loss of transparency is a classical indicator of semi-crystalline behavior as crystallites impede light propagation through the material.

The opaqueness indicator for the formation of crystalline domains with the -S-$(CH_2)_{11}$OH modification was also confirmed with optical microscopy at both room temperature and elevated temperature. PVMS-S-$(CH_2)_{11}$OH was placed over a transparent printout bearing a sign "NCSU" on a heating stage under the microscope. Heating at a rate of 1^oC per minute,

images (5X) were acquired every 30 seconds to track the melting temperature transition. Inspection of the images (*cf.* Figure 4.10) indicated this transition occurs between 28-32^{o}C. At elevated temperatures (>45^{o}C) the letters were clearly visible under the microscope. Upon lowering the temperature, the "NCSU" sign became illegible and almost completely blocked at temperatures below 32^{o}C. This experiment was conducted only for illustrative purposes rather that aimed at pinpointing the exact transition temperature. In addition, while the hot stage used for the temperature ramp had poor control below 30^{o}C, it still demonstrated the substrate's ability to oscillate between either an opaque or transparent state.

Dynamic rheology was performed on PVMS and the three mercaptoalkanol-modified PVMS samples[29]. As noted above, it was obvious through sample handling that the PVMS-S-$(CH_2)_{11}$OH substrate was more rigid than the other modified samples. This observation was further confirmed with a 10-fold increase in the storage modulus G' (*cf.*

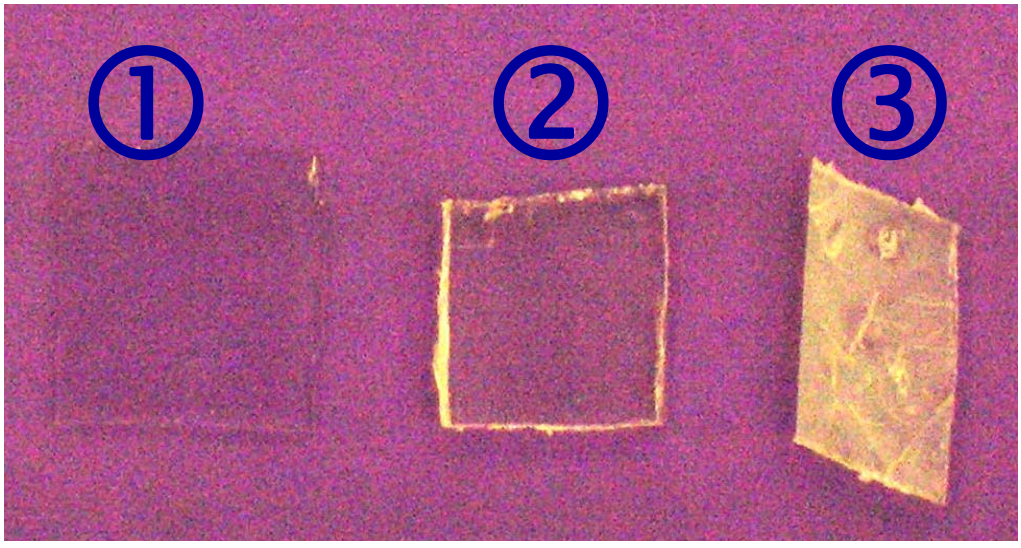

Figure 4.9: Photographs of mercaptoalkanol-modified PVMS substrates in front of an opaque background; ① PVMS ② PVMS-S-$(CH_2)_6$OH and ③ PVMS-S-$(CH_2)_{11}$OH. The opaqueness of ③ is indicative of semi-crystalline structures.

Figure 4.10: A sample of PVMS-S-$(CH2)_{11}$OH observed with optical microscopy (at 5X and in reflectance mode).

Figure 4.11a). Although the modulus did increase, the G' data for PVMS-S-$(CH_2)_{11}$OH is frequency-dependent, indicating an imperfect network (frequency sweep was performed within the linear viscoelastic regime at 0.5% strain). In contrast, PVMS, PVMS-S-$(CH_2)_2$OH and PVMS-S-$(CH_2)_6$OH are considered to be nearly perfectly elastic as a zero slope was obtained for the G' vs. frequency sweeps, as documented by data shown in Figure 4.11a. Upon heating semi-crystalline material, ordered polymer chains will relax into their preferred random coil conformations above a melting transition. To determine if this held true for the PVMS-S-$(CH_2)_{11}$OH substrate, more detailed analysis of the rheological properties was performed by varying the run temperature for the dynamic frequency sweep tests as shown in Figures 4.11b-c. At an operating temperature of 50˚C, the melting transition (melting point of 11-mercaptoundecanol is between 33-37°C [30]) had been reached in Run 2 as this temperature-induced polymer relaxation state resulted in negligible frequency dependency. This indicated the PVMS-S-C_{11}-OH network had reached near-perfect elasticity. Figure 4.11c illustrates that upon cooling there is full network recovery as the Run 3 data replicates Run 1 data. From this work it appears that the ordered alkane chains are acting as filler-like reinforcers at room temperature disrupting the elastic nature of the siloxane network.

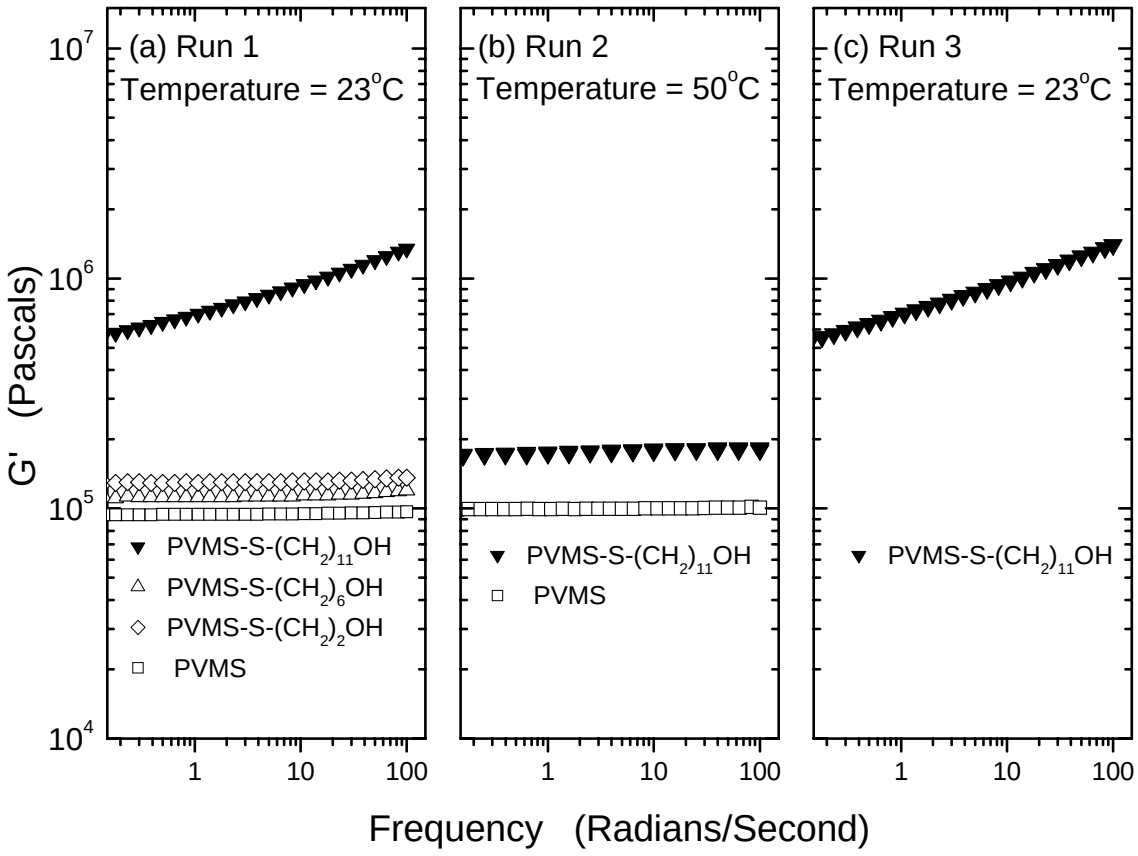

Figure 4.11: Dynamic rheology on PVMS and mercaptoalkanol-modified PVMS substrates. Runs performed at sequential operational temperatures (T): a) T = 23˚C, b) T = 50˚C, and c) T=23˚C. Average standard deviation is ± 33 kPa[29].

FTIR-ATR spectroscopy provided evidence to support our claim that the 11-mercapto-1-undecanol modified PVMS surface had undergone a phase transition with the formation of semi-crystalline domains. Figure 4.12 depicts the decreasing frequency shift for both asymmetric and symmetric C-H stretches of the methylene group. The characteristic frequency for the C-H stretching vibrations (asymmetric) occurs at 2920 cm^{-1} for crystalline polymethylene chains. For the liquid polymethylene state, the C-H stretching vibrations (asymmetric) are detected at 2928 cm^{-1} [24]. A similar downward shift for the symmetrical C-H stretching vibrations is observed for liquid (2856 cm^{-1}) to crystalline (2850 cm^{-1}) transition

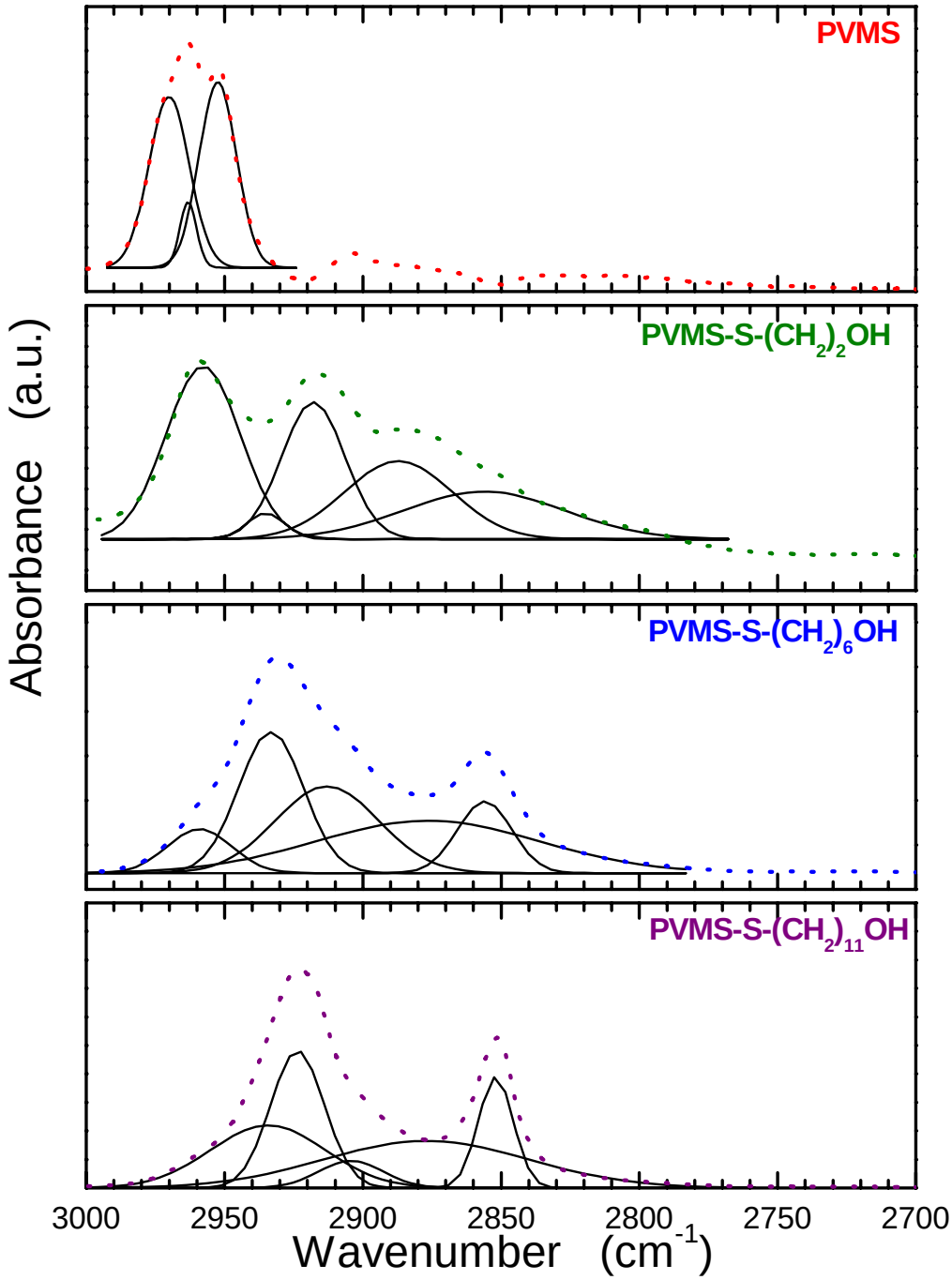

Figure 4.12: ATR-FTIR data (dotted lines) within the methylene stretching region for PVMS and the mercaptoalkanol-modified samples. The resultant chromatogram for each specimen was deconvoluted with multi-peak Guassian fits using OriginLab software (solid lines). The higher wavenumber peak is the characteristic asymmetric methylene stretching vibrations and the lower wavenumber is the characteristic symmetric methylene stretching vibrations. As crystallinity increases, the frequency vibrations shift to lower wavenumbers.

of the polymethylene chain[24]. Our results for the modified PVMS substrates reveal that while the -S-$(CH_2)_6$OH substituted surface is in a liquid-like state, the -S-$(CH_2)_{11}$OH group is in a crystalline-like state. Our observed frequency shifts between these two substrates agree closely with the reported polymethylene transition. Our observations are also in accord with the results of Chaudhury and Owen [25], who showed that adhesion hysteresis can be tuned by varying the surface density of hexadecyltrichlorosilane (HTS) chemisorbed films on PDMS. Highly packed films of HTS were found to be crystalline ($\nu_a(CH_2)$=2919 cm^{-1} and $\nu_s(CH_2)$= 2850 cm^{-1}) with high adhesion hysteresis. The opposite was true for a less dense film of HTS. From all the evidence presented thus far, we believe that after the first wet-dry cycle, -S-$(CH_2)_{11}$OH groups were "trapped" just beneath the surface in a semi-crystalline structure, formed presumably via van der Waals interactions acting among neighboring -$(CH_2)_{11}$- chains, and did not respond to the presence of water on the surface. Annealing the sample appeared to partially "melt" the semi-crystalline regions as the substrate became transparent, hence allowing the mercaptododecanol side-chains to reconstruct moderately at the surface.

As we detected the melting transition for PVMS-S-$(CH_2)_{11}$OH both visually and with dynamic rheology, we expected that FTIR-ATR studies performed at elevated temperatures would result in C-H stretching vibrations characteristic of a liquid-like state. The data in Figure 4.13 illustrates this behavior. We heated PVMS-S-$(CH_2)_{11}$OH from room temperature to 55^oC. At each step interval, the temperature was held constant during the course of the FTIR scan. The inset of Figure 4.13 depicts a steady increase in the methylene stretching vibrations as the temperature is ramped, confirming a reduction in the amount of crystallinity in the probed sample.

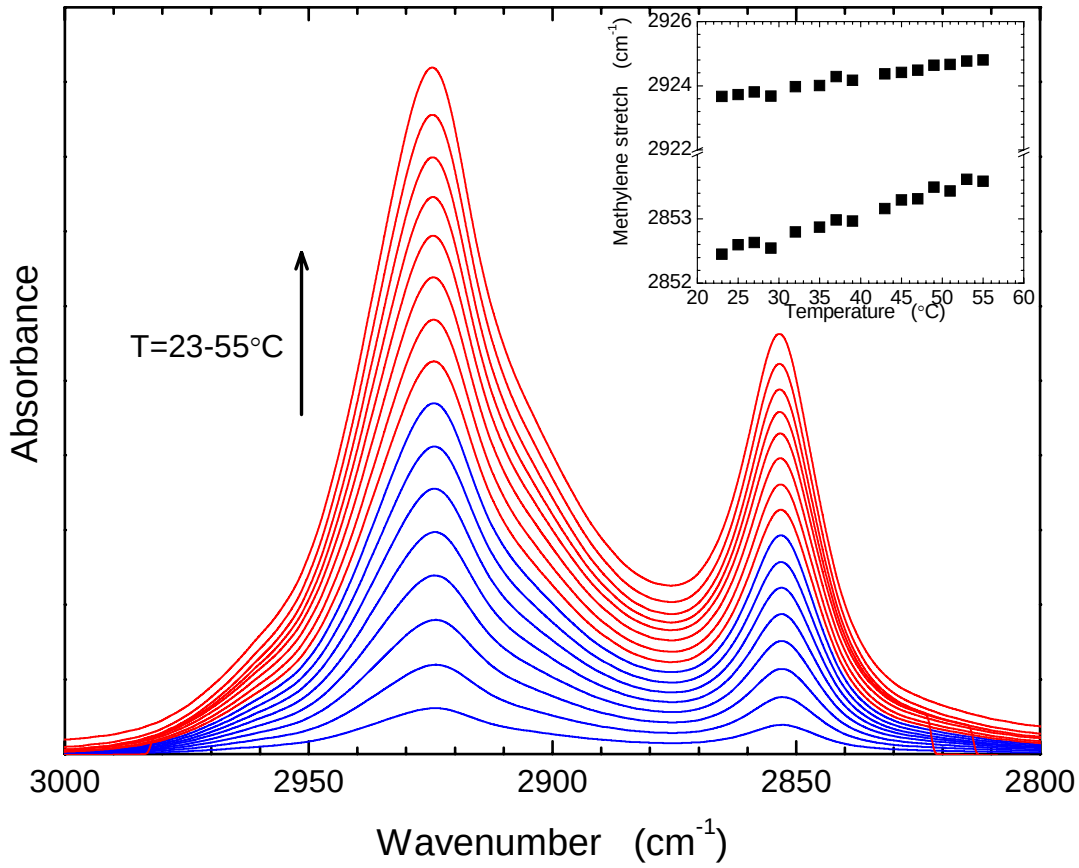

Figure 4.13: ATR-FTIR data recorded between 23-55°C for PVMS-S-$(CH2)_{11}$OH. As the temperature increases the material transitions through a melting region and loses some crystallinity. This is reflected in an upward frequency shift for the characteristic asymmetric and symmetric methylene stretching vibrations with increasing temperature (see inset).

4.5 Confirmation of Temperature Transitions

Two methods were implemented to more accurately define the temperature transitions of PVMS and the modified substrates, dynamic mechanical analysis (DMA) and differential scanning calorimetry (DSC). The DSC instrument for our testing could only reach 180 K, a temperature above the T_g of PVMS. We were, however, able to confirm the melting transition for PVMS-S-$(CH_2)_{11}$OH accurately with DSC as compared to DMA. Quantification of the T_g for PVMS-S-$(CH_2)_2$OH and PVMS-S-$(CH_2)_6$OH did seem to agree

with DMA even though the glassy plateau in DSC was not as apparent due to the lower temperature constraints. Figure 4.14 contains the DSC scans for PDMS, PVMS and the three mercaptoalkanol-modified substrates. PDMS is known to crystallize at ≈225 K.[31] This behavior is not apparent in PVMS, PVMS-S-$(CH_2)_2$OH, and PVMS-S-$(CH_2)_6$OH. There is a melting transition in PVMS-S-$(CH_2)_{11}$OH as shown by the distinct endothermic peak of this scan. Subsequent testing on HS-$(CH_2)_{11}$OH was in agreement with this melting transition. As the glass transition temperature is not apparent with the DSC results, analysis of the temperature transition with DMA provides further insight.

The interpretation of DMA data dictates that the largest step change in elastic modulus E', maxima in loss modulus E", and maxima in tan δ[1] are indications of the glass transition temperature or alpha transition, T_g or T_α.[32,33] The glass transition temperature is largely due to the intramolecular interactions within the backbone, polarity of the substituents, backbone flexibility, and barriers to rotation. As the bulkiness of the substituents increases, a rise in glass transition temperature is typically apparent. Figure 4.15 depicts the DMA temperature ramp behavior to the mercaptoalkanol-modified PVMS samples in comparison to the unmodified PVMS sample. The glass transition temperature rose remarkably in all three modified samples corresponding to other siloxane polymers that have substituent markedly different from the methyl group. Our modified substrates exhibit an increase in both the chain length and polarity of the silicon vinyl substituent. The DMA results for PVMS, PVMS-S-$(CH_2)_2$OH and PVMS-S-$(CH_2)_6$OH are fairly straightforward upon evaluation of the step change in E' and peak maxima of tan δ. For these three samples, the glass

[1] E' ≅ 3·G', E"≅3·G", and tan δ = E"/E'

transitions on E' were 150, 236, and 223 K respectively. As we increased the polarity and chain bulkiness with the addition of $HS(CH_2)_nOH$ an increase in T_g for $SH(CH_2)_2OH$ and $SH(CH_2)_6OH$ is expected. Note that the T_g for the $SH(CH_2)_6OH$ modification is almost 15K lower than the $SH(CH_2)_2OH$ modification. This is consistent with the increase in chain length seen in other polymer systems such as the methacrylates[34]; after the initial rise in T_g with the addition of a polar group and a slightly bulkier group, the longer chain can reduce the glass transition temperature by more easily adopting different conformations and possibly

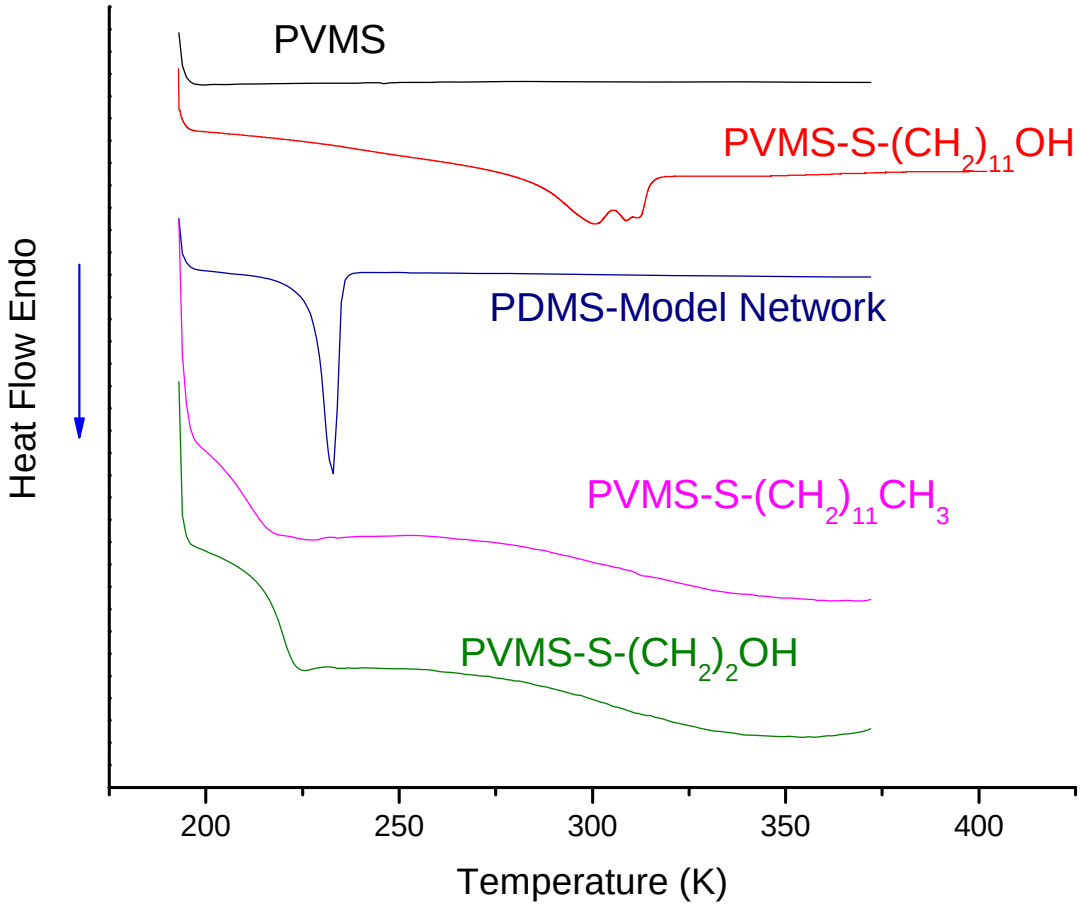

Figure 4.14: Differential scanning calorimetry for PDMS, PVMS and PVMS modified substrates. Heating rate was 3°C/minute, see text for details.

has a "plasticizing" effect on the polymer. The behavior for PVMS-S-$(CH_2)_{11}$OH is more complex due to the induced crystallinity imposed from the van der Waals forces between the alkane chains. As DMA is not the best technique for determining a melting transition of a polymer, we coupled the DMA interpretation with the DSC data. From Figures 4.14 and 4.15 it appears that the melting transition of PVMS-S-$(CH_2)_{11}$OH overlaps with the glass transition temperature due to the large decrease in storage modulus and the tan δ maximum occurring around 300 K. Closer inspection of tan δ for PVMS-S-$(CH_2)_{11}$OH depicts a shoulder in peak that occurs around 250 K. This also corresponds to a peak maximum in the loss modulus E" that is more sensitive to long chain segments and molecular motions in the polymer structure[32]. This explains why secondary dispersions, due to side chain motions, are more easily depicted with evaluation of the loss factors, tan δ and E". The secondary dispersions are often termed the T_β and T_γ transitions in order of decreasing temperature ($T_\alpha > T_\beta > T_\gamma$)[32]. With either analysis, it is obvious that the T_g increased for PVMS-S-$(CH_2)_{11}$OH. Since PVMS-S-$(CH_2)_{11}$OH is a semi-crystalline material, comparing with the amorphous PVMS-S-$(CH_2)_{2,6}$OH substrates is not appropriate. Hence, a deviation from the trend in decreasing chain length with increasing chain length should not be surprising. It is clear that the PVMS-S-$(CH_2)_{11}$OH contains crystallinity and a higher T_g, both attributes that decreased responsiveness and increased surface stability.

Table 4.1 lists the temperature transitions for the various siloxane substrates. It was useful to compare the behavior of the methyl alkane chain counterparts to the

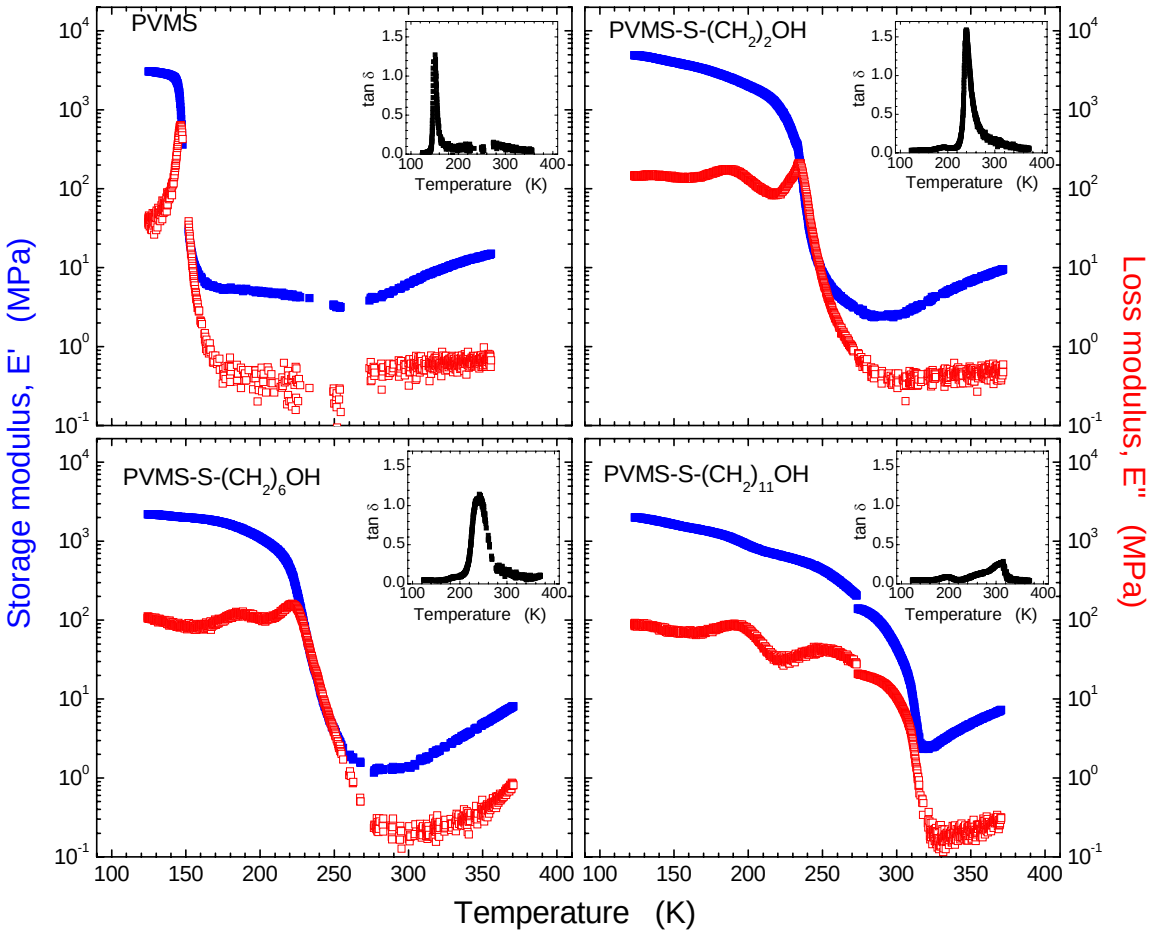

Figure 4.15: Dynamic mechanical analysis for PVMS and PVMS-mercaptanol modified substrates. Temperature ramps were performed at a heating rate of 3°/minute and at 1 Hz. Amplitude was set within the linear viscoelastic regime. Main graph is the measured storage modulus (E'-closed symbols) and loss modulus (E"-open symbols). Inset graph is tan delta (E'/E").

mercaptoalkanol ones to properly assign the temperature transition to the given molecular motion: side chain (T_β) or backbone motion (T_α). We ran several replicates on the PVMS-S-$(CH_2)_{11}OH$ sample of which 2 sets of results are listed in Table 4.1. All testing for

TABLE 4.1: Summary of temperature transitions for PDMS, PVMS and PVMS-modified substrates via DSC and DMA measurements. T_α is assumed to be the glass transition temperature. $T_{\alpha'}$ is assumed to be a melting transition. See text for the description of T_β.

	DSC		***DMA***					
Substrate	$T_g(K)$	$T_m(K)$	$\Delta E'$ $T_\alpha(K)$	*Tan* δ $T_\beta(K)$	*Tan* δ $T_\alpha(K)$	*Tan* δ $T_{\alpha'}(K)$	*E"* $T_\beta(K)$	*E"* $T_\alpha(K)$
PVMS	*	*	150		150	--	--	146
PVMS-S-$(CH_2)_2OH$	215	--	236	190	239	--	187	234
PVMS-S-$(CH_2)_6OH$	208	--	223	190	240	--	186	222
PVMS-S-$(CH_2)_{11}OH$	284.5	299.28 311.83	196 $T_{\alpha'}$: 303	197/ 186	271/ 250	312/ 294	190/ 184	250/ 237
PVMS-S-$(CH_2)_2CH_3$	--	--	190	--	191	--	162	188
PVMS-S-$(CH_2)_{11}CH_3$	210	--	--	--	--	--	--	--
PDMS	--	230	150 $T_{\alpha'}$: 224	--	160.8	--	--	157.7

DMA/DSC took place with a temperature ramp of 3°C/minute for the first data sets. In contrast, the additional testing for PVMS-S-$(CH_2)_{11}OH$ took place in the temperature step mode where equilibration at the given temperature was held for five minutes. This likely contributes to the difference in temperature transitions for the second set of data.

4.6 Conclusion

We summarize this part by emphasizing several key points of the novel design of our surfaces. They represent the only known polymeric system we are aware of that responds almost instantaneously to wettability changes at room temperature ($\Delta\theta \approx 2^\circ$/second for PVMS-S-$(CH_2)_2OH$). This behavior results from the high flexibility of the siloxane

backbone and the large disparity of surface energies between the hydrophobic methyl and the hydrophilic mercaptoalkanol side chains. The response rate depends on the number of methylene spacers in the mercaptoalkanol. While for n = 2 and 6, the surface reconstructs almost instantaneously, n = 11 specimens resist reconstruction because of strong van der Waals forces leading to the formation of semi-crystalline regions. We have shown that liquid-like siloxane surfaces (n = 2, 6) can be continually oscillated between polar and non-polar states for at least ten cycles, with no loss of wettability for the 3-mercaptopropanol modified substrate.

We confirmed the formation of semi-crystalline regions in PVMS-S-$(CH_2)_{11}$OH substrates through dynamic mechanical analysis (DMA) and differential scanning calorimetry (DSC). Both DMA and DSC data revealed a melting transition in PVMS-S-$(CH_2)_{11}$OH that was absent in PVMS-S-$(CH_2)_2$OH and PVMS-S-$(CH_2)_6$OH.

4.7 References

1. Carey, D. H. & Ferguson, G. S. Synthesis and Characterization of Surface-Functionalized 1,2-Polybutadiene Bearing Hydroxyl or Carboxylic-Acid Groups. *Macromolecules* **27**, 7254-7266 (1994).

2. Holmes-Farley, S. R., Reamey, R. H., Nuzzo, R., McCarthy, T. J. & Whitesides, G. M. Reconstruction of the Interface of Oxidatively Functionalized Polyethylene and Derivatives on Heating. *Langmuir* **3**, 799-815 (1987).

3. Boutevin, B., Guida-Pietrsanta, F. & Ratsimihety, A. in *Silicone-Containing Polymers* (ed. Chjnowski, J.) 79-112 (Kluwer Academic Publishers, Dordrecht, 2000).

4. Bauer, J., Husing, N. & Kickelbick, G. Synthesis of new types of polysiloxane based surfactants. *Chemical Communications*, 137-138 (2001).

5. Bauer, J., Husing, N. & Kickelbick, G. Preparation of functional block copolymers based on a polysiloxane backbone by anionic ring-opening polymerization. *Journal of Polymer Science Part a-Polymer Chemistry* **40**, 1539-1551 (2002).

6. Cai, G. P. & Weber, W. P. Synthesis and chemical modification of poly(divinylsiloxane). *Polymer* **43**, 1753-1759 (2002).

7. Chojnowski, J., Cypryk, M., Fortuniak, W., Rozga-Wijas, K. & Scibiorek, M. Controlled synthesis of vinylmethylsiloxane-dimethylsiloxane gradient, block and alternate copolymers by anionic ROP of cyclotrisiloxanes. *Polymer* **43**, 1993-2001 (2002).

8. RozgaWijas, K., Chojnowski, J., Zundel, T. & Boileau, S. Controlled synthesis of siloxane copolymers having an organosulfur group by polymerization of cyclotrisiloxanes with mixed units. *Macromolecules* **29**, 2711-2720 (1996).

9. RozgaWijas, K., Chojnowski, J. & Boileau, S. Optically active dimethylsiloxane copolymers with nucleophilic chiral sulfur groups pendant to the polysiloxane chain. *Journal of Polymer Science Part a-Polymer Chemistry* **35**, 879-888 (1997).

10. Scibiorek, M., Gladkova, N. K. & Chojnowski, J. Controlled synthesis of amphiphilic

siloxane-siloxane block copolymers with carboxyl functions. *Polymer Bulletin* **44**, 377-384 (2000).

11. Herczynska, L., Lestel, L., Boileau, S., Chojnowski, J. & Polowinski, S. Modification of polysiloxanes by free-radical addition of pyridylthiols to the vinyl groups of the polymer. *European Polymer Journal* **35**, 1115-1122 (1999).

12. Crowe, J. A., Efimenko, K., Genzer, J. & Schwark, D. W. in *Responsive Polymer Materials: Design and Applications* (ed. Minko, S.) 184-205 (Blackwell Publishing, 2006).

13. Carey, D. H. & Ferguson, G. S. A smart surface: Entropic control of composition at a polymer/water interface. *Journal of the American Chemical Society* **118**, 9780-9781 (1996).

14. Carey, D. H., Grunzinger, S. J. & Ferguson, G. S. Entropically influenced reconstruction at the PBD-ox/water interface: The role of physical cross-linking and rubber elasticity. *Macromolecules* **33**, 8802-8812 (2000).

15. Khongtong, S. & Ferguson, G. S. Integration of bulk and interfacial properties in a polymeric system: Rubber elasticity at a polybutadienen/water interface. *Journal of the American Chemical Society* **123**, 3588-3594 (2001).

16. Khongtong, S. & Ferguson, G. S. A smart adhesive joint: Entropic control of adhesion at a polymer/metal interface. *Journal of the American Chemical Society* **124**, 7254-7255 (2002).

17. Grunzinger, S. J. & Ferguson, G. S. Coupled, consecutive reconstructions at a polymer/air interface. *Journal of the American Chemical Society* **123**, 12927-12928 (2001).

18. Wong, D., Jalbert, C. & Koberstein, J. T. Surface reorganization kinetics of a model end-functionalized polymer system. *Abstracts of Papers of the American Chemical Society* **216**, U70-U70 (1998).

19. Anastasiadis, S. H., Retsos, H., Pispas, S., Hadjichristidis, N. & Neophytides, S. Smart polymer surfaces. *Macromolecules* **36**, 1994-1999 (2003).

20. Crowe, J. A. & Genzer, J. Creating responsive surfaces with tailored wettability switching kinetics and reconstruction reversibility. *Journal of the American Chemical Society* **127**, 17610-17611 (2005).

21. Holmes-Farley, S. R., Reamey, R. H., McCarthy, T. J., Deutch, J. & Whitesides, G. M. Acid-Base Behavior of Carboxylic-Acid Groups Covalently Attached at the Surface of Polyethylene - the Usefulness of Contact-Angle in Following the Ionization of Surface Functionality. *Langmuir* **1**, 725-740 (1985).

22. Holmes-Farley, S. R. Binding of Phenols to Aluminum-Oxide Surfaces .1. Phenols with a Single Hydroxy Group. *Langmuir* **4**, 766-774 (1988).

23. Allara, D. L., Parikh, A. N. & Judge, E. The existence of structure progressions and wetting transitions in intermediately disordered monolayer alkyl chain assemblies. *Journal of Chemical Physics* **100**, 1767-1764 (1994).

24. Snyder, R. G., Strauss, H. L. & Elliger, C. A. C-H Stretching Modes and the Structure of *n*-Alkyl Chains. 1. Long, Disordered Chains. *The Journal of Physical Chemistry* **90**, 5623-5630 (1982).

25. Chaudhury, M. K. & Owen, M. J. Correlation between Adhesion Hysteresis and Phase State of Monolayer Films. *The Journal of Physical Chemistry* **97**, 5722-5726 (1993).

26. Cammas, S. & Kataoka, K. Functional Poly (Ethylene Oxide)-Co-(Beta-Benzyl-L-Aspartate) Polymeric Micelles - Block-Copolymer Synthesis and Micelles Formation. *Macromolecular Chemistry and Physics* **196**, 1899-1905 (1995).

27. Efimenko, K. et al. Rapid formation of soft hydrophilic silicone elastomer surfaces. *Polymer* **46**, 9329-9341 (2005).

28. Andrade, J. *Surface and Interfacial Aspects of Biomedical Polymers* (Plenum Press, New York, 1985).

29. Crowe, J. A., Efimenko, K. & Genzer, J. in *American Chemical Society Silicone Symposium Series* (ed. Clarson, S.) (ACS, New York, in press 2006).

30. http://www.sigmaaldrich.com/catalog/search/ProductDetail/ALDRICH/447528.

31. Clarson, S. J. in *Siloxane Polymers* (ed. Semlyen, J. A.) 216-244 (PTR Prentice Hall, Englewood Cliffs, New Jersey, 1993).

32. Murayama, T. *Dynamic Mechanical Analysis of Polymeric Materials* (Elsevier Scientific Publishing Company, Amsterdam, 1978).

33. Ferry, J. D. *Viscoelastic Properties of Polymers* (John Wiley & Sons, New York, 1961).

34. Painter, P. C. & Coleman, M. M. *Fundamentals of Polymer Science* (Technomic Publishing Co., Inc., 1997).

Appendix 4.1 Materials and Methods

Elastomeric PVMS network substrates were synthesized by following an alkoxy-cure method as described elsewhere [1,2]. The storage modulus (G') of our networks was measured to be ≈$8x10^4$ Pa after Soxhlet extraction using toluene for at least 48 hours followed by drying at 75°C under 30 mm Hg vacuum. The vinyl moieties on PVMS were subsequently saturated via azodiizobutyronitrile (AIBN)-initiated thiol-ene radical addition of $HS(CH_2)_nOH$ (n = 2,6, and 11)[3]. After the reaction, the samples (denoted as PVMS-S-$(CH_2)_nOH$) were re-extracted, dried, and stored in a low-humidity chamber. Experiments using infrared (IR) spectroscopy confirmed that the grafting density of -$S(CH_2)_nOH$ was approximately equal in each sample.

A4.1 Modification of PVMS Networks

In a typical thiol-ene addition reaction approximately 0.12 grams of the extracted and dried PVMS network was placed at the bottom of a reaction flask. The sample was allowed to swell in 10 grams of N_2-purged toluene overnight. A mixture of 1-dodecanethiol (0.22 g) and AIBN (0.0048 g) was purged with nitrogen and added to the reaction flask. The flask was capped and heated to 60ºC for 5-6 hours. The PVMS-modified sample was removed from the flask then extracted in toluene for 48 hours. After extraction the substrate was dried under 25 mm Hg vacuum at 70ºC for 1 day. The sample was stored in a desiccator until testing was performed. Substrates similarly modified with 3-mercaptopropionic acid were extracted in deionized water, dried with nitrogen, and immediately tested for wettability.

A4.2 Infrared Measurements

Fourier transform infrared spectroscopy in the attenuated total reflection mode (FTIR-ATR) was used to characterize chemical changes that took place on the modified PVMS surface. All spectra were collected using a Bio-Rad/Digilab FTS-3000 Fourier transform infrared (FT-IR) spectrometer using a mounted crystalline Germanium, attenuated total internal reflection (ATR) sampling attachment (Pike Technologies inc., MIRacle™ Single Reflection ATR) with a normal spectral response of 650 to 5500 cm^{-1}. The infrared light is focused onto the photodiode of a liquid nitrogen-cooled, wide band mercury-cadmium-telluride (MCT) detector with a normal spectral response of 650 to 7000 cm^{-1}. There is nominally one reflection with a spot size of approximately 100 μm. The spectrometer and attachment were purged with dry compressed air, which reduces the possibility of atmospheric water or CO_2 contamination of the spectra and samples. For each sample, 64 scans (10 repeats per sample) were collected using Ge-crystal detector with a resolution of 2 cm^{-1} under constant nitrogen flux to eliminate the effect of water vapor on the collected data. The data were analyzed using BioRad-IR software.

In addition the ATR element was fitted with a Peltier thermal heating and cooling chip allowing for temperature control of the samples (± 70° C above ambient). The spectra presented are an average of 1 accumulation of 64 scans. Sample spectra were recorded over a temperature range from ambient to 50° ± 0.5° C in 1-5° C steps, with a resolution of 2 cm^{-1}. The spectra were converted into absorbance units by taking the negative of the log ratio of a sample spectrum to that of an air spectrum. The data were then transferred to data processing software (Microcal Origin, Microcal Software Inc., Northampton, MA.), where numerical

treatment and final graphs were prepared.

A4.3 Differential Scanning Calorimetry

Differential scanning calorimetry was performed using a TA Instrument Q100. Two runs were carried out for each sample in the range of –80^{o}C to 130^{o}C with a heating rate of 3^{o}C/minute under a nitrogen atmosphere. The T_g values were determined as the onset points from the second scans if applicable. The melting point T_m was taken as the maximum of the endothermic peak.

A4.4 Dynamic Rheology

Dynamic frequency sweeps were performed under isothermal conditions from 0.05 to 100 radians/second on a Rheometrics Advanced Rheometric Expansion System (ARES) with a defined strain within the linear viscoelastic regime using a parallel plate geometry. Wall slip was minimized my applying a normal force for optimum plate contact producing repeatable results.

A4.5 Dynamic Mechanical Analysis

Dynamic mechanical analysis was performed using a TA Instrument Q800® operating with a single cantilever geometry. The dried polymers films were cut into approximately 25mm×10mm×1.5mm rectangles. Storage modulus (E'), loss modulus (E"), and loss tangent (tan δ) were recorded at a heating rate of 3^{o}C/minute from –150^{o}C to 130^{o}C and at a test frequency of 1 Hz. The amplitude was set to be within the linear viscoelastic regime.

A4.6 References

1. Efimenko, K. et al. Rapid formation of soft hydrophilic silicone elastomer surfaces. *Polymer* **46**, 9329-9341 (2005).

2. Crowe, J. A. & Genzer, J. Creating responsive surfaces with tailored wettability switching kinetics and reconstruction reversibility. *Journal of the American Chemical Society* **127**, 17610-17611 (2005).

3. Herczynska, L., Lestel, L., Boileau, S., Chojnowski, J. & Polowinski, S. Modification of polysiloxanes by free-radical addition of pyridylthiols to the vinyl groups of the polymer. *European Polymer Journal* **35**, 1115-1122 (1999).

CHAPTER 5: PDMS-PVMS Networks

5.1 Introduction

Basic science studies are needed to inspire more integrative methodologies of scaffold design for tissue engineering and other cell-interfacing devices. The interplay of substrate surface chemistry, topography, and morphology are not yet fully understood in relation to cellular response. This fundamental understanding is paramount to the success of tissue engineering. Two examples are the designs of a synthetic corneal substitute and a cardiovascular stent. A corneal prosthesis should enable the appropriate interactions with epithelial cells and stromal keratocytes. The stromal cells are necessary for the anchoring and overgrowth of the epithelial cells that provide ocular clarity, protection of the underlying membrane, and regulation of corneal hydrations. While both cell types can adhere surfaces such as poly(dimethylsiloxane) (PDMS), epithelial down-growth at the prosthesis/natural tissue interface remains a phenomenon yet to be understood[1]. In order to avoid restenosis, the recurrence of abnormal blood vessel narrowing, during treatment of cardiovascular disease, biomaterial coatings for blood vessel stents need to control the behavior of vascular smooth muscle cells (VSMCs). VSMCs and fibroblasts exhibit "durotaxis", a phenomenon involving preferential cell migration to a more rigid part of the substrate. Figure 5.1 summarizes the result of the work by Zarri and coworkers where they observed VSMCs spreading and migrating at a higher rate for the stiffer poly(acrylamide) (PAAm) regions[2]. Understanding this phenomenon is necessary for its integration as a key design parameter in vascular tissue engineering[3].

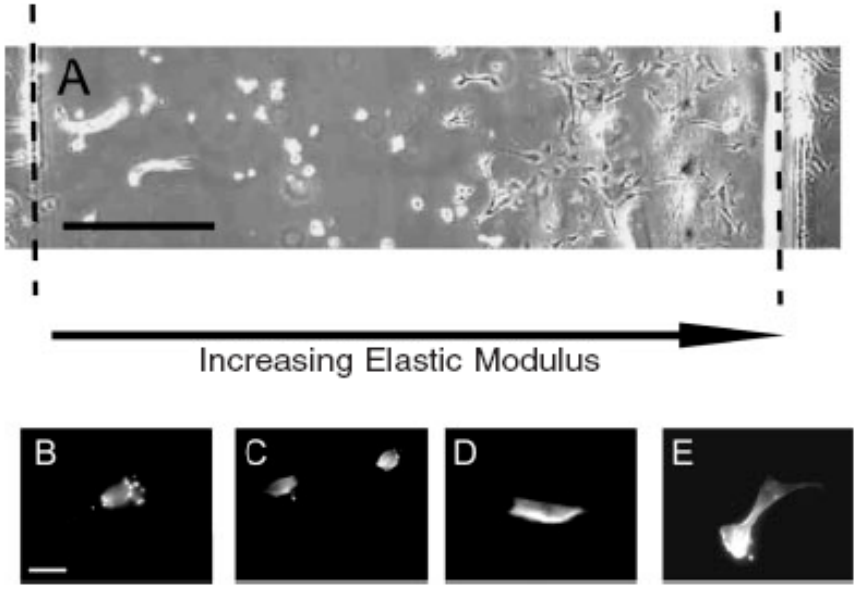

Figure 5.1:VSMC spreading increases and F-actin becomes more well-defined with increasing PAAm stiffness. The arrow shows the direction of increasing elastic modulus. A) Phase contrast image of VSMCs on the gradient gel modified with type 1 collagen; the scale bar is 500 microns. Individual panels (B-E) show representative fluorescent images of F-actin stained with rhodamine-phalloidin. B is from the softer region of the gel (i.e., the leftmost 0.7 mm portion of the gel). (C,D) are from the intermediate regions (i.e. the middle 1.4 mm portion of the gel), and (E) is from the stiffer region of the gel). The scale bar is 50 micron. (Zaari et al. 2004)

While surface chemistry and topology have been probed extensively for their effect on such responses as cellular adhesion and proliferation, studies involving morphology as a surface variable are just beginning to emerge. To achieve timely comprehensive experimental design, there is a need to create novel substrates with tunable mechanical properties (compliance) at the micro and meso-scale level with length scales ranging from individual cells up to whole tissues[4]. Despite the vast amount of research that has been targeted at understanding cellular response to its host scaffold, the choice of material and extrapolation of findings from one cell/material system to another system has proven

difficult. Thus establishing general relationships between substrate compliance and cell behavior cannot be considered independently of the material and cell type.

Cell migration can be influenced through mechanotransduction or tactile sensation. This involves the cell using its sensory abilities to actively explore its environment to determine its behavior, such as preferred migratory direction and destination[5,6]. Wang and coworkers have studied extensively the behavior of an established cell line of National Institutes of Health (NIH) 3T3 cells on PAAm substrates with rigidity gradients (created by varying cross-linker concentration). PAAm is a convenient substrate to use as it is easily modified with cell-adhesive peptides containing the argine-glycine-aspartate (RGD) sequence. Its mechanical properties, namely Young's modulus, have been varied from 10^3 to 10^5 Pascals[7]. As the modulus of most physiological tissues is above 10^6 Pascals (*cf.* Table 5.1)[4], PAAm's

Table 5.1 : Elastic moduli of various soft human tissues.[a]

Tissue	Type	Elastic Modulus (MPa)
Vein	Saphenous	0.027
Artery	Thoracic aorta	1.0
	Abdominal aorta	1.0
	Cartoid artery	1.0-3.0
	Illiac artery	3.0
	Anterior cerebral artery	5.5
Nerve	Sciatic[b]	7.0
	Bovine spinal cord	50 Pascals
	Human gray matter	200 Pascals
Tendon	Patellar	300-350
	Flexor digitorum profundus	1000
	Extensor digitorum longus	1600
Cartilage	Bovine articular	0.5-1

[a] Table adapted from Reference 4 and references within.

[b] Mouse tissue.

mechanical properties simulate only a fraction of human tissue. In addition, PAAm is a synthetic polymer that likely will not be used in vivo due to the known toxicity of the acrylamide monomer[4]. Nonetheless, PAAm has been used as a technology platform for cellular mechanosensing due to its ease-of-use.

As the issues surrounding cell growth and migration are complex, reducing the complexity of the studied surface is key for deconvoluting cell-substrate interactions. Ideally, a substrate capable of variation in surface chemistry, mechanical properties, and topographical features would provide a material platform to thoroughly probe the multi-faceted aspects of cell-substrate interactions. From our work on manipulating siloxane substrates, we believe we can change these three design components in a systematic manner. The work of Efimenko and Genzer on buckled siloxane surfaces provides a platform for understanding topography effects[8]. We can control the surface mobility of modified poly(vinylmethylsiloxane) (PVMS) by tuning the degree of crystallinity[9]. The focus of this Chapter is to address the third component - mechanical property variations. PDMS is a material of choice as it exhibits a physiologically-relevant range of elastic modulus; PDMS is currently used in biomedical devices and implants; preliminary cell-substrate studies exist that probe substrate mechanics in combination with surface[10,11]. The disadvantage of PDMS is its resistance to modification with a stable cell-adhesive layer. We addressed this inherent disadvantage by choosing to make gradients in modulus with PVMS as a significant component of the formulation. PVMS remains attractive to us, as it is more prone to surface functionalization without altering mechanical properties unlike the physical modifications that are necessary to modify a PDMS surface.

5.2 Making siloxane substrates with modulus gradients via interdiffusion

The cross-linking mechanism for fabricating siloxane substrates with gradients in modulus was based on hydrosilation chemistry. As it was desired to utilize PVMS within the network to provide the capability of functionalizing the surface in anticipation for studying cell-surface behavior, we took advantage of the vinyl groups for cross-linking sites. Various networks were made following the mechanism illustrated in Scheme 5.1. Hydride-terminated PDMS was reacted across the PVMS backbone and cured via a platinum catalyst. Another advantage to this chemistry was that it avoided the toxicity of the tin catalyst used in alkoxy-cure cross-linking. The modulus of the network could be varied in two ways: 1) by

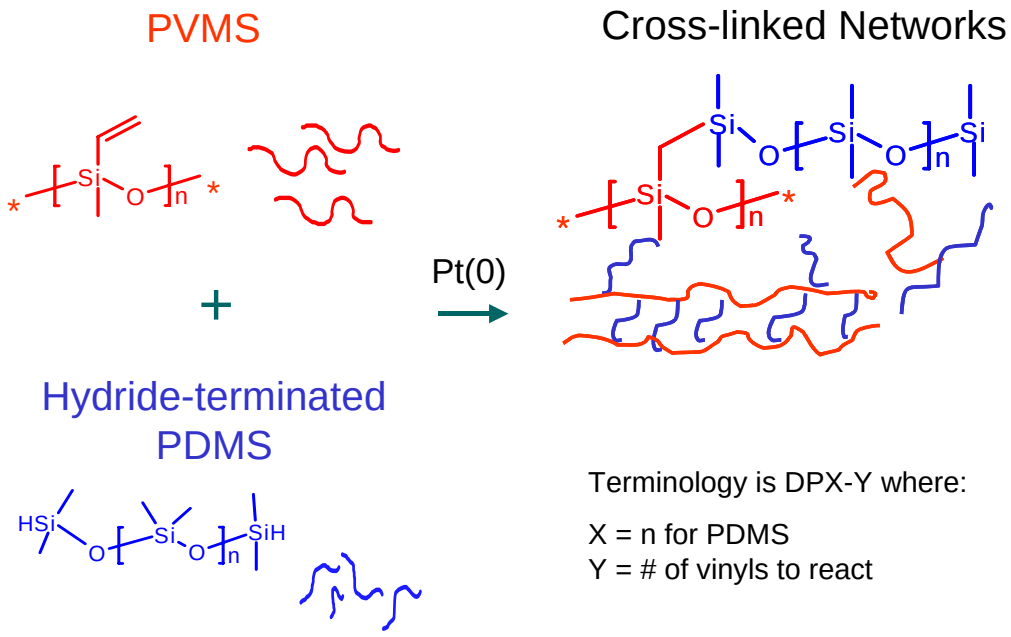

Scheme 5.1: Schematic of PDMS-PVMS cross-linking mechanism. The amount of hydride-terminated PDMS determines the degree of cross-linking.

changing the degree of polymerization of the PDMS linker (we used 11 to 78 repeat units) and 2) by formulating for different amounts of vinyl groups to be reacted. Since the average

PVMS molecular weight was about 40 kDa, the maximum amount of vinyls per mole of PVMS was ≈400. Targeting no more than 300 vinyl groups/mole of polymer for reaction insured intact reactive sites for subsequent functionalization.

The nomenclature for the hydrosilation formulations is DPX-Y, where X represents the degree of polymerization for hydride-terminated PDMS and Y represents the targeted number of vinyl groups for cross-linking. It was expected that upon increasing X the network would be looser with a corresponding decrease in modulus. As Y increased (corresponding to increasing the degree of cross-linking), we expected the stiffness (or modulus) of the material to increase. Figure 5.2 depicts this trend as a formulation labeled DP11-300 had a storage modulus (G') of about 450 kPa and the one labeled DP78-50 had a G' of about 20 kPa. Inspection of the data reveals that the DP15-Y formulations behave in the order of decreasing modulus as Y is varied from 175 to 75. Further increasing the number of vinyls for the DP15-Y series, however, caused G' to drop as the modulus for DP15-200 was roughly 300 kPa compared to 400 kPa for the DP15-175 formulation. Duplicate batches of DP15-200 showed consistent results. It is likely that low molecular weight species were diffusing to the polymer-air interface of these unextracted samples. It is also possible that a maximum had been reached in the incorporated cross-linker molecules and the "extra" hydride-terminated PDMS was acting as a plasticizer.

Allowing equal amounts of three formulations to interdiffuse with each other during the curing process produced a gradient in modulus. The formulations, comprising (1) DP15-30, (2) DP15-125, and (3) DP15-200 were poured into a 30×30cm^2 polystyrene Petri dish in 30-gram amounts covering three adjacent and equal areas. After curing for 3-days in an oven at 70^{o}C, small samples were taken along the substrate in the direction of the formed gradient in order to measure G' (■) as shown in Figure 5.3. Note that the DP15-200 section had a lower modulus than the DP15-125 section consistent with the results shown in Figure 5.2.

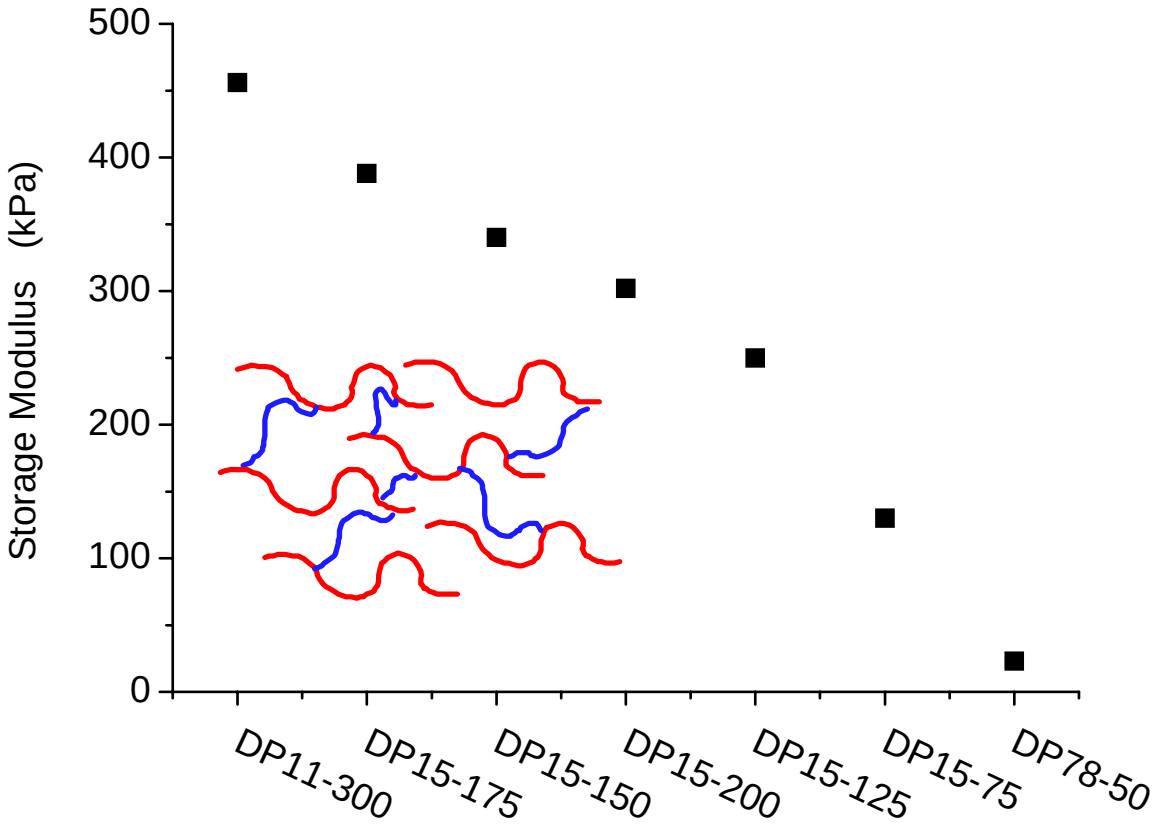

Figure 5.2: Interdiffusion formulations for the PDMS-PVMS blend. Degree of polymerization for PDMS was 11, 15, or 78. The nomenclature for formulations is DPX-Y where X represents the degree of polymerization for the PDMS-hydride terminated fluid and Y is the number of vinyls targeted for cross-linking.

Adjacent samples were also taken from the substrate after an additional 5 days at room temperature. This second set of data, (Δ) in Figure 5.3, is consistently higher in modulus thus all future testing was done on samples that had been cured 3 days in a 70°C oven with an additional 1-week "post-cure".

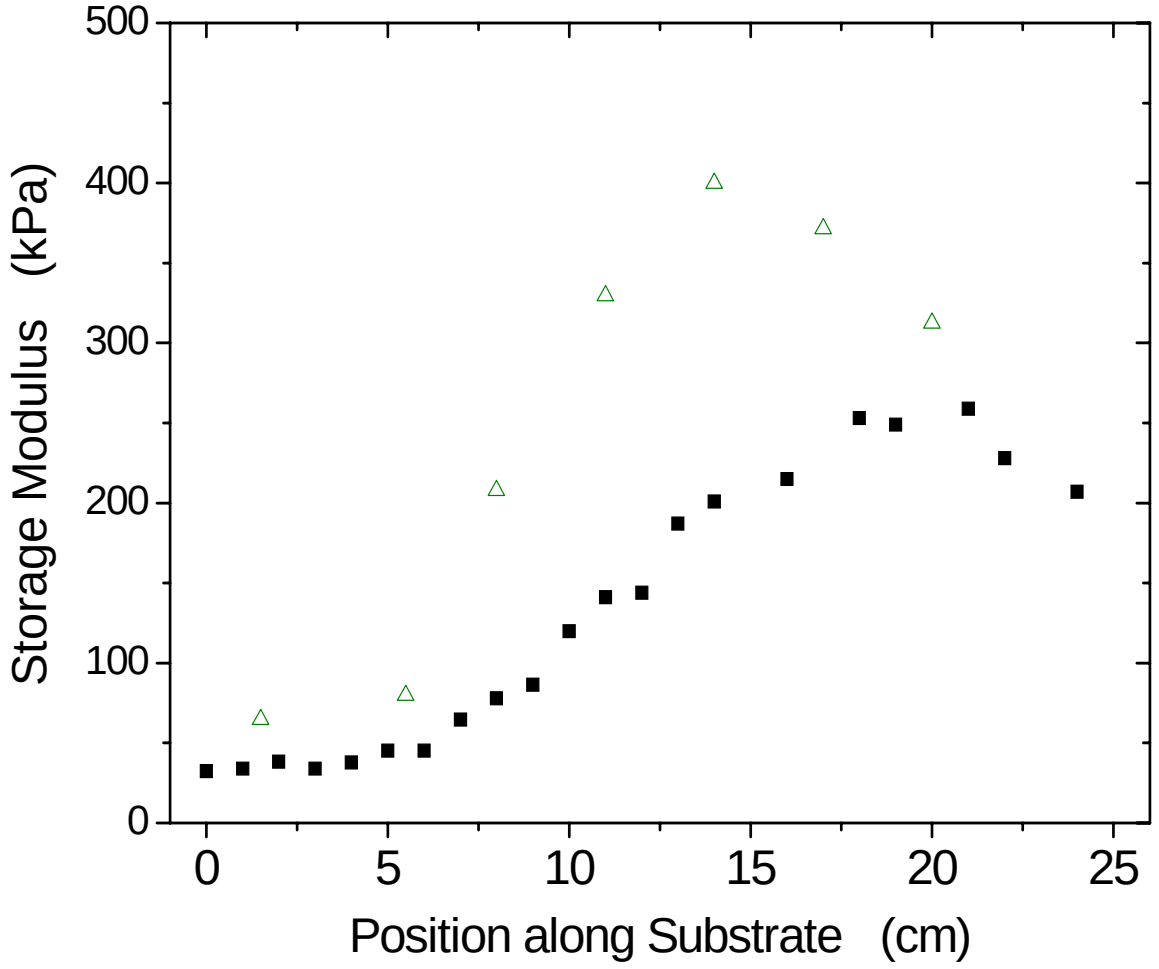

Figure 5.3: Interdiffusion of three formulations of PDMS-PVMS networks. Storage modulus was measured on an ARES 2000 rheometer at 1 radians/second within the linear viscoelastic regime. The first set of data (■) was collected after a 3-day cure time in a 70°C oven and the second set was collected after an additional 5-day room temperature cure time (Δ). The samples were taken from the same cured substrate.

Dynamic mechanical analysis was conducted on two samples, DP11-75 and DP11-250. The specimens were tested as described in Chapter 4 in this Ph.D. Thesis, utilizing the temperature ramp function of the QS-800 at 1 Hz and set amplitude of 40 μm. Figure 5.4 depicts the storage modulus, loss modulus, and tan δ for both samples. The largest step change in modulus for DPD11-250 (top graph (A) in Figure 5.4) is around 150 K, typical of the glass transition temperature of PDMS and PVMS. This large step transition in modulus for DP11-75 occurs at 145 K. Based on tan δ, the glass transition temperature is 150 and 160 K for DP11-75 and DP11-250, respectively. There is a beta transition apparent in the loss modulus for DP11-250 at 141 K that is absent in the data for PVMS and model PDMS networks as shown in Figures 4.15 and 4.16, respectively, and not present in the DP11-75 data (*cf.* Figure 5.4B). In addition, as DP11-250 has more PDMS in the formulation than PVMS (approximately 60 weight % of hydride-terminated PDMS), the cold crystallization behavior that was observed with the model network was also expected with DP11-250. However, this did not occur. We note that while the networks may have a similar molecular make-up, their cross-linking mechanism is different. With the model PDMS and PVMS networks described in Chapter 4, the cross-linking occurred at the end-groups of a molecule, whereas the DPX-Y networks incurred cross-linking along the PVMS backbone. The main backbone in all three networks had a similar molecular weight; thus, while the molecular weight between cross-links M_c for the end-linked networks was the same as the backbone, the DP11-250 has short and non-uniform M_c throughout the network. This may explain the observed differences of the loss modulus' secondary temperature transitions.

There is a large step change in storage modulus for the DP11-75 network ($\Delta E' \approx 7{,}000$ MPa) versus the DP11-250 network ($\Delta E' \approx 1{,}000$ MPa) when transitioning from the glassy to rubbery state. In the amorphous or rubbery state, DP11-250 is a more constrained network with a significant increase in the degree of cross-linking. The glassy state storage modulus for DP11-250 is almost an order of magnitude smaller than that of DP11-75 (10^3 versus 10^4 MPa). While we are not sure of the difference in modulus at temperature below the T_g, it explains the step change difference in $\Delta E'$. A final anomaly in the DMA behavior is that DP11-75 does not show the characteristic rise in modulus at higher temperature (> 298 K). This may be important in the design of surfaces for tissue culture as incubation occurs at ≈ 310 K. Our assimilation of relevant work by other researchers reveals that most mechanical property data is recorded at room temperature. This could be a variable overlooked as the elastic modulus can vary with temperature. It would be prudent to explore two areas for future study: 1) discern the differences between DP11-75 and DP11-250 thermoelastic behavior, and 2) reevaluate the mechanical properties at incubation temperature for the polymers used in biomedical applications.

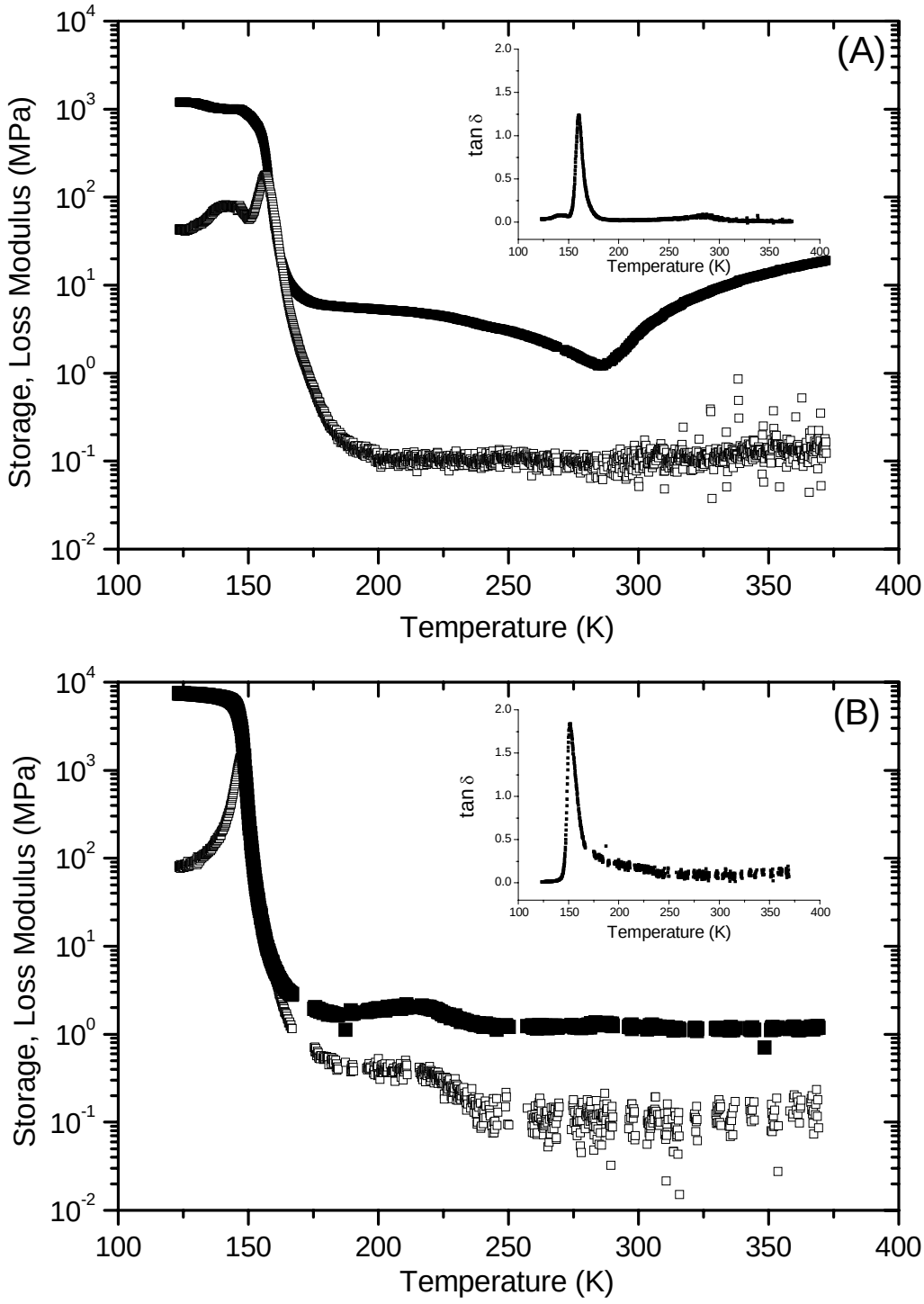

Figure 5.4: Dynamic mechanical analysis data for DP 11-250 (A) and DP11-75 (B) performed at 1 Hz. Storage modulus (■) and loss modulus (□) plotted as a function of temperature.

5.3 Wettability of PDMS-PVMS DPX-Y Substrates

The wettability via static contact angle was measured for DP11-250 and DP11-75 and compared against PVMS and Sylgard-184 (*cf.* Figure 5.5). The results from DP11-250 mirrored those of Sylgard-184; a result that is not surprising as DP11-250 has a higher concentration of PDMS in the formulation. As DP11-75 networks comprise a majority of PVMS, its wettability behavior is similar to that of pure PVMS. The surface reconstruction in the presence of water for DP11-75 is both slower and of lower magnitude than for PVMS. It can be attributed to not only the composition change (about 30% of hydride-terminated PDMS) but possibly due to the reduction in M_c for DP11-75 as compared to PVMS. This reduction in M_c may be decreasing the backbone mobility and hinder the vinyl substituents ability to reconstruct at the surface. As the glass transition temperature for DP11-75 is almost identical to that of PVMS, it seems more probable that the change in reconstruction is primarily due to composition changes.

While the static contact angles did not reveal any significant attributes for the DPX-Y networks as compared to the aforementioned siloxane networks, interesting results were seen when examining dynamic contact angle (DCA) data. Primarily, DP11-250 exhibited dramatically lower contact angle hysteresis for water ($\Delta\theta_{DIW}$). Whereas, PVMS and PDMS typically have a $\Delta\theta_{DIW} \approx 40^o$, DP11-250 resulted in a $\Delta\theta_{DIW}$ of less than 10^o initially.[12] Subsequent cycling of the DP11-250 substrate with DCA only measured an increase to roughly 15^o with little dampening in the CAH with remaining cycles (*cf.* Figure 5.6). DP11-75 proved more difficult to study with DCA. Due to the restructuring that was occurring during the first cycle, the $\Delta\theta_{DIW}$ seemed typical of a PVMS network. A

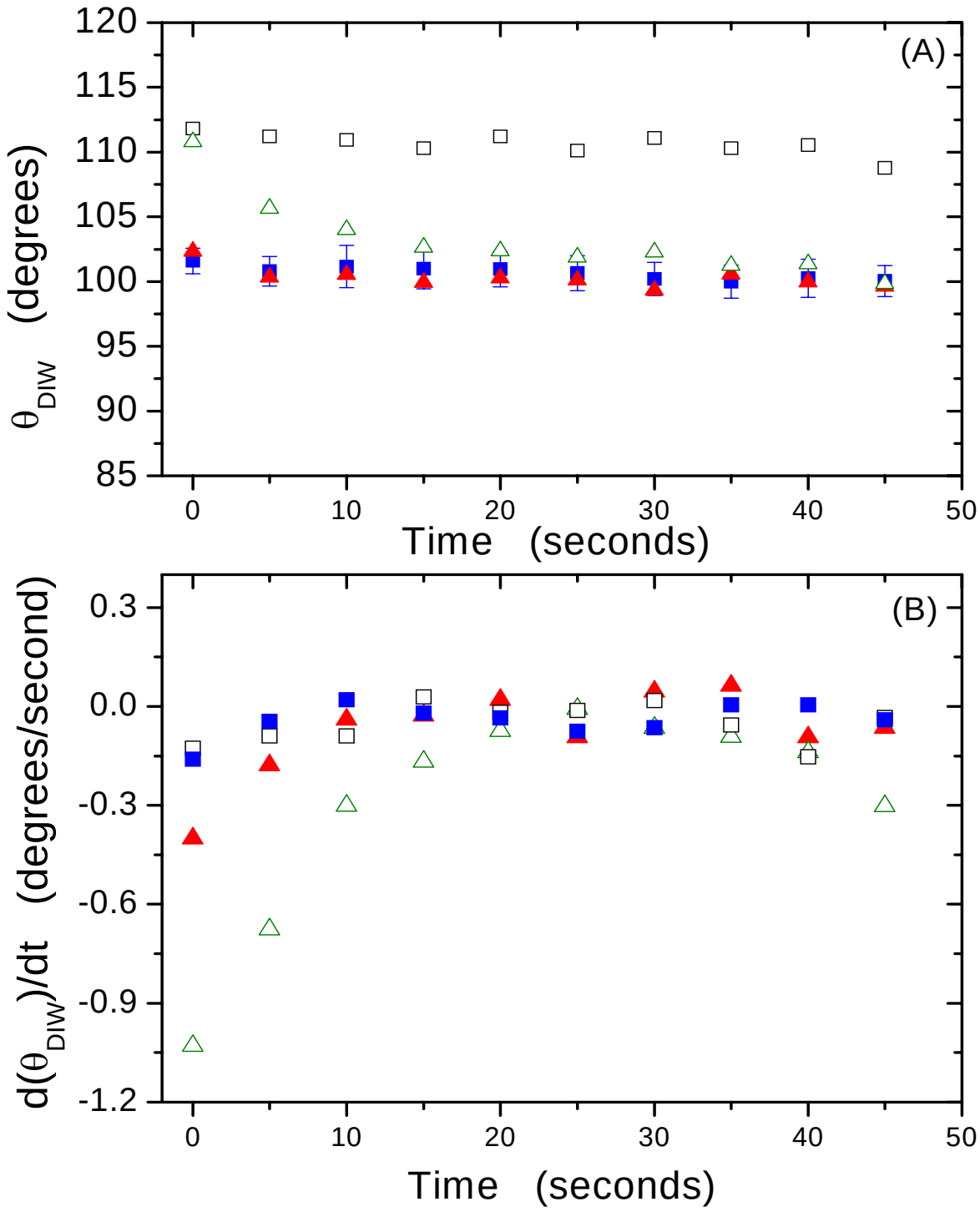

Figure 5.5: Static contact angle (A) and wettability rate changes (B) for PDMS-PVMS DPX-Y networks DP11-250 (■), DP11-75 (▲), PVMS (Δ), and Sylgard 184 (□).

complication arose with the testing as the polymer-air interface side appeared much more hydrophilic than the side that had been in contact with the polystyrene Petri dish. Additional testing was not carried out on DP11-75 as the floating behavior of the substrate complicated the force balance equation used to obtain the contact angle.

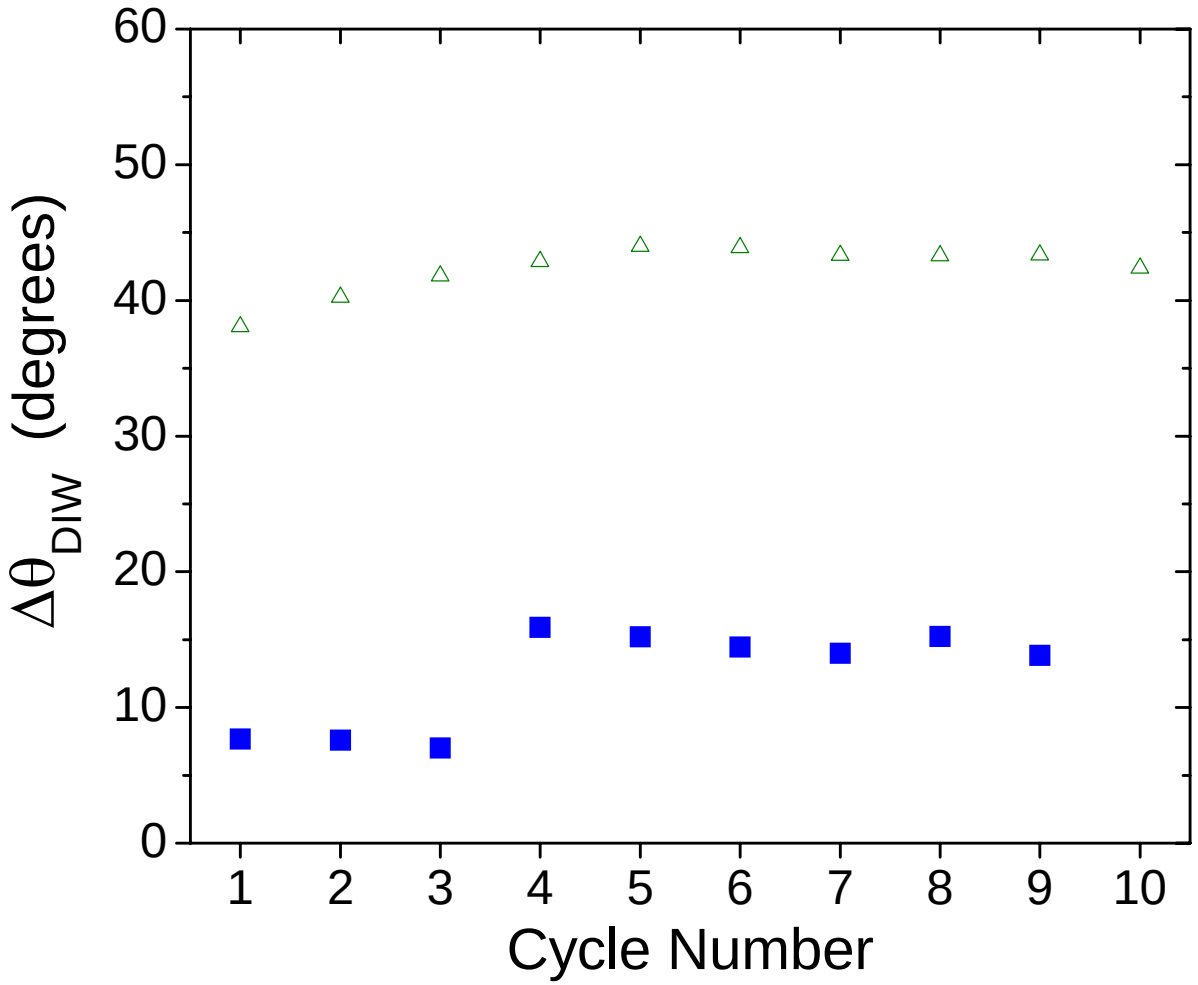

Figure 5.6: The contact angle hysteresis ($\Delta\theta = \theta_{advancing}$-$\theta_{receding}$) via DCA as a function of cycle number for PVMS (△) and DP11-250 (■). Each cycle consisted of immersing the substrate, holding at constant volume for 8.5 minutes and withdrawing the substrate. Substrates were quickly blow-dried with nitrogen between cycles.

General considerations associated with contact angle measurements assume the following properties of a surface: smooth, homogeneous, non-deformable, non-reacting, non-penetrable, with no reorientation.[13] As stated and demonstrated throughout this work, the siloxane surfaces do not fit these categories primarily due to surface reorientation. As the surface properties deviate from ideality, $\Delta\theta_{DIW}$ will typically increase. It is a measure that is often evaluated in applications where superhydrophobicity, anti-fouling, and constant wettability are desired traits. Due to the low $\Delta\theta_{DIW}$ observed for DP11-250, it may be worthwhile to explore the origin of this characteristic in further detail.

5.4 Designing substrates for cell migration/proliferation studies

We designed a very simple cell proliferation study to obtain baselines for the cellular response of NIH3T3 mouse fibroblasts on DP11-75 and DP11-250 in comparison to a polystyrene control. A series of 24-well plates for each polymer studied was prepared by distributing the appropriate formulation in the wells of each individual plate. The multi-well plates enabled evaluating cell proliferation in triplicate for six consecutive days. Each plate was UV-sterilized and treated with a 20 μg/mL fibronectin solution to promote cell adhesion. After each well was seeded with the same number of cells, the plates were cultured in media at 37^{o}C. Every 24 hours, the cells were detached and removed from the designated well to assess the difference in proliferation between substrates via a cell counting protocol.

From the data shown in Figure 5.2, DP11-75 was designated as the more compliant substrate. It is well-accepted that stiffer materials, such as polystyrene and DP11-250, would exhibit greater cell adhesion and proliferation[5]. Contradictory findings were reported by

Wong's group in a study of VSMCs growth behavior on PDMS (Sylgard-184)[11]. It was postulated that optimal cell proliferation occurs at a peak maximum for substrate modulus (biphasic)[11]. Lee et al. reported little variation in mammalian cell growth on essentially the same substrate used by Wong's group[10,11]. The surface treatment of the PDMS substrates was different, however; Lee's study used fibronectin as the cell-adhesive layer where the VSMC study used a layer-by-layer self-assembly of positively and negatively charged polymers. These contradictory findings illustrate the importance of defining the differences in the cell-substrate and cell-type selections as both the absolute value of modulus and the cells' history (primary or transformed cells; the later being cell lines that have been sustained for long-term proliferation) are important factors[5,6]. In our studies, we note two discrepancies from past findings: 1) fibronectin was used as the cell-adhesive layer, and 2) the cells under observation were transformed NIH3T3 mouse fibroblasts (not primary cells). As our data in Figure 5.7 illustrates, we see an inverse relationship between cell proliferation and substrate compliance. These results are surprising on the basis of using transformed cells and a cell-adhesive ligand shown to produce cell aggregates[10,11]. The fibronectin-treatment in our study was not quantified but may be more efficient for the PVMS-PDMS substrates than Sylgard-184. Also, the elastic modulus ranges in the three studies are as follows: 1) Lee et al. evaluated Sylgard-184 with Young's modulus from 0.6 to 2.6 MPa, 2) Brown et al. (VSMC study) evaluated Sylgard-184 with a Young's modulus ranging from 0.048 to 1.78 MPa, and 3) our study evaluated PVMS-PDMS with an elastic modulus ($E' \cong 3G'$) between 0.39 and 1.5 MPa. As our cell proliferation results agree in part with the VSMC study, it does seem to indicate an optimum modulus range. We do note, however, that with regard to

the cell proliferation, we detected ≈150-fold increase in cell growth for our soft substrate compared to the ≈20-fold increase in for the softer substrate in the VSMC study. This difference could be attributed to the differences in cell culturing media. We cultured our cells in complete media, which would result in a higher proliferation. There may be a dynamic synergy between the soluble factors in the media (aiding cell growth) and surface stiffness to achieve an optimum cell proliferation rate. The pioneering study by Wang

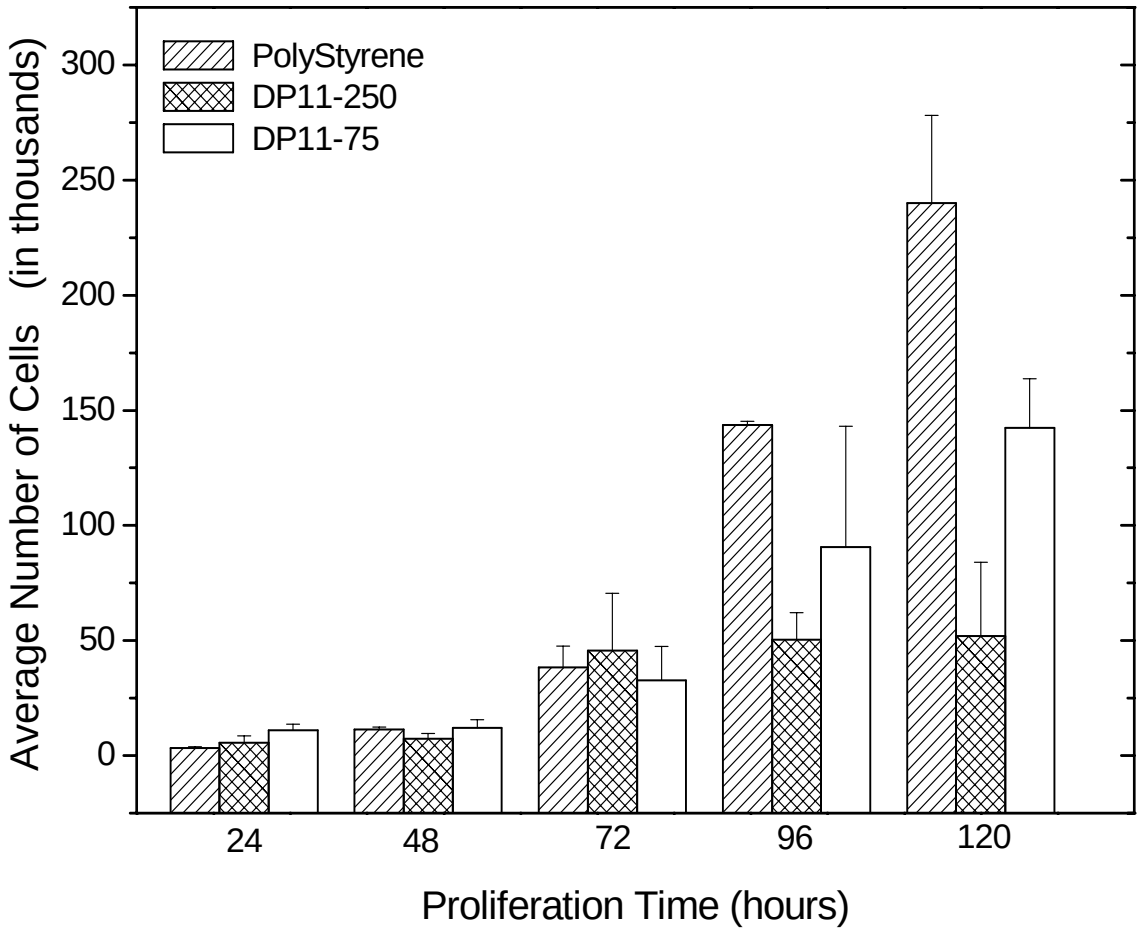

Figure 5.7: NIH 3T3 fibroblast cell counts cultured in DMEM media with 0.1% FBS and 1% PS/G at 37^{o}C. Cells were suspended with trypsin, diluted in PBS, and injected into a hemocytometer for manual counting.

depicted a 2-fold difference in cell proliferation based on substrate flexibility[6]. What is clear is that the interplay between mechanical properties, substrate chemistry, and cell-type needs to be considered before conclusions can be drawn regarding the cell-substrate interactions.

We evaluated the cell growth on the substrates using optical microscopy. Photographs were captured on each well at the time of the cell count. Figure 5.8 depicts the images captured at 48 hours for the three substrates. As the proliferation time increased, the cells reached high confluency, making it difficult to depict differences between the images. As the cell counts at 48 hours showed little variation between the three substrates, the images are inconclusive for proliferation. We do note a possible difference in the morphology of the cells plated on the DP11-75 substrate. They appeared to be slightly more spread out compared to the cells plated on the DP11-250 and the polystyrene substrates. One possibility in the difference in cell proliferation was thought to be a difference in fibronectin distribution. To address this possibility, the DP11-75 and DP11-250 substrates were treated with FITC-labeled fibronectin for evaluation with optical microscopy (*cf.* Figure 5.9). The softer substrate, DP11-75, seemed to contain more agglomerates or "islands" of fibronectin surrounded by smooth areas. The rough nature of the stiffer substrate, DP11-250, was obviously different than its more compliant counterpart. While no conclusions were drawn regarding the adsorption mechanisms, there did appear differences in the surface-makeup between the two substrates prompting additional optical microscopy studies. We considered a couple of different strategies: 1) repeat the fibronectin labeling with FITC or Texas Red labeled fibronectin for imaging with total internal reflection fluorescence (TIRF) microscopy.

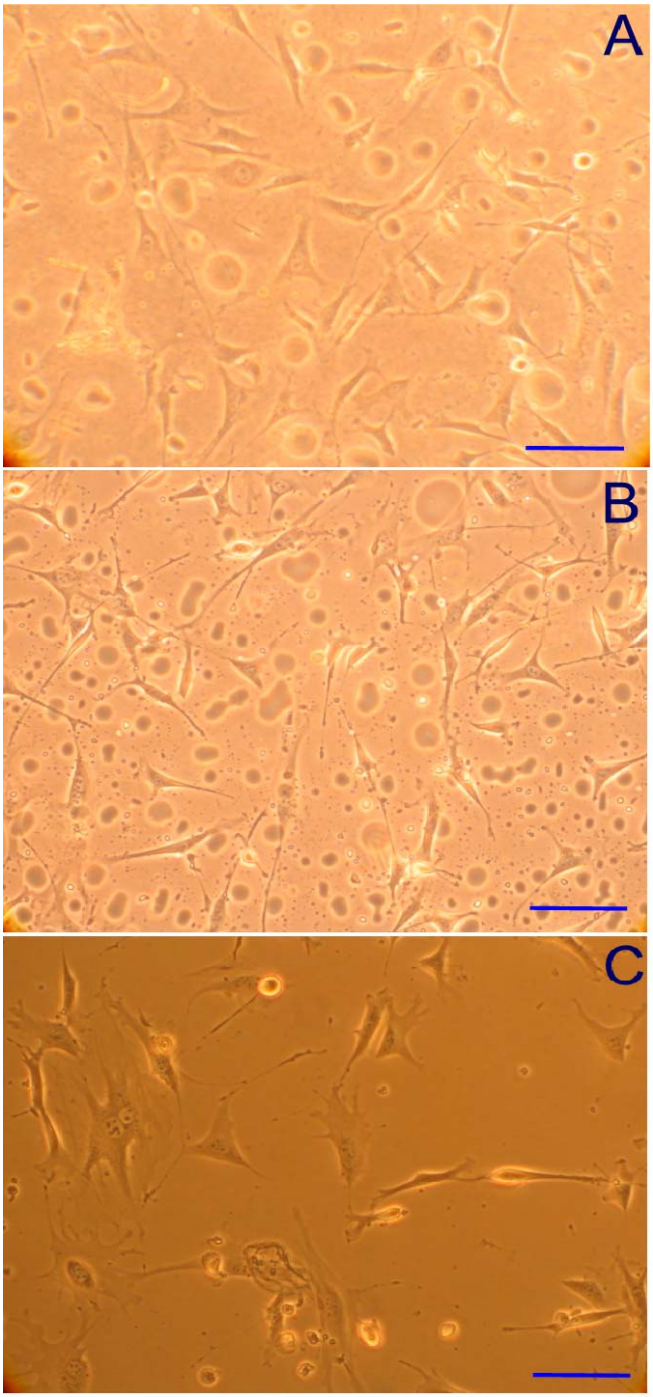

Figure 5.8: NIH3T3 mouse fibroblast growth on A) DP11-75, B) DP11-250 and C) polystyrene substrates. Magnification is at 20X (bar = 5 μm). Photos taken 48 hours after initial seeding.

TIRF is a sensitive microscopy technique, by which fluorophores within ≈100 nm of the substrate are selectively excited or 2) use a fibronectin specific primary antibody, followed by a fluorescent secondary antibody to detect the fibronectin on the surface. This could be performed in a multi-well plate where each well is coated with a different polymer formulation. After the equal concentrations of fibronectin are deposited in the wells, we would detect fluorescence with a plate reader to quantify the amount of surface fluorescence.

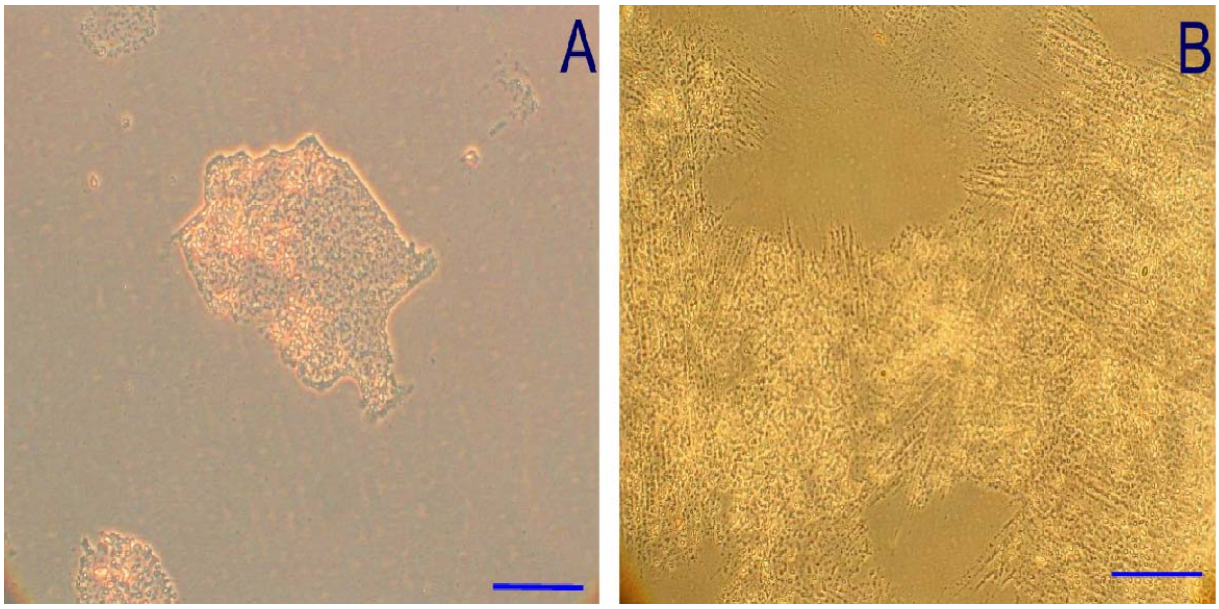

Figure 5.9: Images of substrates A) DP11-75 and B) DP11-250 after exposure to a 20 μg/ml FITC-labeled fibronectin solution. After the substrates were rinsed several times with PBS, the samples were imaged with a 20X (bar = 5 μm) lens transmittance mode optical microscope.

5.5 Morphology studies

We investigated possible surface segregation between the PVMS and PDMS components of the formulation with a phase contrast enabled optical microscope. The photos were obtained on the specimens several weeks after curing the networks so we assume the surface composition was in equilibrium under ambient conditions. Figure 5.10 illustrates the distinct differences in morphologies between the DP11-75 (low concentration of PDMS) and DP11-250 (high concentration of PDMS) substrates. The size domains of DP11-250 are estimated to be about 20 μm, the size of a fibronectin fibril is $60\times2.5\times2.5$ nm^3, and the length scale of NIH3T3 fibroblast cells can be between 10-100 μm[14]. It is possible that the surface segregation between the PVMS and PDMS is driving a different distribution of fibronectin on the cured network surface.

Additional substrates were prepared to monitor the segregation kinetics of DP11-160 and DP11-45 formulations. This study consisted of imaging the substrates every week; we only show the results for time = 0 and 4 weeks, and the sample after it had been exposed to deionized water (*cf.* Figure 5.11). We exposed the substrates to deionized water to ascertain the segregation at the polymer-water interface as the cell proliferation studies are conducted in an aqueous environment. Although the formulations did not exactly mirror those of DP11-75 and DP11-250, there is information to be gleaned from this study. Foremost is that the distinct morphology differences apparent in DP11-250 was also apparent in both DP11-45 and DP11-160 after the specimens were exposed to water. It is likely that DP11-75 also would exhibit the PDMS_PVMS segregation after water exposure; thus the only difference may be in the size domains between the segregated materials.

Given that the PDMS_PVMS segregation creates a complex surface as morphology, surface chemistry (differing vinyl and methyl components), and mechanical properties are dependent variables with one another, understanding the cell proliferation results is difficult. We repeated the cell proliferation study but pretreated the surfaces with water prior to the fibronectin deposition. This insured the surface was in equilibrium with an aqueous environment, similar to the environment for the cell seeding procedure. The substrates evaluated were the tissue culture polystyrene control, DP11-250, and DP11-75. We decided to access the behavior of Sylgard-184 as this material has been the predominant PDMS used in cell-substrate and surface activity studies. While Sylgard-184 is a proprietary formulation

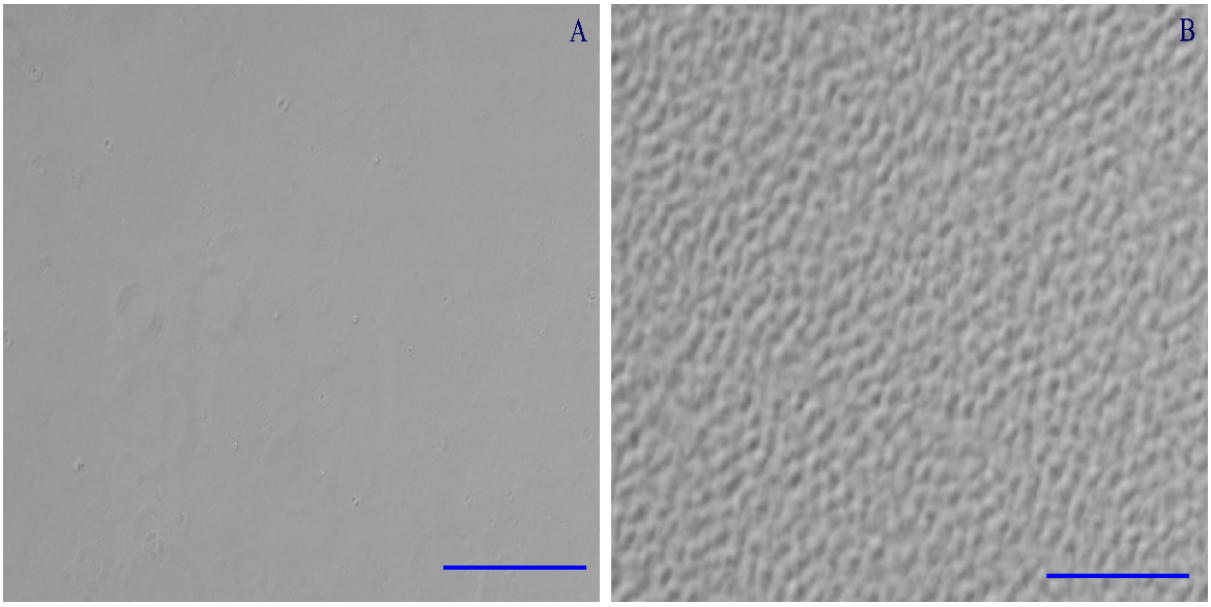

Figure 5.10: DP11-75 (A) and DP11-250 (B) images from phase contrast optical microscopy using a 10X lens in reflectance mode (bar = 200 μm).

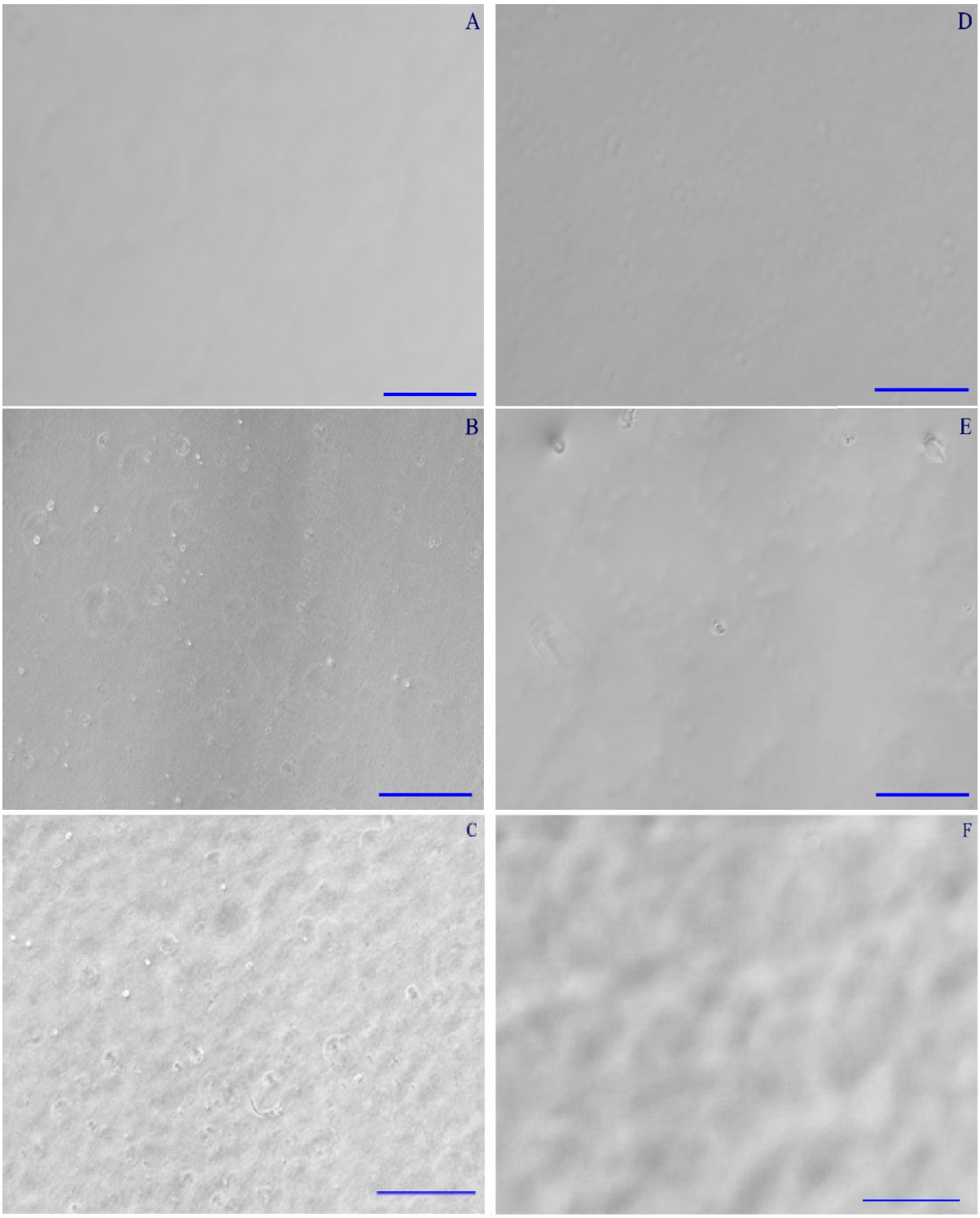

Figure 5.11: Images from phase contrast optical microscopy using a 10X lens in reflectance mode (bar = 200 μm). Images for DP11-45 (A-C) and DP11-160 (D-F) were taken after A,D) initial cure (t = 0), B,E) after 4 weeks, and C,F) after exposure to water.

that comprises 2-D and 3-D PDMS components, the PDMS and PVMS for the DPX-Y formulations consist of only 2-D components. The storage moduli for these three siloxane formulations are depicted in Figure 5.12. Note that the modulus of Sylgard-184 is only slightly higher than that for the DP11-250 formulation.

The same protocol was used for cell seeding, suspension and counting as in the first study with two exceptions: 1) a higher starting cell density was used in the seeding procedure and

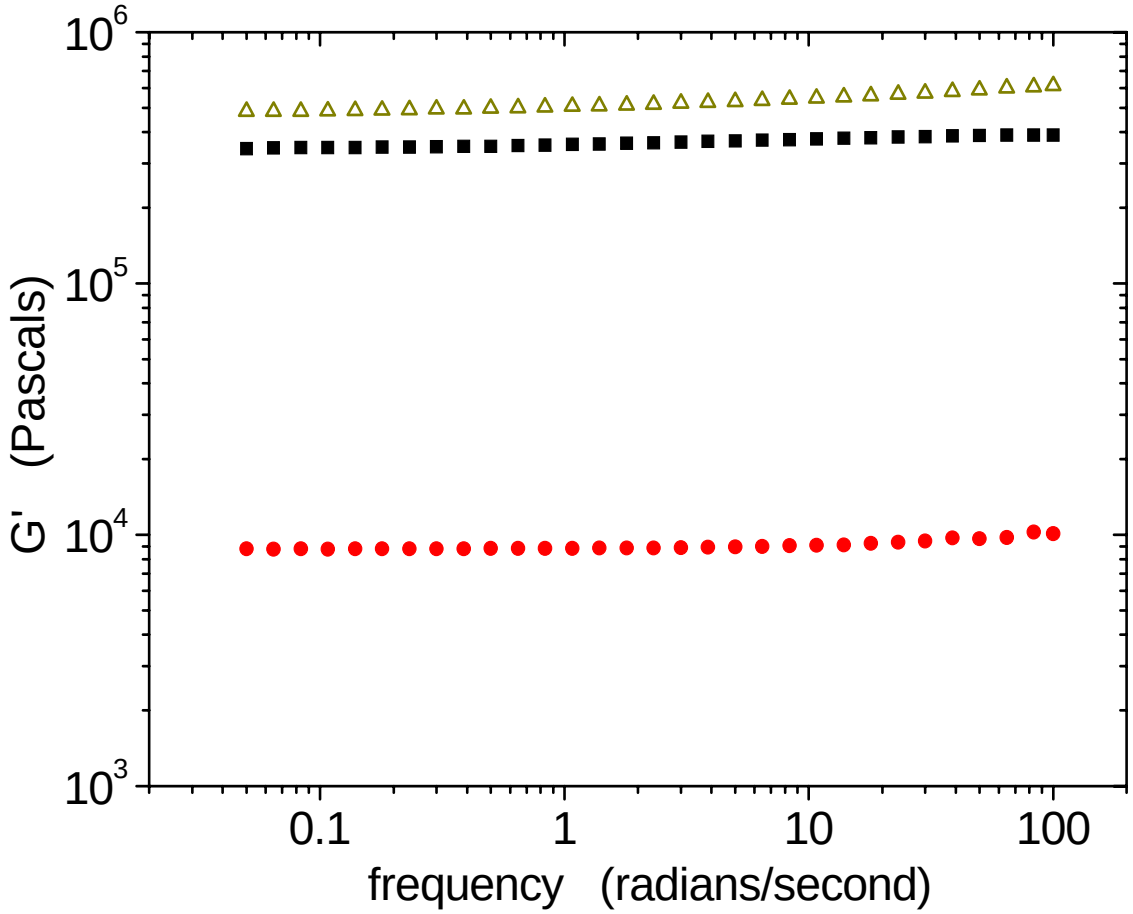

Figure 5.12: Elastic modulus as a function of frequency for Sylgard 184 (Δ) and the high and low modulus (DP11-250 (■) and DP11-75(●), respectively) substrates used in the 2nd cell proliferation study.

2) a BD Coulter® cell counter was used versus a hemocytometer. The results in Figure 5.13 depict that both DP11-75 and DP11-250 produced higher cell counts than Sylgard-184. There appears to be little difference between the substrates that were pretreated with water (*cf.* Figure 5.13B) versus the substrates left in ambient conditions (*cf.* Figure 5.13A). The surprising result is that there appears to be little difference in the cell proliferation for the high and low modulus substrates of the DPX-Y networks. As there was over an order of magnitude difference in modulus between DP11-75 and DP11-250, the conditions of this cell proliferation study clearly did not produce any discernable trends. One possibility is that the higher cell seeding density may have masked any substrate compliance effects on cell proliferation. That Sylgard-184 resulted in a notable reduction in cell proliferation just indicates that more study is warranted for the understanding of NIH3T3 cell proliferation on siloxane networks.

5.6 Conclusion

We were able to demonstrate the viability of generating gradients in modulus for siloxane networks by diffusing different formulations of varying cross-linker concentrations. Substrates with storage moduli (G') varying between 10^4 to over 10^5 Pascals could be generated with the hydrosilation chemistry between a hydride terminated PDMS molecule and PVMS. Surface segregation occurred with the cured networks of PDMS and PVMS where the networks with a high concentration of PDMS showed microscale domains at the air-polymer interface. Further evaluation showed the morphology differences were also

obtained when the specimens were exposed to an aqueous environment. In this case, the vinyl moieties would favor the water-polymer interface.

The studies continue to prove that understanding the interplay between the cellular proliferation behaviors due to substrate mechanics is complicated as it involves delicate interplay between chemistry and topography that are often changed as the substrate is tuned for a mechanical variation. The proliferation studies were only completed for substrates of uniform compliance. Additional work is needed to determine if durotaxis is seen on PVMS-PDMS gradient specimens. Prior to performing this study, the exact make-up of the surface has to be ascertained with a combination of surface characterization techniques. In addition, due to limitations of obtaining microscale variations of modulus with the interdiffusion of cross-linker and polymer, another cross-linking mechanism may be necessary to adopt. Chapter 6 of this Ph.D. Thesis details one such possibility: the synthesis of a UV-curable PVMS-based polymer network. The advantage of this polymer would be to not only utilize the precision of a "mask" to control the UV-exposure time for variations in modulus but also eliminate the PDMS_PVMS segregation with a 100% PVMS formulation.

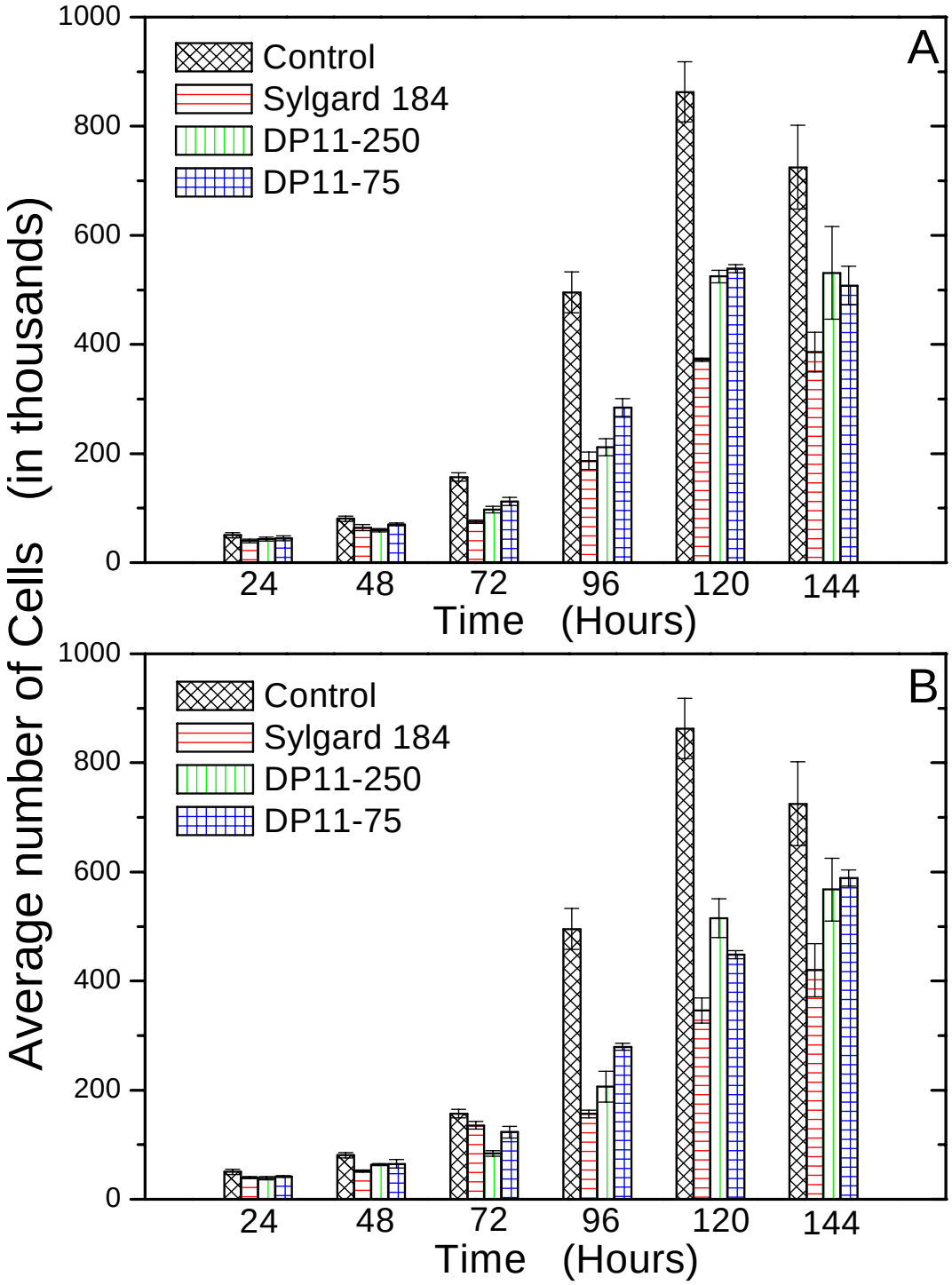

Figure 5.13 A) Cell proliferation results for the 2nd round of substrates evaluated with NIH 3T3 fibroblast cell cutured in DMEM media with 0.1% FBS and 1% PS/G at 37°C. Cells were suspended with trypsin, diluted in PBS, and counter via a BD coulter counter. B) Same samples and cell counting procedure as in (A) except the substrates were pretreated with deionized water to force the surface segregation to equilibrium in an aqueous environment.

5.7 References

1. Merrett, K. et al. Interactions of corneal cells with transforming growth factor beta 2-modified poly dimethyl siloxane surfaces. *Journal of Biomedical Materials Research Part A* **67A**, 981-993 (2003).

2. Zaari, N., Rajagopalan, P., Kim, S., Engler, A. & Wong, J. Photopolymerization in microfluidic gradient generators: Microscale control of substrate compliance to manipulate cell response. *Advanced Materials* **16**, 2133-2135 (2004).

3. Wong, J., Velasco, A., Rajagopalan, P. & Pham, Q. Directed movement of vascular smooth muscle cells on gradient-compliant hydrogels. *Langmuir* **19**, 1908-1913 (2003).

4. Wong, J., Leach, J. & Brown, X. Balance of chemistry, topography, and mechanics at the cell-biomaterial interface: Issues and challenges for assessing the role of substrate mechanics on cell response. *Surface Science* **570 (1-2)**, 119-133 (2004).

5. Wang, H. B., Dembo, M. & Wang, Y. L. Substrate flexibility regulates growth and apoptosis of normal but not transformed cells. *American Journal of Physiology-Cell Physiology* **279**, C1345-C1350 (2000).

6. Wang, H. B. & Wang, Y. L. Substrate flexibility regulates growth and apoptosis of normal but not h-ras-transformed cells. *Molecular Biology of the Cell* **10**, 66A-66A (1999).

7. Peyton, S. R. & Putnam, A. J. Extracellular matrix rigidity governs smooth muscle cell motility in a biphasic fashion. *Journal of Cellular Physiology* **204**, 198-209 (2005).

8. Efimenko, K. et al. Nested self-similar wrinkling patterns in skins. *Nature Materials* **4**, 293-297 (2005).

9. Crowe, J. A. & Genzer, J. Creating responsive surfaces with tailored wettability switching kinetics and reconstruction reversibility. *Journal of the American Chemical Society* **127**, 17610-17611 (2005).

10. Lee, J. N., Jiang, X., Ryan, D. & Whitesides, G. Compatibility of Mammalian Cells on Surfaces of Poly(dimethylsiloxane). *Langmuir* **20**, 11684-11691 (2004).

11. Brown, X. Q., Ookawa, K. & Wong, J. Y. Evaluation of polydimethylsiloxane scaffolds with physiologically-relevant elastic moduli: interplay of substrate mechanics and surface chemistry effects on vascular smooth muscle cell response. *Biomaterials* **26**, 3123-3129 (2005).

12. Uilk, J., Mera, A., Fox, R. & Wynee, K. Hydrosilation-Cured Poly(dimethylsiloxane) Networks: Intrinsic Contact Angles via Dynamic Contact Angle Analysis. *Macromolecules* **36**, 3689-3694 (2003).

13. Andrade, J. *Surface and Interfacial Aspects of Biomedical Polymers* (Plenum Press, New York, 1985).

14. Ohashi, T., Kiehart, D. P. & Erickson, H. P. Dynamics and elasticity of the fibronectin matrix in living cell culture visualized by fibronectin–green fluorescent protein. *Proc. Natl. Acad. Sci. USA* **96**, 2153-2158 (1999).

Appendix 5.1: Materials and Methods

A5.1 Preparation of DPX-Y PDMS-PVMS networks

A typical formulation for a DP11-75 network consisted of 20 grams of PVMS fluid (M_w = 45 kDa), 75 μl of Pt (0) from Aldrich (Karstedt's catalyst), and 6 grams of hydride-terminated PDMS (Gelest H11-Fluid). The order of mixing is important to prevent premature gelation between the catalyst and the hydride-terminated PDMS. The best procedure involves thorough mixing of the PVMS fluid with catalyst prior to the addition of the H11. A lab mixer was used to achieve uniform distribution of the components necessitating de-airing via a vacuum chamber. After the mixture was poured into the desired contained, it was placed in a 70^{o}C oven for 2 days and then at room temperature for at least 5 days prior to use.

A5.2 Preparation of diffusion gradients

Mixtures of varying composition were prepared as described above and poured into the desired container in equal increments. The most successful gradient was generated in the large 30 x 30 cm Petri dish but formulations on a 10 x 25 mm scale were also prepared (data not shown). Once the formulations appeared to have diffused "evenly", they were cured as described above.

A5.3 Wettability measurements

See Chapters 3 and 4 in this Ph.D. Thesis.

A5.4 Dynamic Rheology and Dynamic Mechanical Analysis

See Appendix 4.1 in this Ph.D. Thesis.

A5.5 Cell proliferation protocol

Cell seeding: Using the lab hood UV lamp, sterilize the 24-well plates that have been treated with polymer (PVMS) for 20 min. Treat each well with 500 μL of a 20 μg/mL fibronectin (FN) solution made by diluting the FN stock with sterile deionized water. Treat at 37 ˚C for 1 hour, then remove FN solution and wash once with 1 mL of sterile phosphate buffer solution (PBS). NIH3T3 mouse fibroblasts (American Type Culture Collection, Manassas, VA) were sub-cultured in 10-cm tissue culture polystyrene dishes using Dulbecco's modified Eagle's medium (DMEM) with 10% fetal bovine serum, 2 mM L-glutamine, and the antibiotics penicillin and streptomycin as the growth medium. Unless otherwise noted, all tissue culture reagents were from Invitrogen (Carlsbad, CA). Cells were seeded in growth medium into either the 24-well tissue culture dishes either coated with the appropriate polymer network. One set of wells was left uncoated to be used as the tissue-cultured grade polystyrene control.

A5.6 Cell suspension and counting

Flush the well with sterile PBS and detach the cells from the surface with 0.5 mL/500μL of Trypsin (37 ˚C). Remove the suspended cells from the well and add the appropriate suspension volume to hemocytometer (10 μL) or in a vial (100 μL) for the BD coulter counter. Total number of cells is calculated by multiplying the cell density (ρ) by the total well volume. The cell density for the hemocytometer is calculated from:

(Ave. cell number) x (dilution factor (if used)) x 10^4 = ρ (cells/mL) (5.1)

The cell density for the hemocytometer is calculated from:

$$\rho = \left(\frac{AVE\ count\ \#}{0.5\,mL} \right) \bullet \left(dilution\ factor \right) \quad , \tag{5.2}$$

where the dilution factor is 101 and 201 for 100 and 50 μL of cells, respectively.

CHAPTER 6: UV-Curable Siloxanes

6.1 Introduction

The networks with gradients in compliance prepared by the interdiffusion method described in Chapter 5 of this Ph.D. Thesis were convenient but lacked the precise control of generating gradients on the micro-scale; the length-scale of cells. The disadvantage of this preparation route for generating variations in Young's modulus is its dependence on a diffusion mechanism constrained by the viscous nature of the flow path between the high and low modulus formulations. There may be ways to circumvent this constraint, however. For instance, the surface chemistry of the formulation support substrate (a glass slide or tissue culture Petri dish) has an effect on the siloxane diffusion pattern. As discussed in Chapter 5, our investigation of the diffusion-limited variants revealed a surface segregation between poly(dimethylsiloxane) (PDMS) and poly(vinylmethylsiloxane) (PVMS) components in the cured network. There may be advantages of this segregation that could aid in the design of novel substrates for studying cell-surface interactions. We will discuss these possibilities for future work in the Outlook section of this Ph.D. Thesis. The aim of this Chapter, however, is to first give a brief overview of the compliance-gradients generated to-date, possible UV-curable siloxane systems, and most importantly, to describe our concurrent efforts of generating a photo-curable siloxane polymer to produce micro-scale gradients in mechanical properties.

Poly(acrylamide) (PAAm) has been an attractive polymer for use in tissue engineering research for the ability of the acrylamide monomer to be photo-cured into a network, the

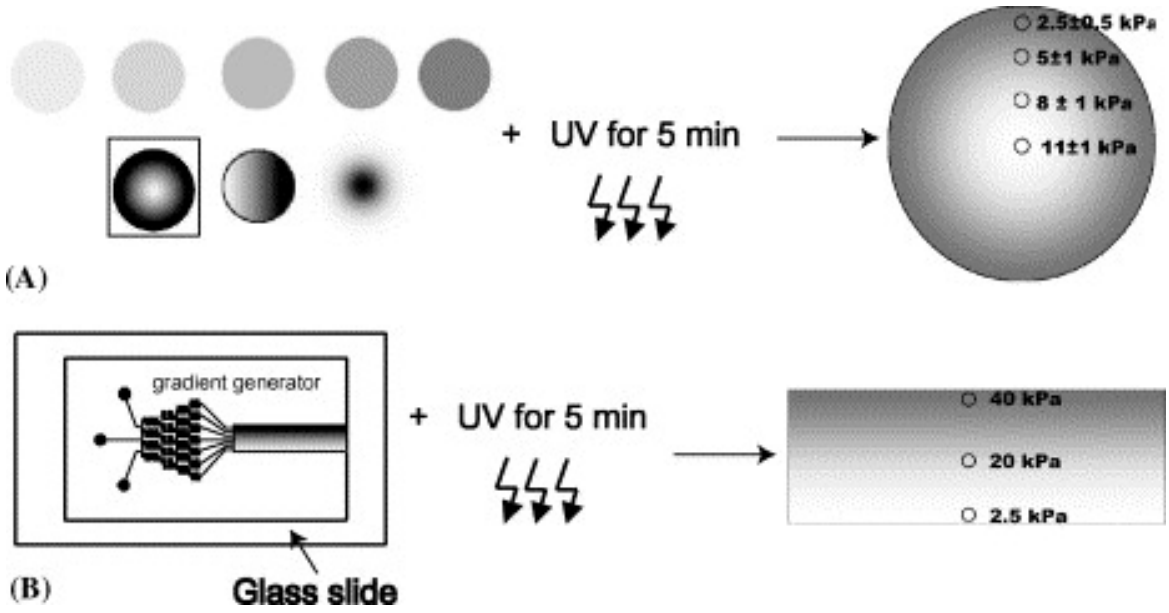

Figure 6.1: "Methods for generating elastic substrata with gradients in mechanical properties. (A) Acrylamide is photopolymerized under transparency masks with varying degrees of opacity. The radial gradient pattern boxed on the left can be used to create a substrate shown on the right with the 'map' of its mechanical properties (Young's modulus). (B) Acrylamide is photopolymerized using a combination of microfluidics and photopolymerization. The gradient generator is used to create a gradient in the crosslinker (bis-acrylamide). The width of the gel is 3 mm, and the gradient in the Young's modulus (as determined from atomic force microscopy) is approximately 12 Pa/μm. In (A), the lighter the shading, the higher the compliance. In (B), the lighter the shading, the lower the compliance." From reference 4.

ability to subsequently modify the pendant $–OCNH_2$ substituents with cell-adhesive ligands, and that it has been well-characterized due to the extensive research with this polymer-system. The pioneering work that demonstrated the cellular behavior of durotaxis utilized a simple compliance gradient formed by letting two different concentrations of bis-acrylamide to diffuse through an acrylamide solution prior to curing. The formed PAAm rigidity-gradient of roughly 40 μm in length demonstrated that National Institutes of Health 3T3 mouse cells migrated from the softer region (Young's modulus ≈14 kPa) to the stiffer regions (Young's modulus ≈ 30 kPa). If the cell migration path originated from the stiffer region in

the direction of the softer region, it was observed that the cells would reverse their direction upon reaching the rigidity-gradient boundary[1]. Improving upon the fabricated PAAm rigidity-gradients, Wong and co-workers implemented two different techniques (*cf.* Figure 6.1)[2]: A) by using a transparency mask over a photo-curable acrylamide solution, they imparted spatial control of the light intensity from the UV source. After 5 minutes of UV-exposure time, the Young's modulus varied in a radial-direction from 11 kPa at the center to 2.5 kPa at the perimeter of the exposed solution and B) with the use of a microfluidic gradient generator, the amount of bis-acrylamide, the cross-linker, was controlled to result in its linear distribution throughout the solution. Upon photo-curing, the area with the most cross-linker resulted in a Young's modulus of 40 kPa versus 2.5 kPa for the area with the least amount of cross-linker[3]. Both compliance-gradient substrates were cultured with vascular smooth muscle cells (VSMCs) that exhibited preferential migration to the stiffer regions of the substrates [4].

While the results of the early PAAm rigidity-gradient experiments demonstrated that the cell behavior was dictated by substrate mechanical signals, a siloxane-based substrate for tissue engineering scaffolds is more desirable for cell-surface study than a PAAm support due to the physiologically relevant mechanical properties of PDMS and its applicability as a FDA-approved biomaterial[5,6]. However, there are complications with utilizing PDMS as a substrate; these arise due to PDMS's resistance to modification with cell-adhesive ligands[4]. Thus, we set out to determine if we could make a photo-curable PVMS network. This would enable us to make gradients in modulus for a 100% vinylmethylsiloxane network eliminating surface segregation issues seen with the PDMS/PVMS blends, preserve the vinyl moiety for

subsequent modification, and use a parallel strategy of controlling the spatial distribution of the light intensity during the UV-curing step via transparency masks.

6.2 UV-curable Silicones

Despite the wide range of available UV-cure mechanisms that have been implemented with siloxane precursors, commercial grade UV-curable silicones were not suitable to our studies. These included elastomers by Loctite Corporation that utilized dual-curing mechanisms. The primary role of this elastomer class is to provide the construction industry with a rapid surface-cure via UV-induction in conjunction with a secondary (and slower) alkoxy-cure mechanism for the complete substrate cure. This precluded these elastomers for use in a gradient-cure mechanism, as they would eventually cure uniformly throughout the substrate with the secondary cure. Gelest and Dow Corning provided UV-curable silicone formulations but they were aimed for resin-grade coatings. Use of the commercial-grade elastomers would also limit surface modification as they are formulated with 100% PDMS.

Products by Dow Corning Corporation, General Electric Company, and Loctite Corporation dominate the majority of UV-curable siloxane synthesis work under various patent landscapes. Siloxane polymers have been formulated with UV-curable functionality such as acrylates, epoxides, norbornene, and thiols[7-15]. Each mechanism presented had it own unique challenges; due to the desire to utilize our PVMS-OH fluid, we opted for a condensation reaction of PVMS-OH with mercaptoalkoxysilanes[16]. This seemed to be a logical choice as 1) it avoided the oxygen inhibition presented by acrylate functionality (of a concern since siloxanes are highly permeable to oxygen, 2) epoxide functionalization of

PVMS-OH would prove challenging due to moisture inhibition, and 3) the desired norbornene intermediate would require additional synthesis steps. The thiol-ene reaction has regained popularity due to the excellent mechanical properties realized in the products, new synthesis routes to mask the odor characteristic of thiol monomers, low inhibition due to oxygen and moisture, and the development of new photoinitiators that allow for better oxidative stability (low-yellowing)[17]. End-capping PVMS-OH with thiol functionality seemed straightforward; it would lead to a siloxane system comparable to a PDMS analog that was reported to exhibit a rapid-cure and produced elastomers with superior mechanical properties[14].

6.3 Synthesis of 3-mercaptopropylmethyl-terminated PVMS

Our synthesis route was adapted from the condensation process of linear dimethyl silanols (*cf.* Scheme 6.1)[16]. This process was performed under vacuum to obtain very high molecular weight materials with the option of adding end-blockers to the formulation enabling various terminus functionality of the resulting siloxane fluid. Adjusting the process to produce a mercapto-terminated PVMS fluid did not require the use of vacuum as we were

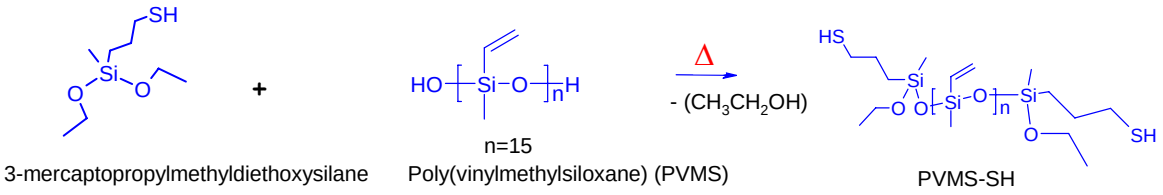

Scheme 6.1: Schematic for making mercapto-terminated poly(vinylmethylsiloxane). Reaction is performed in reflux mode at ≈60°C for ≈2 hours.

not trying to build the molecular weight of the starting PVMS-OH fluid. Ideally, the mercaptoalkoxysilane would be monofunctional to prevent cross-linking and gelation during the synthesis. This monoalkoxysilane was not available commercially. Since its synthesis was not straightforward, 3-mercaptopropylmethyl dimethoxysilane was employed as the end-blocker[18]. In order to promote the condensation reaction between the primary alkoxysilane and the –OH terminal moieties of PVMS, the reaction was heated under reflux to 65^{o}C with 0.1 wt % barium hydroxide. The reaction completion was determined with FTIR, which monitored the disappearance of the hydroxy peaks of the siloxane due to the capping with the 3-mercaptodimethoxysilane (*cf.* Figure 6.2A). As the degree of polymerization (N) of PVMS-OH increased from N=15 to 300, the dimethoxysilane was added in 2-4 fold excess formulated at 2:1 moles of end-blocker per mole of PVMS-OH to limit step-growth polymerization. With high molecular weight PVMS-OH (N = 300), branching occurring during the end-capping reaction could result in an uncontrollable rate of reaction. To limit the molecular weight increase, the catalyst was added after the reaction temperature reached 60^{o}C. The material was removed from heat and filtered after $\approx$1.5 hours at 65^{o}C. The resultant product was precipitated in methanol to remove residual 3-mercaptodimethoxysilane.

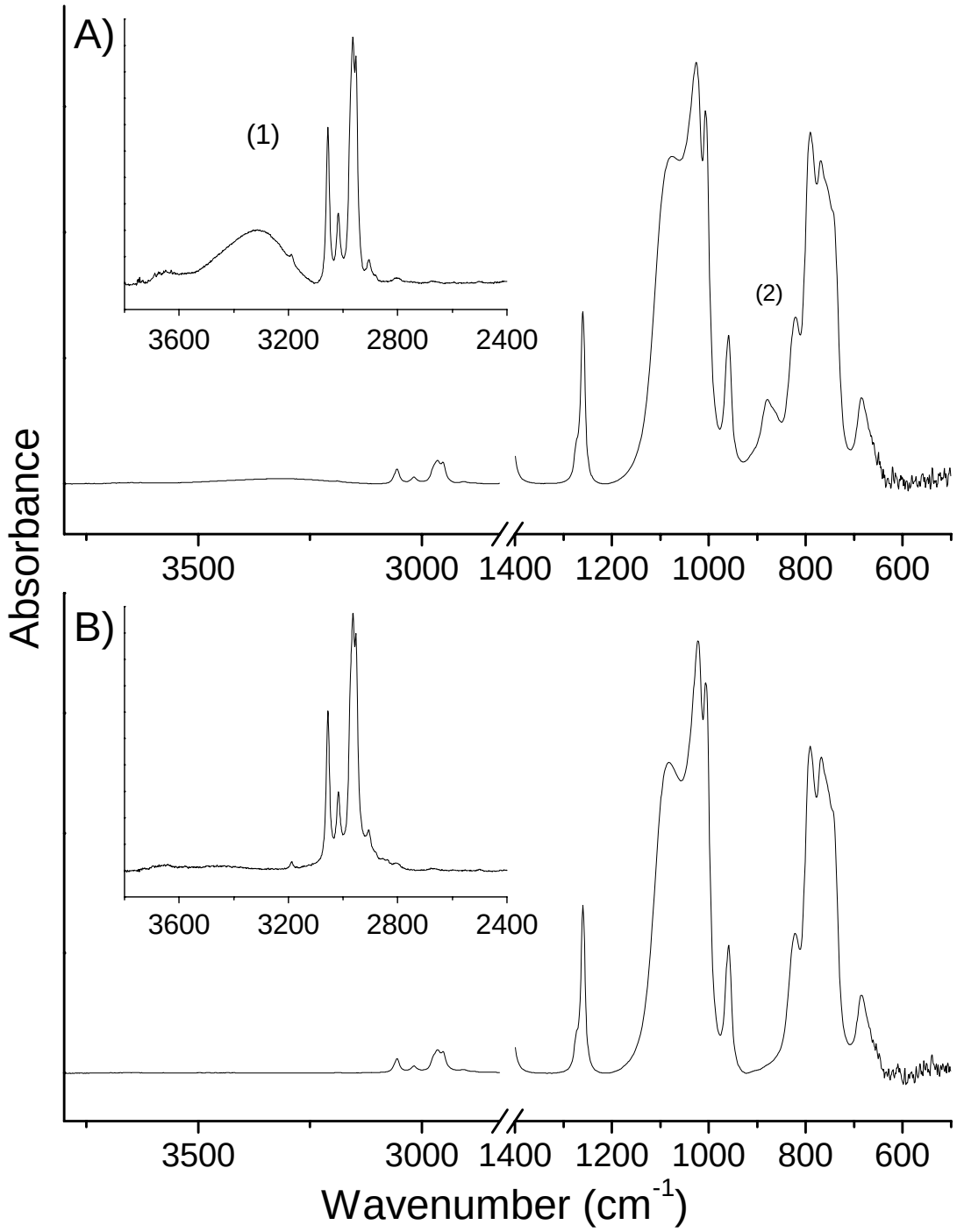

Figure 6.2: FTIR spectra for PVMS (Dow Corning PJ Fluid®) (A) and after the end-capping reaction with mercaptopropylmethyldimethoxy silane (B). Peak (1) is the –OH stretching and peak (2) is the ≡Si-O stretching from the terminus groups of PVMS (≡Si-OH). Note that these peaks are absent in the lower spectrum.

As the hydroxy peaks in the precursor PVMS-OH (N =300) were not apparent with FTIR and –($SiOCH_2CH_3$) and –SH stretching vibrations exhibit weak frequency signals (2840 cm^{-1} and 2560cm^{-1}, respectively), we confirmed that the reaction took place with ^{13}C and ^{1}H NMR (*cf.* Figure 6.3). Upon inspection of the spectra for both PVMS-OH (N=15, PJ Fluid) and PVMS-OH (N=300) in comparison to PVMS-SH, there were obvious differences in the 0.5-3.5 ppm region for ^{1}H and in 12-53 ppm region for ^{13}C indicating chemical shifts due to the mercapto- termination[19,20]. Specifically, in the Figure 6.3B the ^{1}H chemical shifts for PVMS-SH that are absent for PVMS include: 1) the protons on the methoxy group occurs ≈3.5 ppm, 2) the proton on the -S- atom occurs around 1.3-1.6 ppm, and 3) the propyl spacer between sulfur and silicon has proton chemical shifts ranging from 0.9 to 2.5 ppm. The significant peaks in the ^{13}C NMR spectra occur at 50 ppm for the carbon from the methoxy group and between 15-35 ppm for the carbons in the propyl spacer.

After synthesizing PVMS-SH with both short chain PVMS-OH (N=15) and PVMS-OH (N=300), their molecular weight was determined with gel permeation chromatography (GPC) as outlined in Chapter 3 in this Ph.D. Thesis. Figure 6.4 illustrates the GPC differential refractive index (DRI) detector traces for the nominal N=300 PVMS-OH (A) and the resultant PVMS-SH (B). Note that the weight-average molecular weight (M_w) increased from 28 to 57 kDa after the end-capping condensation reaction indicating either branching from the secondary alkoxysilane group or chain extension with PVMS-OH step-growth condensation. The DRI traces show 3 peaks for each sample. The first peak represents the linear PVMS polymer, the second peak corresponds to either vinylmethyl cyclics or low molecular weight linear species, and the third peak is associated with the solvent from the

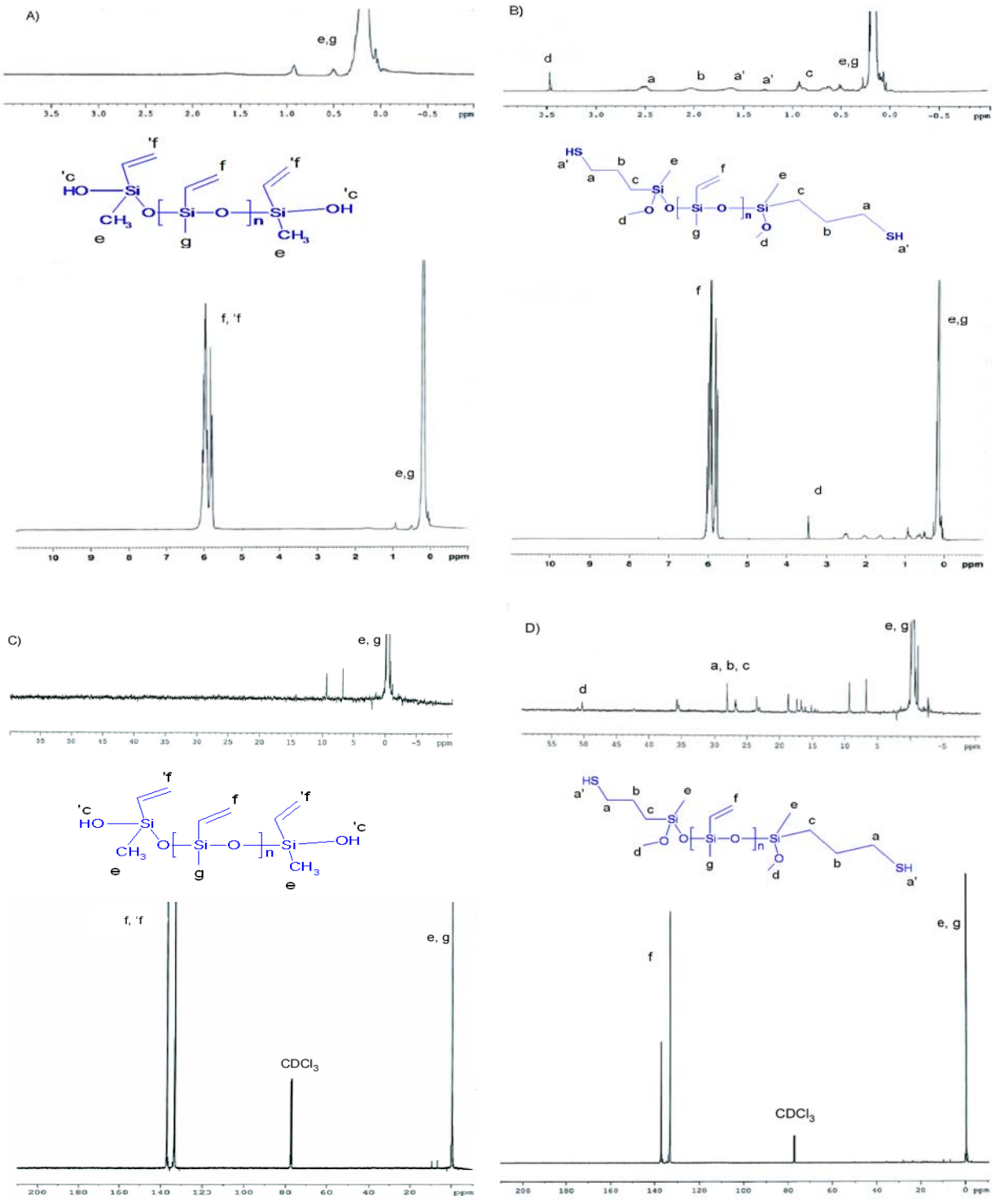

Figure 6.3: ^{1}H NMR for PVMS (A) and PVMS-SH (B). ^{13}C NMR for PVMS (C) and PVMS-SH (D). See text for explanation of chemical shifts.

sample solution. Consistent with the increase in molecular weight is the decrease in short chain/cyclic siloxanes in the PVMS-SH (B) trace as well as a broadening of the main peak. It is interesting to note that even when starting out with low molecular weight (N=15) PVMS-OH, the molecular weight increases from ≈1.5 to ≈42 kDa. The concentration of the condensation catalyst for the N=15 PVMS-OH run was one third the amount used for the high molecular weight PVMS-OH illustrating the differences in reaction rates for the different viscosity fluids. As the mixing apparatus was the same for both runs, the catalyst amount was a means to overcome the mass transfer limitations of the low molecular weight

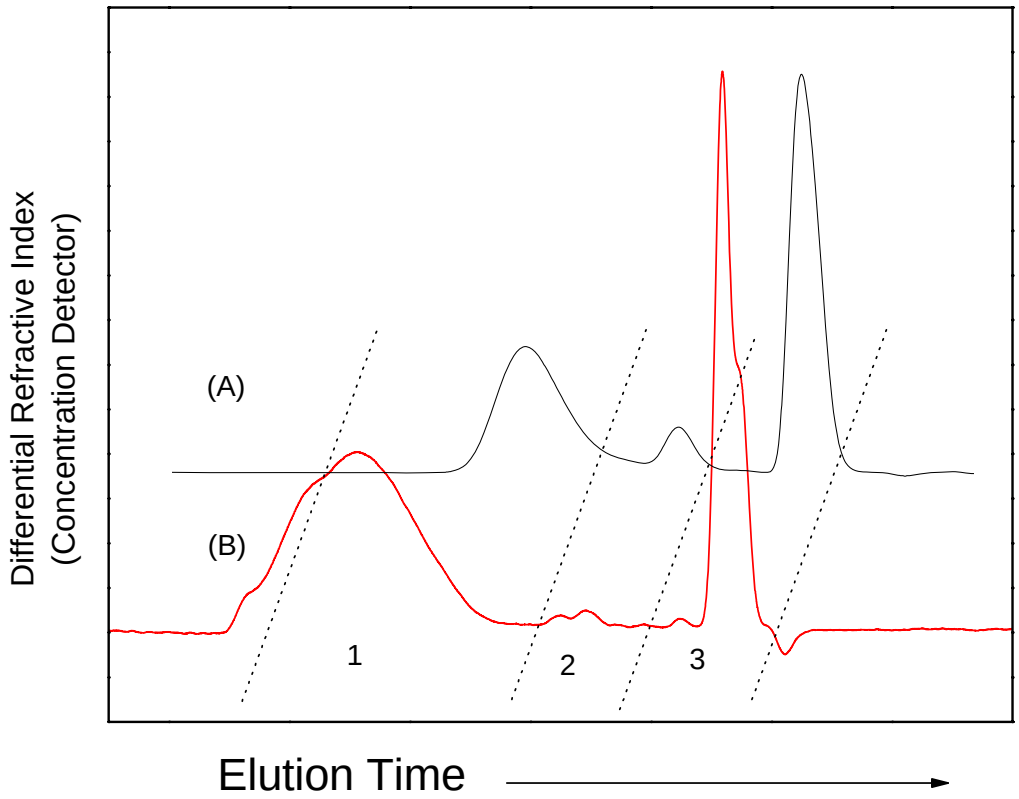

Figure 6.4: GPC traces for PVMS (A) precursor (n=300) and the resultant PVMS-SH terminated fluid (B). Peak 1 is the liner siloxane fluid, Peak 2 corresponds likely low molecular weight PVMS species (or cyclics) and Peak 3 represents the mobile phase (toluene).

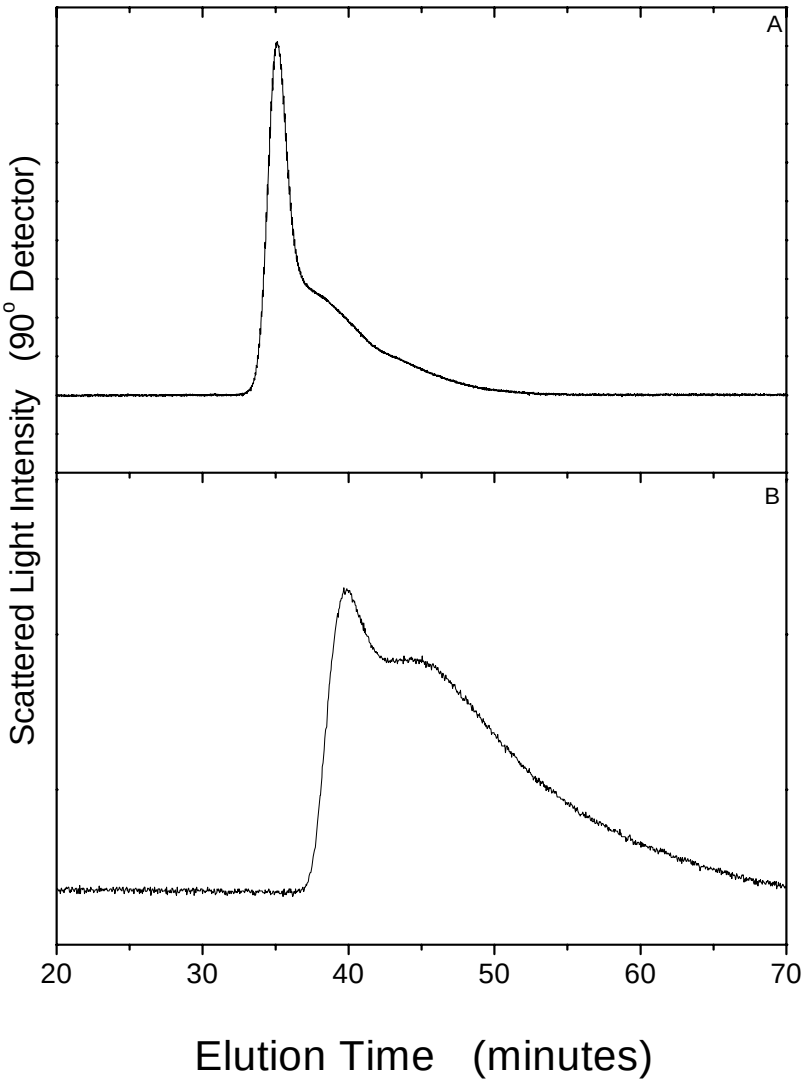

Figure 6.5: Molecular weight distribution for mercapto-endcapped PVMS with the starting PVMS fluid possessing a M_w of 28 kDa (A) versus 1.5 kDa (B).

end-blocker species throughout the more viscous PVMS-OH fluid. The reaction starting with PVMS-OH (N=15) demonstrates that the synthesis of PVMS-SH can be a one-step reaction of end-capping and step growth condensation occurring simultaneously. Starting with the higher molecular weight material was an attempt to control the amount of branching and prevent the reaction between the secondary methoxysilane and the hydroxy group from

occurring. Inspection of the GPC traces in Figure 6.5 reveals that while the resultant product with the higher molecular weight PVMS-OH material produced a narrower molecular weight distribution of final polymer, a low molecular weight tail was present in both cases.

Qualitative analysis of the NMR spectra, molecular weight analysis, and successful UV-curing of the PVMS-SH product validated our reaction scheme and process. We proceeded to investigate ways of generating variants in modulus with the formulated PVMS-SH fluid.

6.4 Formation of UV-curable PVMS networks

As the synthesis of a mercapto-terminated PVMS fluid was successful, the next step was to produce networks with the material cured via ultraviolet light. It was our observation that the mercapto-terminated PVMS possessed little odor and a photoinitiator (2-hydroxy-2-

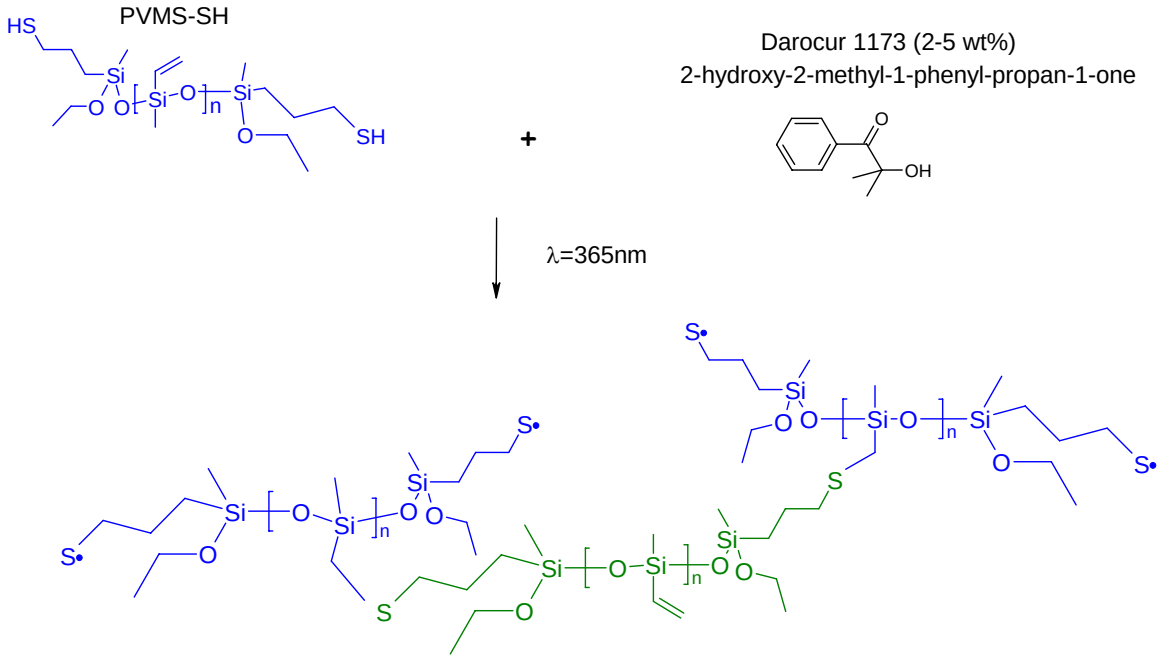

Scheme 6.2: Steps to making a UV-cured PVMS network. The UV exposure duration dictates the degree of cross-linking.

methyl-1-phenyl-propan-1-one, Darocur® 1173) commonly used for biomedical applications was soluble in PVMS. We explored two simple formulations for our networks: 1) a blend of 65% of PVMS-SH (≈41 kDa) and 35% (w/w) of PVMS-OH (≈28 kDa) with 2-3% of photoinitiator and 2) 100% PVMS-SH (≈58 kDa) with 2-3 % photoinitiator. The blend formulation was an attempt to incorporate PVMS with a lower polydispersity index into the mixture, reduce the amount of available cross-linking, and provides a broader distribution of cross-linked density throughout the cured elastomer. Scheme 6.2 depicts the general synthesis of a network with 100% of PVMS-SH polymer. The reaction proceeds with hydrogen abstraction from the sulfur atom after UV-initiation of the photoinitiator. The thiol

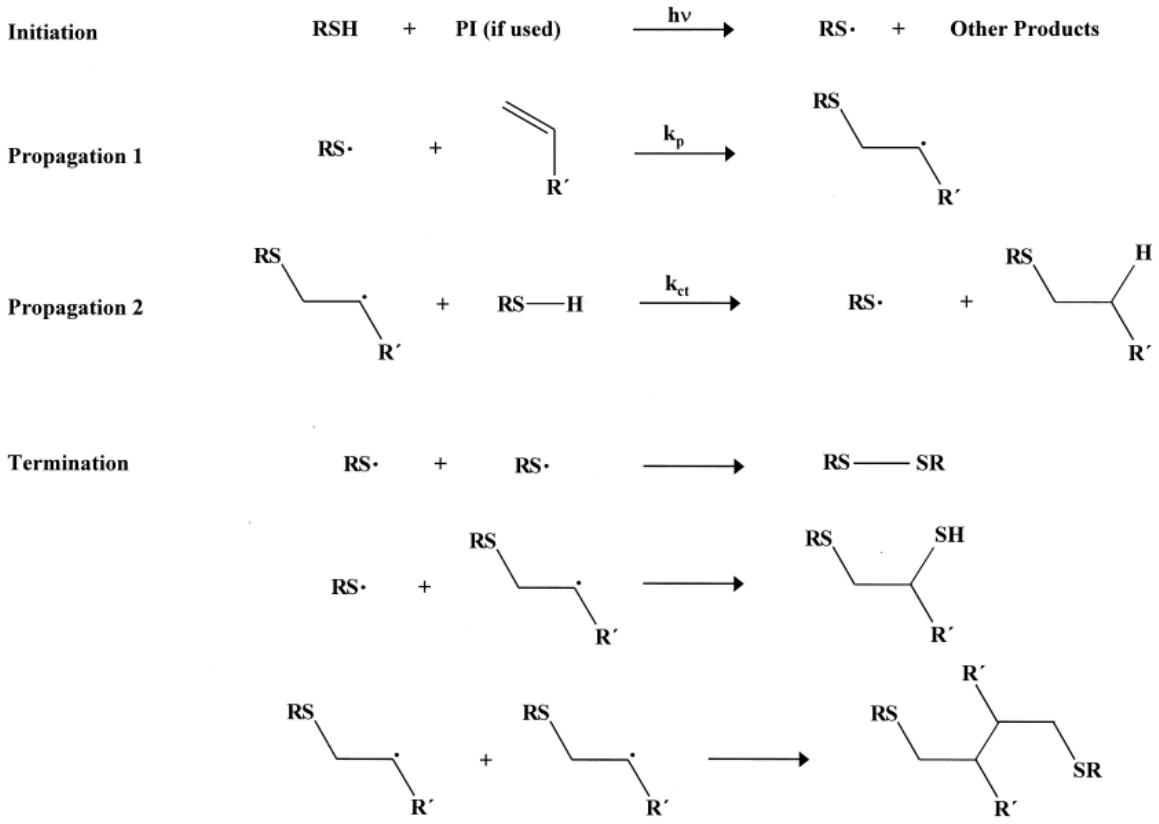

Scheme 6.3: General thiol-ene photopolymerization process[17].

radical attacks the vinyl substituent, whereas the formed carbon radical abstracts hydrogen from another mercapto- group. Cross-linking of the siloxane-ene and thiol-terminated siloxane continues until the radicals are terminated or UV-exposure is eliminated (*cf.* Scheme 6.3). As homopolymerization of the siloxane–ene component is not favored, only with prolonged UV-exposure will vinyl-to-vinyl cross-linking likely occur. This undesirable cross-linking will reduce the overall elasticity of the substrate.

Forming networks with 100% PVMS-SH increases the likelihood that more siloxane chain segments are incorporated in the network. As the number of available cross-link sites greatly outnumbers the potential of thiol radicals generated, formulating with a blend of PVMS-SH and PVMS-OH reduces the total number of PVMS-S• available to react across the C=C substituent of the siloxane backbone. This could result in some "dangling" PVMS chains in the network. With either formulation, if termination occurs between two PVMS-S• segments, it would act as a chain extender, as shown in Scheme 6.3. A common concern regarding the formation of the -Si-C-C-S-C- bond is its thermal stability due to the predicted liability of heteroatomic bonds beta to the silicon atom as shown in Scheme 6.4[13]. For example, when a PDMS-ran-PVMS copolymer was modified with 2-(2-benzimidazolyl)

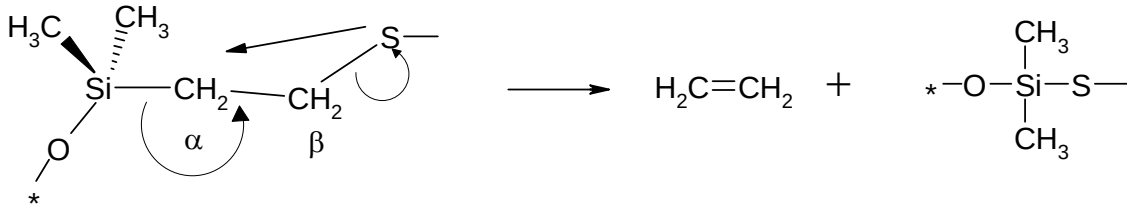

Scheme 6.4: Rearrangement to -Si-S- due to thermal instability of the Si-C-C-S bond. Redrawn from reference 13.

ethanethiol, there was a significant reduction in weight loss at 360°C compared to 500°C with the unmodified polymer[21]. While this thermal instability may preclude the use of siloxane thiol-ene elastomers at high temperatures, they are still suitable for current research where temperatures will remain below 100°C.

Rheological properties were obtained with an ARES rheometer operating isothermally at 30°C within the linear viscoelastic regime for elastomers cured at 365 nm for various times

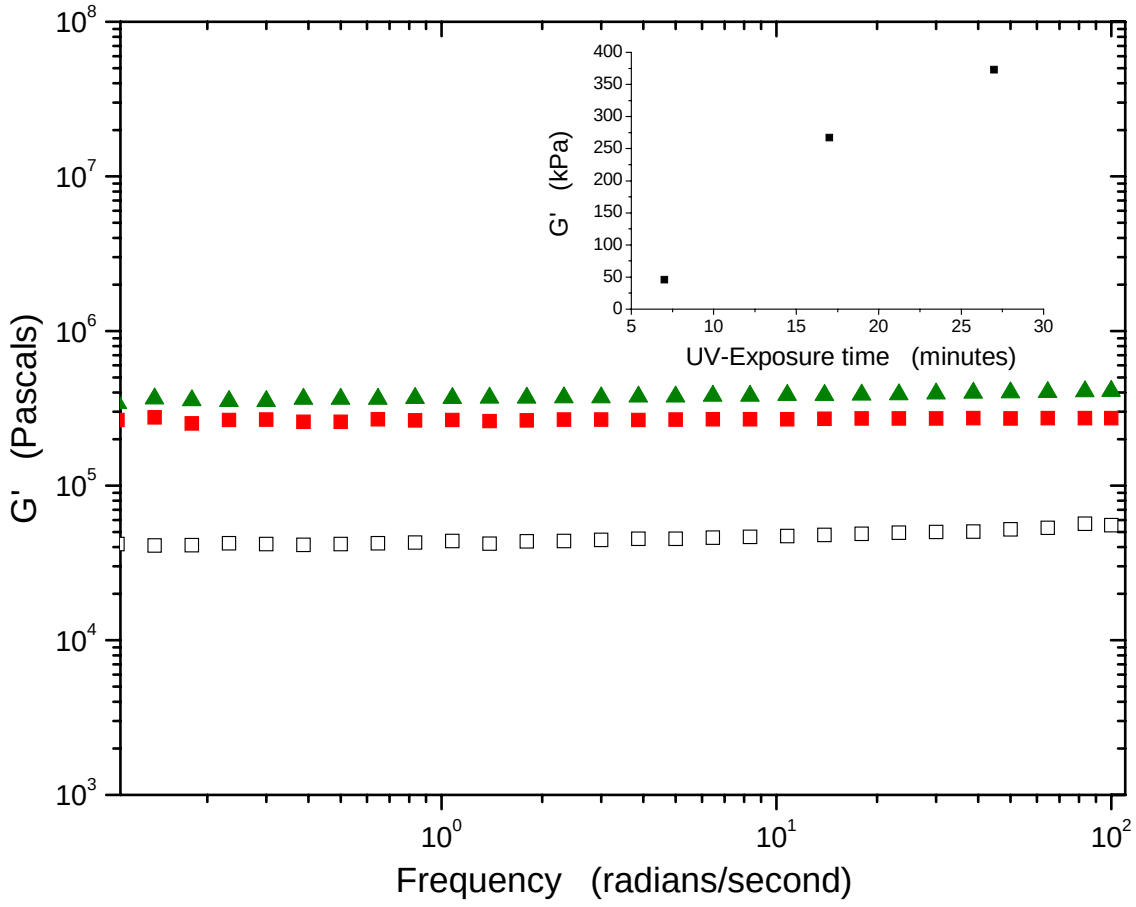

Figure 6.6: Dynamic rheology frequency sweep data for a network of 65/35 PVMS-SH/PVMS. UV cured at 365 nm for 7 (□), 17 (■), and 27(▲) minutes. Scan performed at 30°C and at low strain (0.1%) determined to be within the LVE region. The inset shows the range of G' versus cure time.

(*cf.* Figure 6.6). Increasing the exposure time from 7 to 27 minutes resulted in an order of magnitude change (from 30 to 300 kPa) in the storage modulus (G'). This range in modulus showed promise for generating compliance gradients by simply varying the time (or intensity) of UV-exposure.

A control sample for the 100% PVMS-SH formulation was analyzed with Dynamic Mechanical Analysis (DMA) in the temperature ramp mode. The glass transition temperature was determined by the large step change in E' was 150 K, similar to standard alkoxy-cure PVMS (*cf.* Figure 6.7). Closer inspection of the DMA data reveals a large disparity between the tan δ for PVMS and PVMS-SH. With standard alkoxy-cure PVMS, the cross-linking occurs at the chain ends. This is not the case for PVMS-SH where backbone cross-linking is the mode for network formation. As tan δ = E"/E', it is apparent with the data for PVMS-SH that the elastic component is significantly higher for PVMS-SH in the rubbery regime as tan δ approaches zero; indicative of a solid-like behavior. This result is logical as the backbone flexibility is reduced through cross-linking of the vinyl substituents thus reducing the molecular weight (and motion) between cross-links. Although the modulus goes up as a function of temperature as seen in other siloxane networks (*cf.* Chapter 4 in this Ph.D. Thesis), it increases at a much higher rate (dE'/dT = 4.8 MPa/K for PVMS-SH versus 0.181 MPa/K for PVMS). In addition, this temperature-dependent increase in modulus occurs at ≈310 K for the PVMS-SH network versus ≈285 K for the PVMS network. Two phenomena could be influencing the increase in modulus with respect to temperature. The first could be simply additional cross-linking occurring throughout the network. This was not the case with PVMS as post-testing after the temperature ramp did

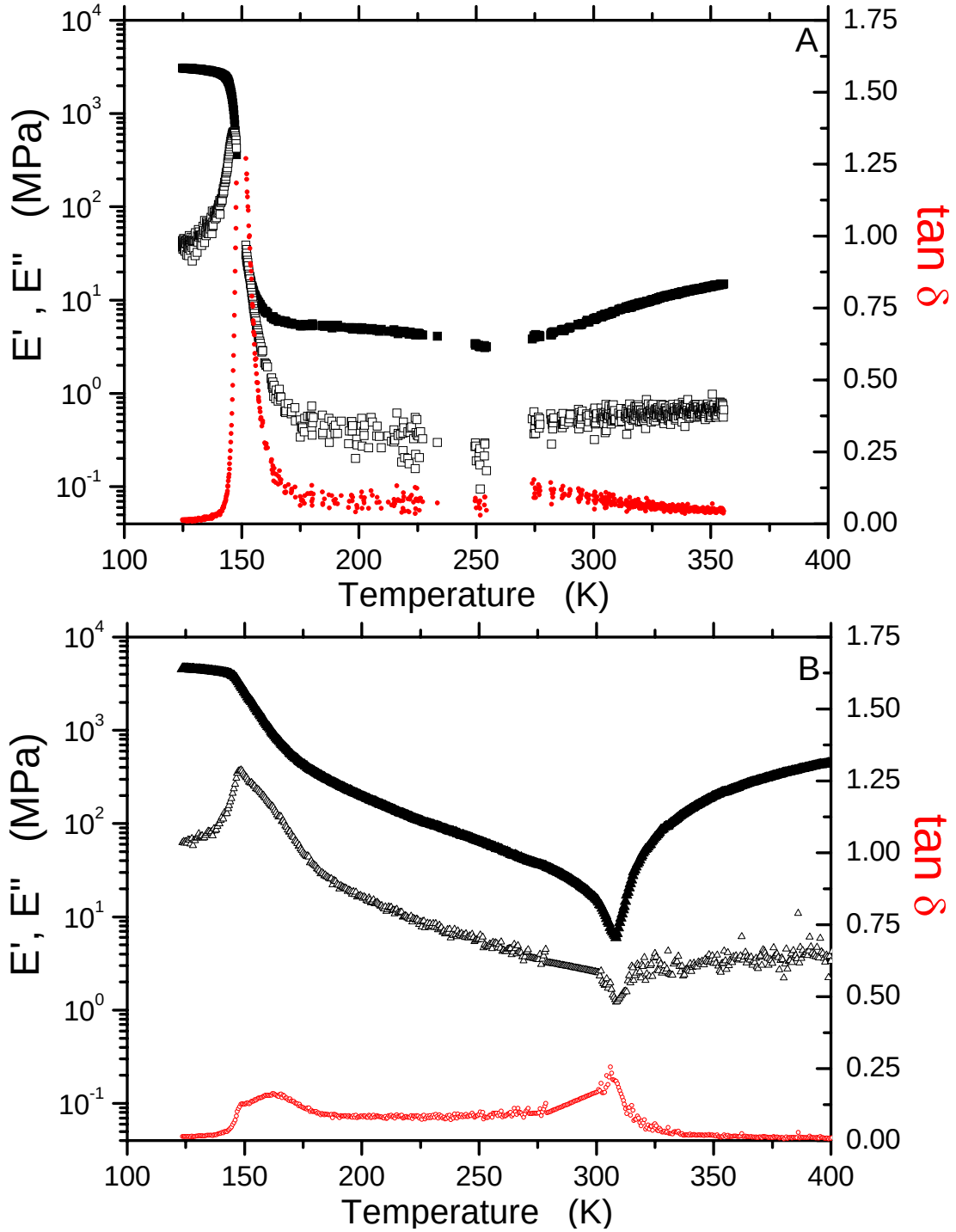

Figure 6.7: Dynamic Mechanical Analysis for PVMS cured via an alkoxy mechanism (A) and 100% PVMS-SH UV-crosslinked material (B). UV cure performed at 365 nm for 7 minutes. Storage modulus E'(closed symbols ■ , ▲), loss modulus E" (open symbols □ , △) and tan delta (●,○) as a function of temperature (Frequency = 1 Hz and set amplitude of 30 micron for LVE region).

not indicate an increase in E'. Post-testing was not performed with the PVMS-SH network which is necessary to determine if further crosslinking is occurring at elevated temperatures. The other phenomenon would follow the theory of rubber elasticity where the elastic modulus is directly proportional to temperature as described by

$$E' = 3 \cdot \frac{\rho RT}{M_c} \tag{6.1}$$

where ρ is the polymer density, R the gas constant and M_c the molecular weight between crosslinks[22]. Equation 6.1 assumes that the overall polymer strand molecular weight is much larger than M_c, which is the case for PVMS-SH networks but does not hold for alkoxy-cured PVMS networks. Instead the following relation would apply:

$$E' = 3 \cdot \frac{\rho RT}{M_c}\left(1 - \frac{2 \cdot M_c}{\bar{M}_n}\right) \tag{6.2}$$

where M_n is the average polymer strand molecular weight[22]. As M_n approaches M_c this relation fails as the quantity $(1\text{-}2M_c/M_n)$ becomes negative. Nonetheless, it is instructive to assess the degree of cross-linking for PVMS-SH networks in relation to alkoxy-cured PVMS networks. As can be expected due to the differing cross-linking methods, the slope of a linear fit of E' versus temperature is 30 times steeper for PVMS-SH than alkoxy-cured PVMS indicating increased crosslinking for PVMS-SH. Comparing E' at room temperature and at 310 K (cell incubation temperature) yields additional information worthy of further investigation. Essentially, at 310 K the moduli of PVMS-SH and PVMS are very similar (8.24 MPa and 6.31 MPa, respectively). At room temperature, the modulus of PVMS-SH is

twice as high as that of PVMS. More dynamic rheology experiments performed isothermally would elucidate if these relative differences are accurate.

To ascertain if PVMS-SH could be used to generate gradients in modulus, several slides were coated with the uncured formulation, covered with a patterned transparency film, and exposed to UV for 12-20 minutes (*cf.* Figure 6.8). After the desired exposure time, the film was removed from the UV-source and placed in the dark to prevent subsequent cross-linking. Mechanical probing of the material surface to nm-scale depths was performed with a Hysitron Triboindenter in constant force mode. Results for specific regions of two cured substrates are shown in Figure 6.9. The change in Young's modulus was reported in relative values due to the tip's geometry resulting in erroneously high values. The overall trend in modulus change is valid, however, and the data indicates values ranging from 50 to 100% of the maximum obtained modulus value of ≈300 kPa (obtained on the ARES rheometer).

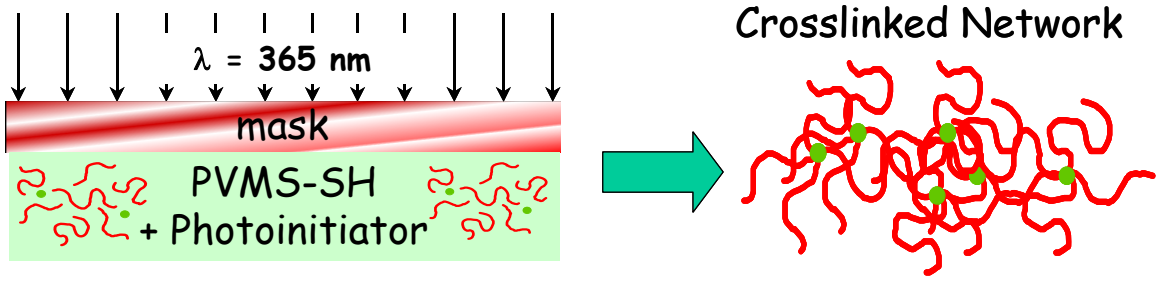

Figure 6.8: Illustration of gradient/pattern formation of UV-curable PVMS-SH fluid.

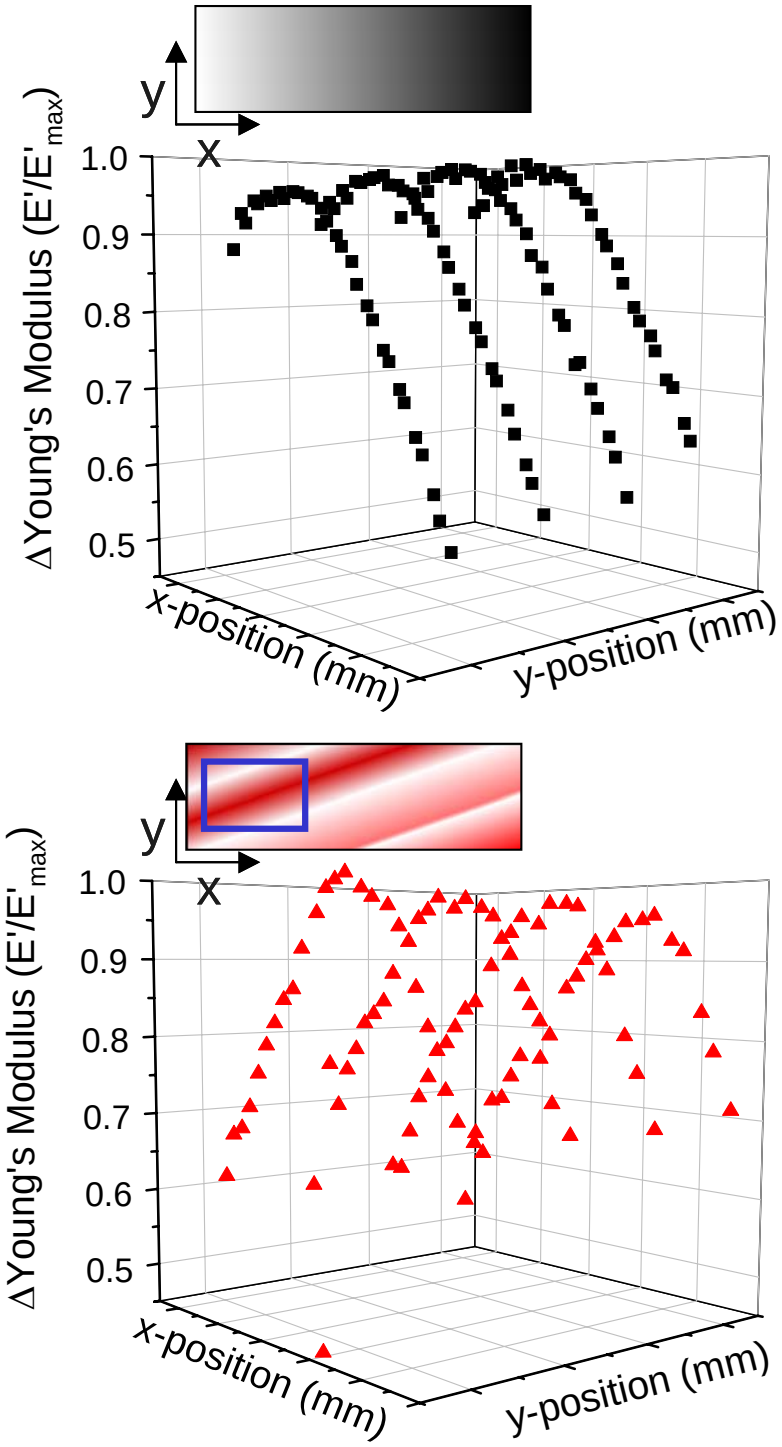

Figure 6.9: Nanoindentation of PVMS-SH cured networks. Material was cured beneath a patterned mask for a specified amount of time. The boxed region in the lower mask is the area tested with nanoindentation. Gradients in modulus were successfully produced with this technique.

6.5 Conclusion

As in Chapter 5 in this Ph.D. Thesis, the compliance-gradients can be of aid in the understanding of cell growth, proliferation, and migration on synthetic materials. To insure that the PVMS-SH networks would be conducive to cell proliferation, the cured substrate was exposed to complete cell-culture media, seeded with NIH3T3 mouse fibroblasts, and observed for over 6 days. Qualitatively the cells appeared to be migrating to the softer regions of the material and atypical cell apoptosis was not observed. Unfortunately, we stopped tending to the cells before a picture and quantitative cell count was obtained but we were encouraged by these preliminary results. Additional studies of cell behavior on these surfaces are currently in progress.

The synthesis of an UV-curable PVMS fluid enables the generation of compliance gradients. The reaction time for a cured network is less than 10 minutes with a direct UV-source of 365 nm and is about 30 minutes for the networks subject to the gradient transparency masks. Future work includes the utilization of the vinyl substituent for surface functionalization; both uniform and gradient in nature.

6.6 References

1. Lo, C.-m., Wang, M.-B., Dembo, M. & Wang, Y.-l. Cell movement is guided by the rigidity of the substrate. *Biophysical Journal* **79**, 144-152 (2000).

2. Wong, J., Velasco, A., Rajagopalan, P. & Pham, Q. Directed movement of vascular smooth muscle cells on gradient-compliant hydrogels. *Langmuir* **19**, 1908-1913 (2003).

3. Zaari, N., Rajagopalan, P., Kim, S., Engler, A. & Wong, J. Photopolymerization in microfluidic gradient generators: Microscale control of substrate compliance to manipulate cell response. *Advanced Materials* **16**, 2133-2135 (2004).

4. Wong, J., Leach, J. & Brown, X. Balance of chemistry, topography, and mechanics at the cell-biomaterial interface: Issues and challenges for assessing the role of substrate mechanics on cell response. *Surface Science* **570 (1-2)**, 119-133 (2004).

5. Colas, A. & Cutis, J. in *Biomaterials Science: An introduction to Materials in Medicine* (ed. Buddy Ratner, A. H., Fredrick Schoen, and Jack Lemons) (Elsevier, Inc., 1996).

6. Colas, A. & Cutis, J. in *Biomaterials Science: An introduction to Materials in Medicine* (ed. Buddy Ratner, A. H., Fredrick Schoen, and Jack Lemons) (Elsevier, Inc., 1996).

7. Crivello, J. & Lee, J. in *Radiation Curing of Polymeric Materials* (eds. Hoyle, C. & Kinstle, J.) 398 (American Chemical Society, Washington D.C., 1990).

8. Eckberg, R. P. & Riding, K. D. in *Radiation Curing of Polymeric Materials* (eds. Hoyle, C. & Kinstle, J.) 382 (American Chemical Society, Washington D.C., 1990).

9. Fouassier, J. P. *Photoinitiation, Photopolymerization, and Photocuring* (Hanser Publishers, Munich, 1995).

10. Gordan, D. J. & Ziemelis, M. J.,Radiation-curable organopolysiloxane coatings. Dow Corning Corporation, USA 4107390, 1978.

11. Goudy, W. G. & Keil, J. W.,Organic rubbers with mercaptoorganosiloxanes having improved elongation. Dow Corning Corporation, USA 3,380,196, 1968.

12. Homan, G. R. & Lee, C.-l.,Sulfur containing silicone elastomer and method of preparation. Dow Corning Corporation, USA 4066603, 1978.

13. Jacobine, A. & Nakos, S. in *Radiation Curing* (ed. Pappas, S. P.) 181- (Plenum Press, New York, 1992).

14. Lee, C.-l. & Lutz, M.,Fast ultraviolet radiation curing silicone compositions. Dow Corning Corporation, USA 4780486, 1986.

15. Mine, K., Nalto, H. & Yamakawa, K.,Method for curing ultraviolet-curable silicone compositions. Dow Corning Toray, European Patent 0 728 799 A1, 1996.

16. Rees, S. & Westall, S.,Process for producing organosilicon products. Dow Corning Limited, European Patent Application 0 382 365, 1990.

17. Hoyle, C. E., Lee, T. Y. & Roper, T. Thiol-Enes: Chemistry of the Past with Promise for the Future. *Journal of Polymer Science: Polymer Chemistry* **42**, 5301-5338 (2004).

18. Korth, K., Albert, P. & Klefer, I.,Process for preparing(mercaptoorganyl)alkoxysilanes. Degussa AG, USA 6995280 B2, 2006.

19. http://www.acdlabs.com/products/spec_lab/predict_nmr/, ACD/HNMR Predictor & ACD/CNMR Predictor, ACD / Labs, Toronto, 2007.

20. Taylor, R., Parbhoo, B. & Fillmore, D. in *The Analytical Chemistry of Silicones* (ed. Smith, A. L.) 347-420 (John Wiley & Sons, INC., New York, 1991).

21. Persson, J. C. & Jannasch, P. Intrinsically Proton-Conduction Benzimidazole Units Tethered to Polysiloxanes. *Macromolecules* **38**, 3283-3289 (2005).

22. Murayama, T. *Dynamic Mechanical Analysis of Polymeric Materials* (Elsevier Scientific Publishing Company, Amsterdam, 1978).

Appendix 6.1: Materials and Methods

A6.1 Synthesis of PVMS-SH

A standard reaction consisted of 300 grams of Dow Corning PJ Fluid®, 10.52 g of 3-mercaptopropylmethyldimethoxysilane (Aldrich) and 0.342 g of $Ba(OH)_2 \cdot 8H_2O$ (Aldrich) that was agitated in a 3-neck flask in reflux mode. The reaction was held at 60°C for 2.5 hours. The barium catalyst was removed from the resultant product by filtering through a cake of diamateous earth (Celite 545 from Aldrich) twice, which effectively terminated the reaction. The product was a clear viscous liquid that was further purified by extraction into methanol.

Disapperance of the –OH stretching (3200-3500 cm^{-1}) and the SiOH stretching (850-925 cm^{-1}) in FTIR confirmed the reaction of the -ethoxysilane with the -hydroxy endgroup on PJ Fluid.

A6.2 Network Formation

Darocur® 1173 (Ciba-Geigy) was added at a 2-3% (w/w) relative to the amount of PVMS-SH. This mixture was de-aired, poured into 30-60 mm Petri dishes and exposed to a 365 nm UV source for 7 minutes. The residual photoinitiator was extracted with methanol and the sample was dried before testing.

A6.3 Nanoindentation

Testing of the mechanical properties of modified and unmodified PVMS networks were performed by using Hysitron Triboindenter. The instrument was equipped with quasi-static and dynamic mode of operation, force and displacement controlled (feedback) and an

integrated AFM head. Indentations were performed at room temperature in the acoustic enclosure of the Triboindenter. Two different tips were used to perform indentations, a 150 nm Berkovic and a 46 μm conical diamond tip, the calibration of the diamond tips was performed on standard fused quartz. Force-displacements curves of indents were analyzed by using Oliver-Pharr method by using the software TriboScan supplied by Hysitron. Only the results of displacement controlled quasi-static indentations are reported. The reduced modulus is calculated using equation 6.1:

$$E_r = \frac{S\sqrt{\pi}}{2\sqrt{A}} \quad \text{and} \quad \frac{1}{E_r} = \left(\frac{1-\nu^2}{E}\right)_{sample} + \left(\frac{1-\nu^2}{E}\right)_{indenter} \tag{6.1}$$

where (S) is the stiffness of the unloading curve, (A) is the projected contact area, and ν is Poisson's ratio. The initial unloading contact stiffness (the slope of the initial portion of the unloading curve) is defined as:

$$S = \frac{dP}{dh}. \tag{6.2}$$

For a standard diamond indentor probe, $E_{indenter}$ is 1140 GPa and $\nu_{indenter}$ is 0.07. Poisson's ratio varies between 0 and 0.5 for most materials.

The samples were cured on glass slides which were mounted on the magnetic plate by attaching metal AFM disc with super glue. A series of indentations were performed on each sample by considering the minimum distance not to effect the neighboring indentations and the size of the each sample.

In separate experiments standard deviation of the tips were calculated on homogenous modulus samples and they are found to be ≈3% of the modulus values. In addition, the

indented surface was scanned with the integrated AFM in non-contact mode and no visible deformation or cut on the network was observed. The same test conditions were used for each sample and the test parameters for displacement-controlled indentations are as follows: 500 nm/sec loading, 5 seconds of hold period and 500 nm/sec unloading.

Force controlled indentations: In this mode the software calculates the force needed to extend the springs of the capacitor transducer during the test and adjusts the total force applied on the moving plate of the transducer to apply the set-point force on the sample.

*Displacement controlled indentations***:** the moving plate of the transducer penetrates in to the surface as much as the set-point and records the force vs. displacement data.

A6.4 NMR Spectroscopy

All of the pulsed field NMR experiments were performed on a Bruker AVANCE 500 MHz Spectrometer (1996) with Oxford Narrow Bore Magnet (1989), SGI INDY Host Workstation, XWINNMR Software version. The instrument is equipped with three Frequency Channels with Wave Form Memory and Amplitude Shaping Unit, with three Channel Gradient Control Unit (GRASP III), variable Temperature Unit, Pre-Cooling and Temperature Stabilization Unit. 5 mm ID 1H/BB (^{109}Ag-^{31}P) Triple-Axis Gradient Probe (ID500-5EB, Nalorac Cryogenic Corp.) has been used for all measurements.

The NMR probe was tuned to C-13 frequency, which is 125.75 MHz in the 500 MHz spectrometer (^{1}H frequency -500.128 MHz). The NMR probe was tuned to Si-29 frequency, which is 99.36 MHz in the 500 MHz spectrometer (^{1}H frequency -500.128 MHz). A combination of homonuclear ^{1}H, ^{13}C and ^{29}Si methods were applied to study the structure of polymer. Chromium(III) acetyl acetonate, Aldrich 202231 was used as an efficient

relaxation reagent for ^{29}Si NMR studies. ^{13}C (1D) and ^{1}H spectrum were also run with proton decoupling for confirmation of the peak assignments.

Sample Preparation and Instrumental Parameters

The NMR samples were prepared by dissolving 0.2 grams of each sample in approximately 0.5 grams of $CDCl_3$ then transferring the solution to a 5-mm NMR tube for analysis. Tubes were carefully washed and dried for 24 hours in an oven and bubbled with nitrogen before being capped for storage. Samples for ^{29}Si were prepared with 1% of relaxation agent to shorten the T_1 relaxation time[1].

All spectra were acquired at 298 K. Tetramethylsilane was used as an internal standard. Data were processed with Bruker software XWINMR 3.6. and standard processing parameters. The instrumental parameters for acquisition of the one-dimensional proton and carbon data are listed in Table A6.1 below:

Table A6.1: NMR instrument parameters for ^{1}H, ^{13}C, and ^{29}Si.

Parameter	^{1}**H** value
Spectrometer frequency (MHz)	500.128
Spectral width (Hz) and (ppm)	6613.7 Hz or 13.2 ppm
Number of data points	32 K
Relaxation Delay (s)	1
Acquisition time (s)	2.47
Pulse width (μs) and tip angle	10.5 at 90^{o}
Number of transients	16
Number of dummy scans	0

Table A6.1 continued.

Parameter	**^{13}C v**alue
Spectrometer frequency (MHz)	125.76
Spectral width (Hz) and (ppm)	30303 Hz or 240ppm
Number of data points	32 K
Relaxation Delay (s)	1
Acquisition time (s)	0.3
Pulse width (μs) and tip angle	14 at 90^{o}
Number of transients	1K
Number of dummy scans	16

Parameter	**^{29} Si value**
Spectrometer frequency (MHz)	99.36
Spectral width (Hz) and (ppm)	9936 Hz or 103ppm
Number of data points	32 K
Relaxation Delay (s)	1
Acquisition time (s)	0.3
Pulse width (μs) and tip angle	14 at 90^{o}
Number of transients	4K
Number of dummy scans	16

A6.4 References

1. Taylor, R., Parbhoo, B. & Fillmore, D. in *The Analytical Chemistry of Silicones* (ed. Smith, A. L.) 347-420 (John Wiley & Sons, INC., New York, 1991).

CHAPTER 7: Summary and Outlook

7.1 Summary

The overall aim of this Ph.D. Thesis was to study the characteristics of siloxane surfaces; a $9.3 billion industry that is viable with forecasted growth for a material with intrinsic chemical and physical characteristics that ascertain technical advances not always possible with hydrocarbon materials. Combining silicones with organic materials leads to hybrid structures that possess the best features from both technologies. A few years ago, our research group achieved such a hybrid material by marrying the flexible silicone backbone with a densely packed monolayer of semi-fluorinated alkane chains coined “mechanically assembled monolayers” (MAMs). The high degree of elasticity in silicone elastomers enabled the cured network to be “stretched” during surface modification. Upon release from its stretched state, it recovered its original length simultaneous with the formation of an ordered alkane chain mono-layer upon its surface.

We probed controlling the surface mobility of siloxane elastomers extending the material platform established by the MAMs technology. Recognizing that while we prevented surface reconstruction utilizing the MAMs technique, there are certain advantages of achieving reconstruction. As we went from studying poly(dimethylsiloxane) (PDMS) to poly(vinlymethlsiloxane) (PVMS) elastomers, we assessed the dual-energy nature of the surface imparted from the differing characteristics of the vinyl and methyl substituents. Due to the intrinsic mobility of the siloxane backbone, the surface chemical make-up of PVMS will oscillate between the lower surface energy methyl groups and the higher surface energy vinyl groups depending on the contacting media at its interface. Utilizing time-dependent

static contact angle of water (θ_{DIW}) measurements enabled the evaluation of the surface restructuring kinetics between wet and dry states of the elastomeric interface. Further increasing the energy differences between the two silicon substituents magnified the effects of the surface reconstruction. Thiol-ene addition reactions to the vinyl substituent enabled the opposing methyl substituent to comprise a -carboxy or -hydroxy terminated alkane chain. For example, the functionalization of the PVMS elastomer with mercaptopropionic acid resulted in a rapid surface restructuring as measured by θ_{DIW} at -2^{o}/second upon exposure to water. To our knowledge, this change in surface energy states is the fastest of any known polymer system.

The restructuring kinetics of PVMS-modified networks was further evaluated by tuning in wettability and switch hysteresis through controlling the degree of surface mobility imparted from the surface modifier. This was accomplished by varying the number of methylene spacers between the silicon atom and the hydroxy terminus. Once the a critical number of methylene groups was achieved, the van der Waals interactions between methylene groups were capable of inducing crystallinity, which resulted in decreasing dramatically the rate of surface reconstruction. Whereas a liquid-like surface modifier could easily conform to the lowest energy-state, the formed semi-crystalline regions resulted in a solid-like modifier incapable of easily switching its conformation for differing polymer interfaces. This crystallinity-induced surface "stability" could be reverted to a liquid-like surface by increasing the enthalpic energy of the network by raising the temperature above its melting transition. These findings were confirmed with dynamic mechanical analysis, differential scanning calorimetry, and optical microscopy where PVMS modified with a

-$(CH_2)_{11}OH$ spacer possessed a melting transition of about 37°C. While the PVMS-S-$(CH_2)_2OH$ and PVMS-S-$(CH_2)_6OH$ glass transition temperature (T_g) was significantly higher than unmodified PVMS, the T_g of alkyl-modified PVMS was still well below room temperature keeping the surface mobility intact for our studies.

An attractive feature of PVMS elastomers is that the vinyl substituent lends itself to surface modification. This trait is of essence in biomaterials where modification with cell-adhesive ligands is often necessary for a viable application. We explored possibilities of generating PVMS with varying surface characteristics to make the study of complex cell-surface interactions on one substrate. Cell-surface interactions are affected by topology, surface chemistry, and mechanical properties. The 3rd variant, namely the elastic modulus of the surface, is one that is just being explored by several researchers. With gradients in modulus of the substrate, the cell migration path changes due to the way the cells adhere and sense their surroundings. As siloxane elastomers are currently used in biomaterials it is an attractive substrate for evaluation. Its drawback lies in its resistance to surface modification. Our work in defining the wettability characteristics of PVMS led us to evaluate it as a material to first control its mechanical properties in a systematic manner and then control its surface chemistry.

In this Ph.D. Thesis we defined two approaches for generating networks with tunable mechanical properties. We implemented hydrosilation chemistry to cross-link chains across the PVMS backbone with hydride-terminated PDMS (H-PDMS). By varying the concentration of ≡Si-H and the degree of polymerization of H-PDMS, we produced elastomers with elastic moduli (G') ranging from 20 to 400 kPa. We designed varying ≡Si-H

cross-linker formulations to interdiffuse upon casting the network mold to produce a substrate with a gradient in modulus. Upon evaluation of cell proliferation with these networks, surface segregation was observed between the PDMS and PVMS components. While this complicated the interpretation of the proliferation results, our work did lead to some interesting leads for future study, as discussed in the next section. Our second approach for producing substrates with micro-scale gradients in modulus was to utilize an UV-curable siloxane to finely control the spatial intensity of the resultant cross-link junctures. Synthesizing mercapto-terminated PVMS provided this capability and cell-work with the formed networks is just beginning.

7.2 Recommendations for Future Work

Throughout the research of this Ph.D. Thesis the options and opportunities for future work seem unlimited. While the focus through Chapter 4 was on the design and manipulation of responsive surfaces, the findings could be carried over into the remaining of the research work. For instance, concern about reconstruction could be avoided if the polymer interface were kept constant and allowed to reach equilibrium before proceeding forward with additional experiments. While we initially thought that inducing the crystalline structure of PVMS-S-$(CH_2)_{11}$OH was undesirable in regards to surface responsiveness at room temperature, it may have certain advantages for systems where the end-use is at elevated temperatures performing as a thermoresponsive network. In the remainder of this chapter, we will discuss some possibilities for additional work that stem from some preliminary work with surface modification of PVMS, mechanical analysis of the formed

networks, and using the surface segregation of the PVMS-PDMS networks as a way to vary the topography of the networks.

7.2.1 Surface modification of PVMS via UV-activation of thiol-ene addition reactions

Preliminary work was carried out with growing polymer brushes on PVMS through the functionalization of the surface with ω-mercaptohexanyl bromoisobutryrate, an atom transfer radical polymerization (ATRP) initiator. The ATRP initiator was mixed with Darocur 1173 (2-hydroxy-2-methyl-1phenyl-propan-1-one), coated on the surface of an alkoxy-cured

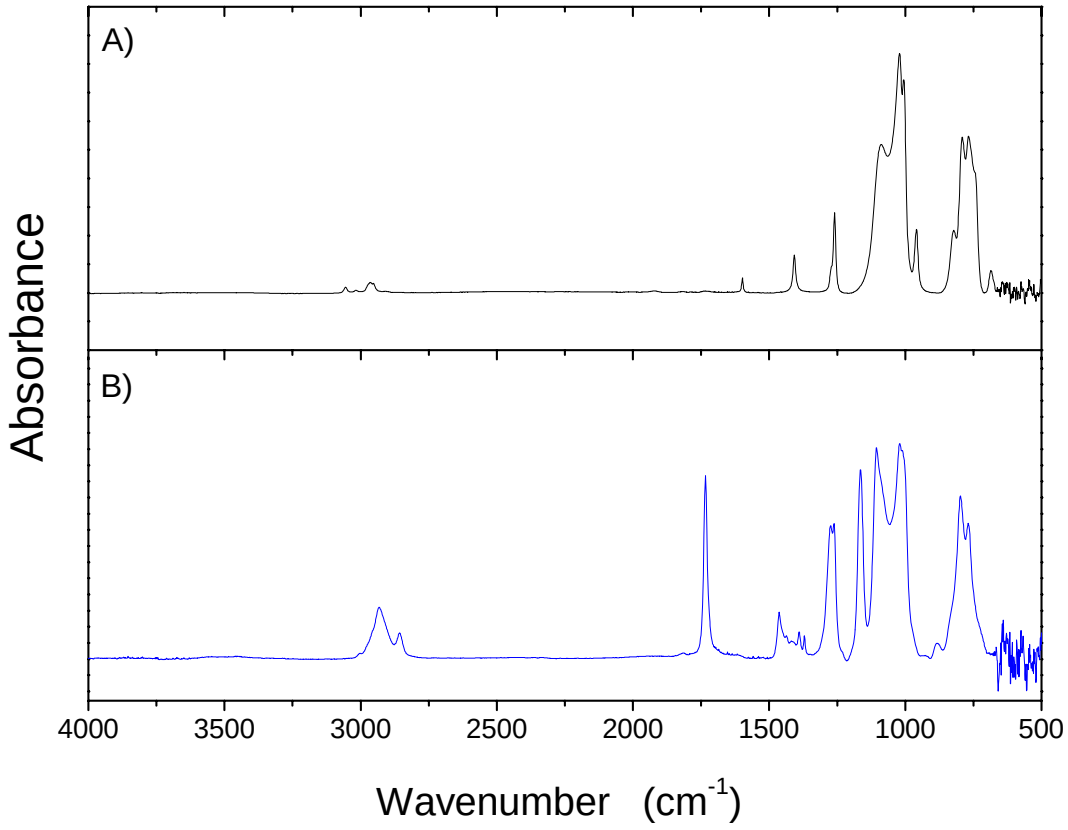

Figure 7.1: ATR-FTIR spectra for A) untreated side of PVMS and B) treated with ω-mercaptohexanyl bromoisobutryrate.

PVMS network, and covalently bound via UV activation. Figure 7.1 depicts the FTIR spectra for the side of the substrate that had been coated with the initiator versus the reverse side that was not, where the appearance of the carbonyl stretching vibration at 1760 cm^{-1} indicates the attachment of ω-mercaptohexanyl bromoisobutryrate. The one-sided addition of the thiol initiator was in contrast to the bulk addition reaction of the mercaptoalkanols of Chapter 4 of this Ph.D. Thesis. This minimized the amount of thiol that was necessary for the reaction in addition to more closely obtaining a true surface functionalization. The PVMS-initiator substrate was subsequently polymerized with N,N-dimethyl aminoethyl methacrylate following a standard ATRP procedure used in our laboratory. Testing of this sample was not completed although visual changes of the sample occurred; namely a precipitate colored with copper-residue. As poly(N,N-dimethyl aminoethyl methacrylate) is a well-studied thermo-responsive polymer system, surface polymerization from an elastomeric substrate could lead into some interesting opportunities for scientific study.

L-Cysteine was also attached to the PVMS surface via UV-activation. This molecule is of interest as it would be a building block for modifying surfaces with various peptides. A saturated solution of L-Cysteine in ethanol was mixed with Darocur 4265, applied to the surface of PVMS, and irradiated at 365 nm for 20 minutes. ATR-FTIR indicated the presence of cysteine with a characteristic carbonyl stretching vibration at 1735 cm^{-1} (*cf.* Figure 7.2A). Further confirmation that surface modification occurred was with phase contrast optical microscopy where the morphology of the PVMS was dramatically altered (*cf.* Figure 7.2B).

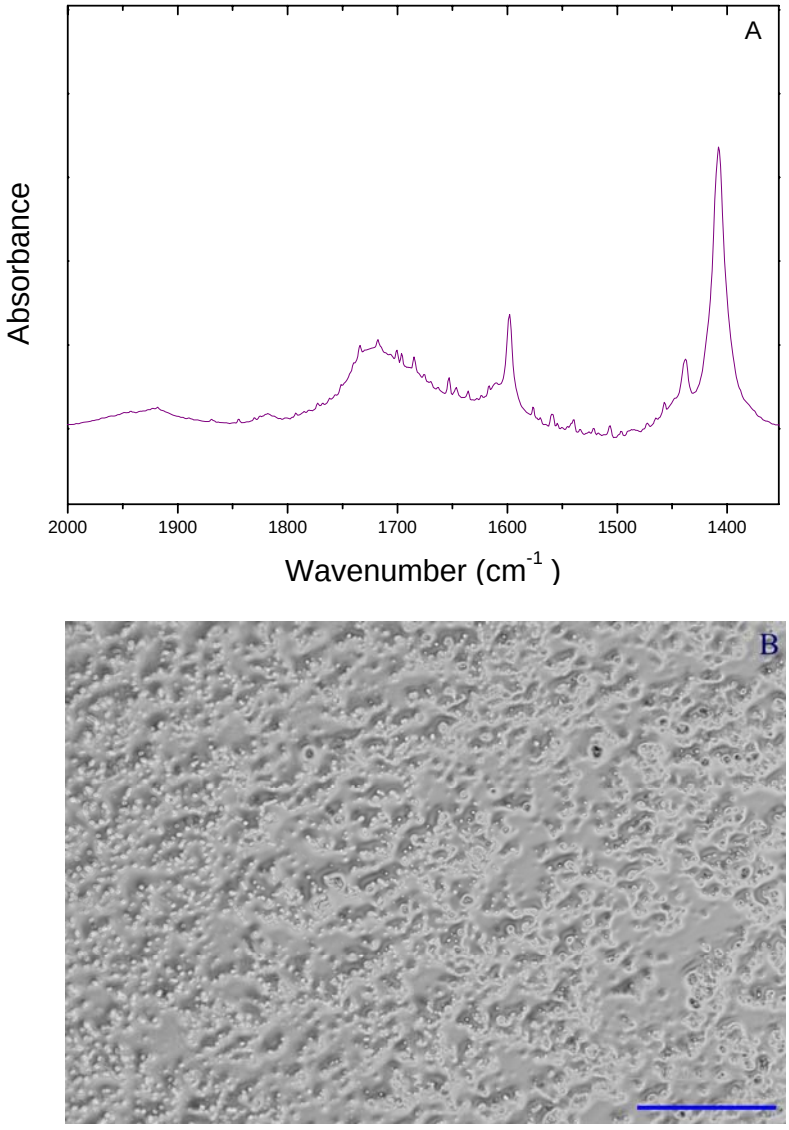

Figure 7.2: A) ATR-FTIR spectra of a PVMS surface modified with L-cysteine. The presence of a broad carbonyl peak –COOH is indicative of the cysteine molecule and B) optical microscopy illustrates a dramatically different surface morphology than standard PVMS (bar is 200 microns).

Another route to modify PDMS surfaces to promote cell adhesion through conjugation of RGD peptides was suggested by Li and coworkers [1]. This two-step process of 1) soaking the PDMS substrate with a solution of N-sulfo-succinimidyl-6-(4'-azido-2'-nitrophenyl-

amino)hexanoate followed by exposure to UV light for 30 minutes and 2) incubating the modified substrate with a RGD peptide solution at room temperature for 24 hours. The researchers saw a remarkable improvement in the attachment and proliferation of human skin fibroblasts, almost equivalent to the tissue culture polystyrene substrate. In addition to the adhesion and proliferation improvements, the RGD-conjugated PDMS was extremely durable and maintained their integrity for reuse after subsequent cleaning and sterilization. One interesting aspect is the duration of UV exposure time. As discussed in Chapter 2 of this Ph.D. Thesis, our research group demonstrated, that prolonged UV exposure altered the surface elasticity of PDMS elastomers[2]. Utilizing PVMS networks in place of PDMS networks may keep the desired surface elasticity intact.

The need to understand the surface chemistry characteristics after treating the siloxane networks with cell-adhesive ligands is critical for deconvoluting the contributing parameters for cell-substrate interactions. One method could be to use an atomic force microscopy (AFM) tip under cell-culture media that has been functionalized with an appropriate cell receptor. Mapping the surface with the AFM tip to determine the uniformity of the surface would qualitatively confirm the surface modification. Alternatively, we could label an adhesive protein, such as fibronectin, with fluorescent markers, deposit onto the siloxane surface, and determine the uniformity of fluorescence upon excitation of the surface.

7.2.2 Additional mechanical analysis

We and other researchers have observed that surface modification can alter the mechanical compliance of the modified substrate[3]. Thompson and co-workers noted that

polyelectrolyte multilayers (PEMs) conjugated with peptide sequences through a heterobifunctional cross-linker realized an increase in elastic moduli from 10^5 to 10^7 MPa. The main mechanism increasing the material stiffness occurred via increased interchain hydrated cross-linking through bulk poly(allylamine hydrochloride) adsorption. The adsorption step was necessary to promote the conjugation between the peptide and the cross-linker. By reducing the bulk adsorption time, Thompson and coworkers were able to minimize the elasticity changes.

The change in PEMS surface compliance during the peptide conjugation procedure is an illustration of the importance of probing the material properties of the final modified substrata. Ideally, this would occur in the cell culture media and at incubation temperature (37^oC). The vast majority of the cell-substrate interaction behavior is assessed from material properties obtained in environmental conditions differing from cell-culturing conditions. Not only could the modulus be changing, but also the surface chemistry could be different when exposed to media due to possible surface reorientation effects.

As follow-up to the UV-curable PVMS-SH networks prepared by us, we should ascertain any post-curing occurring during dynamical mechanical analysis (DMA) testing. This would involve simply evaluating the modulus after equilibration at elevated temperatures. It would also be advantageous to improve upon the robustness of the formed network for increased durability during extraction and cell plating procedures. The networks are simple in structure in order to make understanding their surface characteristic less complex. Typical silicone elastomers are formulated with 3D resins and silica fillers. The incorporation of vinyl functional resins into the PVMS-SH may increase the elongation and

tensile strength at the point of break. Lee and Lutz produced similar networks with a mercapto-functional siloxane cross-linker and a combination of vinyl-terminated PDMS and dimethyvinylsiloxy resins possessing tensile strengths around 3 MPa with 150% elongation[4]. Finally, although we avoided the synthesis of norbornenyl-functional PVMS it could be advantageous to do so as it would have a higher reaction rate with the mercapto-groups as the –ene component. This process may enhance the cross-linking control with the formed network[5-7].

7.2.3 Surface Segregation in PDMS-PVMS

While we observed surface segregation with PDMS-PVMS networks; these systems could present some interesting characteristics for additional study. For instance, nanotopographic interfaces were formed with poly(styrene-co-4-bromostyrene) random copolymers for the evaluation of human foetal osteoblastic cellular behavior on this substrate[8]. The researchers found that the cellular activity depended on the size of the nanoisland that was formed by the polymer-demixing (11-85 nm in size). If it is still desired to use the interdiffusion technique for forming variants in modulus but avoid surface segregation, vinyl terminated PDMS and a copolymer with hydride functionality throughout the backbone could be employed. The drawback would be the lack of a reactant substituent for subsequent cross-linking. It may, however, be a first step approach to deconvoluting the modulus effects versus surface chemistry effects. Conversely, we have just begun testing of a PVMS-OH (N=15) formulated with excess mercapto-alkoxy silane. If norbornenyl substituents could be incorporated into a PVMS-PVMS-NB copolymer combined with a SH-

PVMS (N=15), the resultant network would be closer to the DPX-Y networks described in Chapter 5 of this Ph.D. Thesis.

7.3 References

1. Li, B., Chen, J. & Wang, J. H.-C. RGD peptide-conjugated poly(dimethylsiloxane) promotes adhesion. proliferation and collagen secretion of human fibroblasts. *Journal of Biomedical Materials Research Part A* **79**, 989-998 (2006).

2. Efimenko, K. et al. Formation of hydrophilic silicon elastomer surfaces by ultraviolet/ozone treatment of poly(vinylmethyl siloxane) networks. *Manuscript in preparation* (2004).

3. Thompson, M. T. et al. Biochemical Functionalization of Polymeric Cell Substrata Can Alter Mechanical Compliance. *Biomacromolecules* **7**, 1990-1995 (2006).

4. Lee, C.-l. & Lutz, M.,Fast ultraviolet radiation curing silicone compositions. Dow Corning Corporation, USA 4780486, 1986.

5. Muller, U. & Kunze, A. Photocrosslinking of Silicones. Part 13. Photoinduced Thiol-ene Crosslinking of Modified Silicones. *J Macromol Sci Pur Appl Chem* **33**, 439 (1996).

6. Jacobine, A., Glaser, D. & Nakos, S. in *Radiation Curing of Polymeric Materials* (eds. Hoyle, C. & Kinstle, J.) 160-175 (American Chemical Society, Washington DC, 1990).

7. Hoyle, C. E., Lee, T. Y. & Roper, T. Thiol-Enes: Chemistry of the Past with Promis for the Future. *Journal of Polymer Science: Polymer Chemistry* **42**, 5301-5338 (2004).

8. Lim, J. Y., Hansen, J. C., Siedlecki, C. A., Runt, J. & Donahue, H. J. Human foetal osteoblastic cell response to polymer-demixed nanotopographic interfaces. *Journal of the Royal Society Interface* **2**, 97-108 (2005).